IMPLEMENTATION OF VENTED FUEL ASSEMBLIES IN THE SUPERCRITICAL CO_2-COOLED FAST REACTOR

By Stephanie A. McKee

B.S. Nuclear Engineering
The University of Tennessee, Knoxville, 2007

SUBMITTED TO THE DEPARTMENT OF NUCLEAR SCIENCE AND ENGINEERING IN PARTIAL FULFILLMENT OF THE REQUIREMENTS FOR THE DEGREE OF

MASTER OF SCIENCE IN NUCLEAR SCIENCE AND ENGINEERING
AT THE
MASSACHUSETTS INSTITUTE OF TECHNOLOGY
[June 2008]
APRIL 2008

Signature of Author: _____
Department of Nuclear Science and Engineering
April 25, 2008

Certified by: _____
Dr. Michael J. Driscoll, Thesis Supervisor
Professor Emeritus of Nuclear Science and Engineering

Certified by: _____
Dr. Jacopo Buongiorno, Thesis Reader
Carl R. Soderberg Professor of Power Engineering
Associate Professor of Nuclear Science and Engineering

Accepted by: _____
Dr. Jacquelyn C. Yanch
Chair, Department Committee on Graduate Students

IMPLEMENTATION OF VENTED FUEL ASSEMBLIES IN THE SUPERCRITICAL CO_2-COOLED FAST REACTOR

By

Stephanie A. McKee

Abstract

Analysis has been undertaken to investigate the utilization of fuel assembly venting in the reference design of the gas-cooled fast reactor under study as part of the larger research effort at MIT under Gen-IV NERI Project No. 05-044, "Optimized Competitive Supercritical-CO_2 Cycle GFR for Gen-IV Service." The focus of this work is on selection and optimization of a fuel assembly configuration best suited for venting, assessment of the radionuclide release of such an assembly design, and identification of plant systems which must be altered in order to support fuel venting.

The innovative tube-in-duct design of the reference GFR fuel assembly is particularly well suited to venting, allowing fission products to diffuse into a common header before being routed along a vent path and eventually being released to the primary coolant system. A set of equations were developed which model the transport of fission products from fuel to vent path to primary coolant inventory and then into the containment atmosphere, with emphasis on conservatism in calculations of coolant impurity levels. Using these equations in a computer code, the lengthy list of radioactive and chemically volatile fission products for study was reduced to only fifteen species of any great concern. Of these, ^{85}Kr and ^{137}Cs were considered conservative bounding cases on the behavior of the other nuclides.

The chemistry of the fission products released to the coolant was explored. In particular, reactions between fission products and their surroundings were identified, and estimates of deposition of both compounds and free atoms on steel surfaces were made. Investigation of reactions between fission products and CO_2 revealed that the formation of stable oxides would lead to deposition of most volatile species within the fuel assembly's debris trap. The radioactive volatiles which remain in the primary comprise only tritium, two isotopes of iodine, two isotopes of tellurium, and three isotopes of cesium. These species deposit on primary surfaces to a great enough degree to preclude hands-on primary system maintenance. In addition, techniques for removal of volatile and radioactive species from the primary coolant were identified, and a scheme for purification of the primary coolant volume was selected. The analysis confirms that primary coolant activity can be maintained at acceptable levels when purification of the primary coolant volume occurs once per hour.

The response of the vent system to changes in primary system pressure was also investigated. In particular, the small periodic pressure transients known as breathing were studied, as were loss-of-coolant type scenarios. Both cases were investigated using hand calculations and computational techniques, and the radiological consequences of each were addressed. The analysis demonstrated the ability of the vented fuel assembly to

quickly equalize pressure in the event of a sudden drop in operating pressure, and also showed the ability of a succession of plena to prevent the expulsion of much of the activity inventory of the plena during a breathing transient. Conversely, the use of a single plenum results in reduced activity release during a LOCA. After consideration of both results, a two-plenum approach, with a large lower annular plenum following a small upper axial plenum, was selected as the final design.

Thesis Supervisor:	Michael J. Driscoll
Title:	Professor Emeritus of Nuclear Science and Engineering
Thesis Reader:	Jacopo Buongiorno
Title:	Carl R. Soderberg Professor of Power Engineering Associate Professor of Nuclear Science and Engineering

Acknowledgments

Like any other scientific endeavor, this work would not have been possible without the assistance of a great number of people. First and foremost is my advisor, Prof. Michael J. Driscoll, who was a constant source of guidance and was persistently helpful in fact-checking and providing new leads. Prof. Ron Ballinger provided a great deal of assistance in the forms of the HSC computer code used for the analysis in chapter 5, and in the use of his laboratory equipment for the experiment which aided in the development of a coolant purification scheme. A special thanks goes out to Dr. Tom McKrell for his invaluable help in setting up this experiment.

Thanks also go out to Prof. Andrew Kadak, for the wealth of technical documents which helped provide a background for the present work, and to Dr. Pavel Hejzlar for his assistance in using RELAP. I am also grateful to both Matt Memmott and Anna Nikiforova for their help in completing my calculations.

I especially want to thank Richard St. Clair, for a great deal of time spent in assisting with preparation of this finished report. Without his help, there would be many fewer illustrations for clarity.

Chapter 1: Introduction

Foreword

The objective of the present work was to investigate the implementation of vented fuel assemblies in the reference design of the MIT Gas-Cooled Fast Reactor (GFR), currently under development as part of a larger research effort, "Optimized, Competitive Supercritical CO_2 Cycle GFR for Gen-IV Service" (Project 05-44), which has been funded by the Nuclear Energy Research Initiative (NERI). This goal of this larger project is the development of an integrated plant design for the GFR, based on the direct supercritical CO_2 Brayton cycle. This project is defined by three major tasks and nine subtasks:

1. **Core design and performance assessment**
    - 1.1 Optimization of the features of the vented fuel concept using tube-in-duct fuel assemblies
    - 1.2 Development of pin-type core as benchmark for comparisons and fallback option
    - 1.3 Confirm capability of GFR to burn transuranics and minor actinides
2. **PRA guided design of safety systems**
    - 2.1 Development of decay heat removal for accident, shutdown, and refueling
    - 2.2 Development of improved emergency power systems, such as microturbines and fuel cells
    - 2.3 Development of active and passive means of shutdown assurance to preclude an anticipatory transient without scram (ATWS)
3. **Overall plant design and economic assessment**
    - 3.1 Design of power cycles for core exit temperatures ranging from 550 to 700 °C
    - 3.2 Demonstration of integration with high-temperature electrolysis of steam for H_2 production
    - 3.3 Estimation of busbar costs of electricity generation relative to other reactor options.

To date, all but subtasks 1.1, 2.1 and 3.1 have been completed. The present work builds on the previously completed subtasks to complete subtask 1.1, vented fuel optimization.

1.0 Motivation

As nuclear power continually grows in favor as a source of clean, reliable energy for the ever-expanding needs of the U.S. and world markets, it is clear that fast reactors should eventually be relied on to produce much of this power. Though research on fast reactor systems slowed in the 1980s due to concerns over proliferation and expense, and pessimism on the part of the public, the work of the 1960s and 1970s on fast reactors in general and on gas-cooled fast reactors (GFRs) in particular has received a great deal of renewed interest, as embodied by the current Gen-IV and GNEP projects [GNEP, 2007]. This renaissance has come as the result of a number of driving forces: the availability of proliferation-resistant fuel reprocessing technology, the need for recycling of the growing inventory of spent thermal reactor fuel, the decades of safe and economically stable operating experience of nuclear reactors in the U.S. and abroad, and the overwhelming importance of shifting to methods of energy generation which do not contribute substantially to global warming. While many of these factors may spur construction of additional light water reactors, a few of the concepts listed cannot be forwarded through the use of traditional nuclear power systems. Only fast reactors can achieve the goals of long term sustainability, while reducing spent fuel inventories and continuing to support the operation of light water reactors as a means for safe, environmentally friendly power generation.

As the importance of using fast reactors increases, so too does the importance of ensuring that these reactors can operate as safely as possible with the highest fuel burnup possible. As it stands, the lifetime of fuel within a fast reactor is most severely constrained by the acceptable strain on the cladding, rather than by neutronic limitations of the fuel. Creep occurs in materials which are under stresses lower than their yield strength for extended periods of time. The rate of increased strain is affected both by the mechanical stress placed on the material, in this case the internal pressure on the cladding, and the temperature at which the stress occurs. The presence of other disruptive forces, such as radiation fields, also influences the creep rate by inducing dislocations in the microstructure. While it may not be possible to reduce the damage to the cladding due to the radiation field or elevated temperature present in a nuclear reactor, venting can effectively reduce the creep rate of the cladding by decreasing the mechanical stress

caused by pressure. While it may appear reckless to effectively remove the first barrier to fission product release, in light of the high pressures and high cladding temperatures common to the GFR, it is more prudent to plan for small continual fission product releases than to allow creep to contribute to cladding damage and eventual large-scale fission product release. Accordingly, venting of fission products from GFR fuel is the principal subject of this thesis research project.

In addition to reduction of cladding strain, the venting of fuel may be motivated by several other phenomena. First, the presence of large quantities of fission gases in the space between the fuel surface and its cladding reduces the thermal conductivity of that gap. This leads to reduced heat transfer capability from fuel to coolant and in turn causes the fuel to remain at a higher temperature than desired. Venting of fission gases can improve the thermal conductivity of the gap by reducing the quantity of fission gas present in the gap at any instant, as CO_2 has a thermal conductivity higher than Kr and Xe by a factor of 2 or 3 [CRC Handbook, 2007]. While a small amount of CO_2 may be displaced by the fission gases which emerge from the fuel, it is expected that the slow rate of release of the gases from the fuel will allow continuous diffusion of fission gases through the CO_2 and out of the fuel assembly, rather than large-scale slug-flow displacement of CO_2.

Venting of fuel may also make it possible for a system to operate under more favorable neutronic conditions. Since cladding strain would be significantly reduced by the removal of the gaseous fission products from the gap, the cladding thickness could likewise be reduced. The reduction of cladding thickness would improve the neutron economy of the system. This improvement in neutron economy means that the system would be able to sustain a higher reactivity-limited burnup, or alternatively, operate with a lower initial enrichment.

Another benefit of using vented fuel assemblies, if they are kept at a slightly lower pressure than that of the gas coolant which flows through them by venting to a plenum in the grid plate, is that the collection system can be used to detect the location and size of a leak in the cladding. The lower pressure inside the cladding means that any opening will cause a leak of clean coolant into the fuel element, and not leakage of gaseous fission products into coolant. The higher than normal concentration of the

coolant in the gas making its way to the collection system can be detected by in-line monitoring, alerting management that a cladding breach has occurred.

The emphasis in the present work, however, will be in delayed venting of fission products directly to the coolant.

1.1 History of Vented Fuels

Prior to the study of vented fuel assemblies for the GFR, analysis had been performed on a number of vented fast reactor designs. One of the early designs was of the Fast Flux Test Facility (FFTF), developed by General Electric and Pacific Northwest Laboratory for the U.S. Atomic Energy Commission [Gee, 1969]. This work drew on previous venting experience in the Dounreay test reactor, and established the feasibility of venting fission gas to sodium coolant, despite key fuel form differences between the FFTF and Dounreay reactors. A similar study undertaken by GE evaluated vented fuel favorably for use in a ceramic fueled, sodium cooled reactor from both technical and economic standpoints [O'Neill, 1965], and made an important innovation in the form of a "diving-bell" type structure which would allow venting of gaseous fission products while preventing the influx of sodium coolant into the cladding. Contemporary to both the analyses performed by GE and the operation of the Dounreay test reactor was the operation of Peach Bottom Unit 1, an HTGR which utilized vented fuel.

In parallel with work on the FFTF, irradiation tests were performed during the fuel element development program for the General Atomics Gas-Cooled Fast Reactor (GCFR) [Campana, 1973], which vented fission products to its helium coolant for collection and sequestration, as shown in Fig. 1. The measurements of fission gas release from the irradiated test elements were intended to verify the conservatism in previous design calculations, and were successful in doing so. Many of the conclusions drawn as a result of these irradiation tests should lend weight to the calculations performed in the present work.

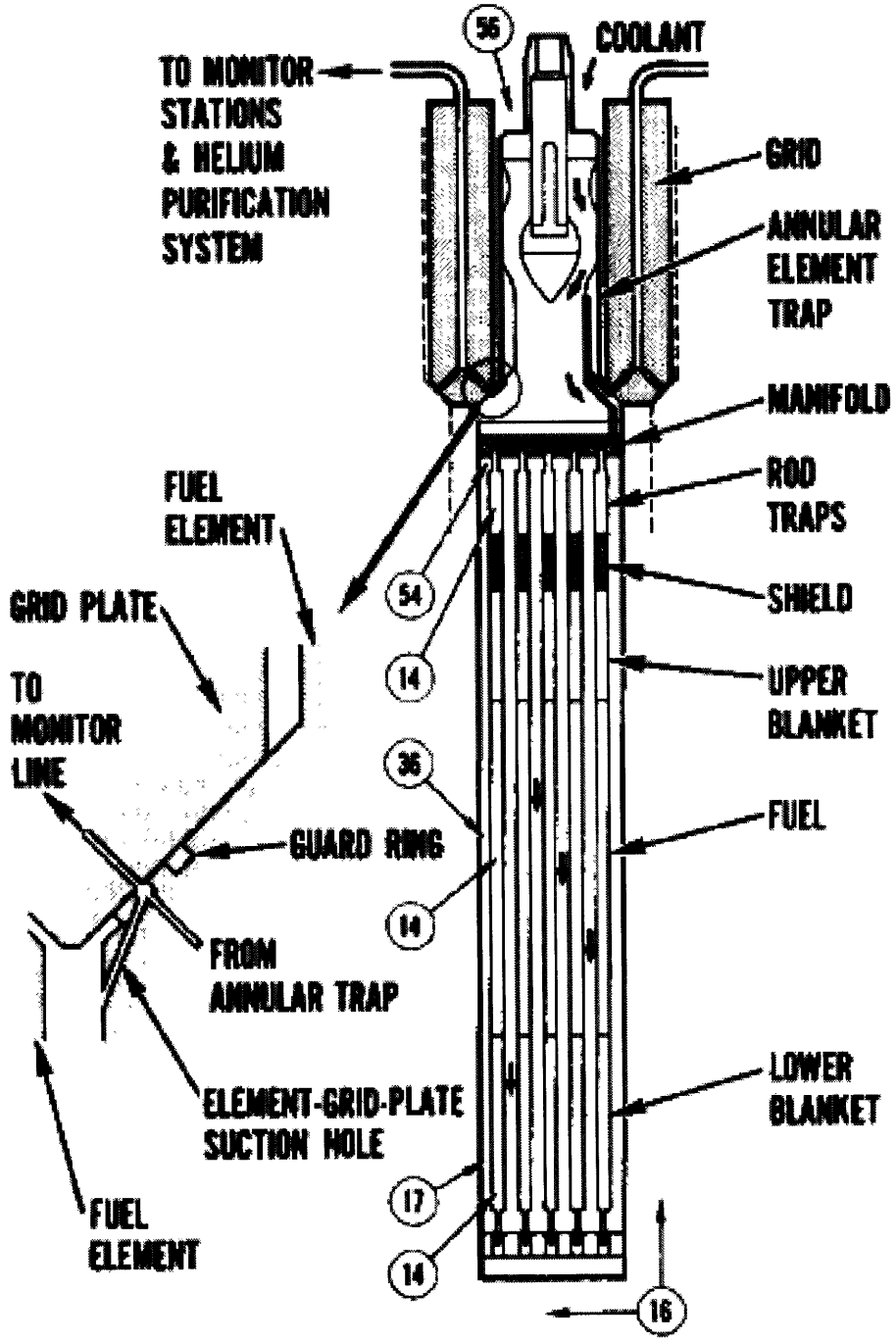

Figure 1.1:Schematic of GCFR Assembly, Showing Path of Fission Gas Transport [Campana,1973]

Efforts to assess the use of vented fuels are also ongoing. At present, a team at Idaho National Laboratory is investigating the behavior of vented carbide pin-type fuel for a GFR design similar to that of the present work [Gan, 2008].

1.2 Objectives and Contributions of this Work

The primary objective of the present work is a complete assessment of the venting of fission products from the fuel assemblies to the coolant of the Gas Cooled Fast Reactor (GFR), which has been the subject of ongoing research at MIT. Particular emphasis is placed on assessment of the licensability of the GFR with vented fuel. The contributions of this work are

- Identification of nuclides of particular interest in the venting process.
- Estimation of primary coolant activity levels.
- Investigation of interactions of fission products with their surroundings.
- Recommendation of purification rates and methods for achieving these rates.
- Examination of vent system response to transients.
- Estimation of radiation released during accidents.
- Identification of areas of work required for refinement of design.

1.3 Achievement of Goals Through Venting

The efforts in GFR development at MIT have taken place with the goals of the Generation IV International Forum in mind. These goals include [Gen IV Roadmap, 2002]

- Sustainable energy generation that meets clean air goals
- Long-term availability and effective fuel utilization
- Minimization and responsible management of nuclear waste
- Excellence in safety and reliability
- Low likelihood and degree of reactor core damage
- Clear life-cycle cost advantage over other energy sources
- Resistance to proliferation.

In this spirit, the present work endeavors to preserve the achievements made toward these goals by previous work, and to make additional advances in these areas. For example, as mentioned in section 1.0, it has been mentioned that vented fuel assemblies can operate for longer periods of time than their non-vented counterparts, due to the reduction in cladding strain afforded by venting. This lifetime extension would clearly fit with the goal of effective fuel utilization. Alternatively, instead of lengthening the fuel lifetime,

the initial fuel enrichment could be reduced. This would correspond to both reduction in fuel costs and added resistance to proliferation. Finally, the venting of fuel assemblies increases the safety of the fuel form by reducing the probability of cladding rupture due to overpressure.

1.4 Transient Scenarios

For any nuclear system, there exist a number of transient scenarios which must be addressed in order to ensure safe operation of the system. The most important of these in establishing the safety of vented fuel assemblies are those transients which involve deviation from standard operating pressure. Both small and large changes in pressure can be expected at some point during the reactor's operational lifetime. For example, direct cycle energy conversion systems often experience a phenomenon known as "breathing", where small changes in local pressure result in oscillations of the gas volume. While such a phenomenon is of little concern in non-vented systems, it becomes important in vented fuel assemblies because the periodic decreases in system pressure can lead to increased escape of fission products. Therefore, in order to fully assess the fission product inventory of the coolant, such transients must be investigated.

A less common transient, but one just as important to a discussion of reactor safety, is that of a large-break Loss-of-Coolant Accident (LOCA). Two effects of the LOCA are of particular concern in this analysis: the ability of the vented fuel assembly to follow a sudden drop in primary system pressure, and the ability of the vent and purification systems to reduce the radioactive inventory of the coolant both prior and subsequent to the LOCA. Both are discussed in chapters 6 and 7.

While a number of other transients occur in the reactor environment, many can be considered bounded by the discussions of pressure transients in chapter 7. For example, depressurization for refueling or shutdown can be described using the same methods used for breathing and LOCA transients. On the other hand, many other transients, such as loss of external load, may occur which require different treatment. The bulk of these transients do not involve the fission product vent system, and so they are not investigated in the present work. For information on such transients, the reader is referred to M. Pope's 2006 work.

1.5 Previous Work at MIT

The vented fuel assembly under study is intended for use with the 2400 MWth Supercritical CO_2-Direct Cycle GFR, researched by the Center for Advanced Nuclear Energy Systems (CANES) at MIT. Previous work has outlined the complete neutronic [Handwerk, 2007] and thermal hydraulic design [Pope, 2006] of the reactor, and has made mention of the benefits of venting to such a design, but has not explicitly determined the feasibility of its use.

In addition to these design analyses, an additional project described the supporting systems required for the direct cycle operation of the GFR [Freas, 2007]. This work generically described the coolant makeup and charging systems, the coolant purification system and the coolant leak detection system. Because each of these systems must differ slightly from their traditional forms in a system utilizing vented fuel assemblies, this work will be useful in identifying areas in which changes are required.

1.6 Organization of This Report

Chapter 2 describes the reference design of the GFR and its unique tube-in-duct fuel assembly design. The vented fuel concept is introduced, and the integration of vented fuel assemblies into the GFR plant is discussed.

Chapter 3 introduces the mathematical models used to describe transport of radionuclides from the fuel, through the upper axial reflector, and through one or a series of plena and vent tubes. Techniques for computational analysis of fission product transport are also discussed.

Chapter 4 identifies nuclides which are problematic due to their radioactivity and/or volatility. A set of nuclides are identified which serve as bounding cases for the full range of fission products.

Chapter 5 investigates the chemical properties of the fission products released to the coolant and examines the potential for the chemical interaction of these products with each other and with their surroundings. In addition, the deposition of solids onto reactor surfaces is addressed, as is the potential for decontamination of primary system surfaces.

Chapter 6 sets guidelines for the purification of the primary coolant, and outlines potential purification methods. Purification of containment air is also addressed.

Chapter 7 investigates the effects of small and large pressure transients on vented fuel assemblies. The radiological consequences of sudden primary system depressurization are also examined.

Chapter 8 summarizes the present work and identifies a number of areas for future research.

Appendices are included, documenting sample computer inputs, and relevant supplementary data.

Chapter 2: System Description

2.0 Introduction

This chapter outlines the reference design of the GFR under analysis at MIT, as well as the particular features of the fuel assembly design which allow venting to take place. Because venting can take place by two different methods, venting of fission products directly to coolant and venting to a grid-plate collection and sequestration system, the two concepts are compared. In addition, this introduction to fuel venting addresses changes which must be made to other plant systems when use of vented fuel assemblies is planned.

2.1 GFR Reference Design

The GFR design which has been the subject of recent investigation at MIT is a 2400 MWth fast spectrum reactor cooled by supercritical carbon dioxide. Energy conversion occurs through the use of a direct Brayton cycle. The design was constrained by a number of unique requirements imposed due to the desired use of the GFR in Generation IV service [Pope, 2007]. For example, the desire to reduce proliferation risk led to the elimination of the ^{238}U blankets common to fast reactors. With the elimination of plutonium-producing blankets arose the need to increase fuel volume fraction in order to support a long fuel lifetime and high conversion ratio. In addition, the increase in fuel volume fraction coincided with a decrease in coolant volume fraction, an important characteristic since fast reactors usually suffer from a positive void coefficient.

The reduction in coolant volume fraction, however, placed additional requirements on the design of the fuel. Because the increase in fuel volume and decrease in coolant volume tend to cause difficulty in cooling the fuel, the geometry of the fuel had to be modified. The result is a tube-in-duct fuel assembly, consisting of inverted fuel pins, where a cylindrical coolant channel extends through the center of a stack of hexagonal fuel pellets, shown in figure 2.1. The effect of cooling the fuel internally is to place the fuel mass closer to the coolant channel, resulting in overall cooler fuel and

lower pressure drop across the core than would be experienced with pin-type fuel [Pope, 2006].

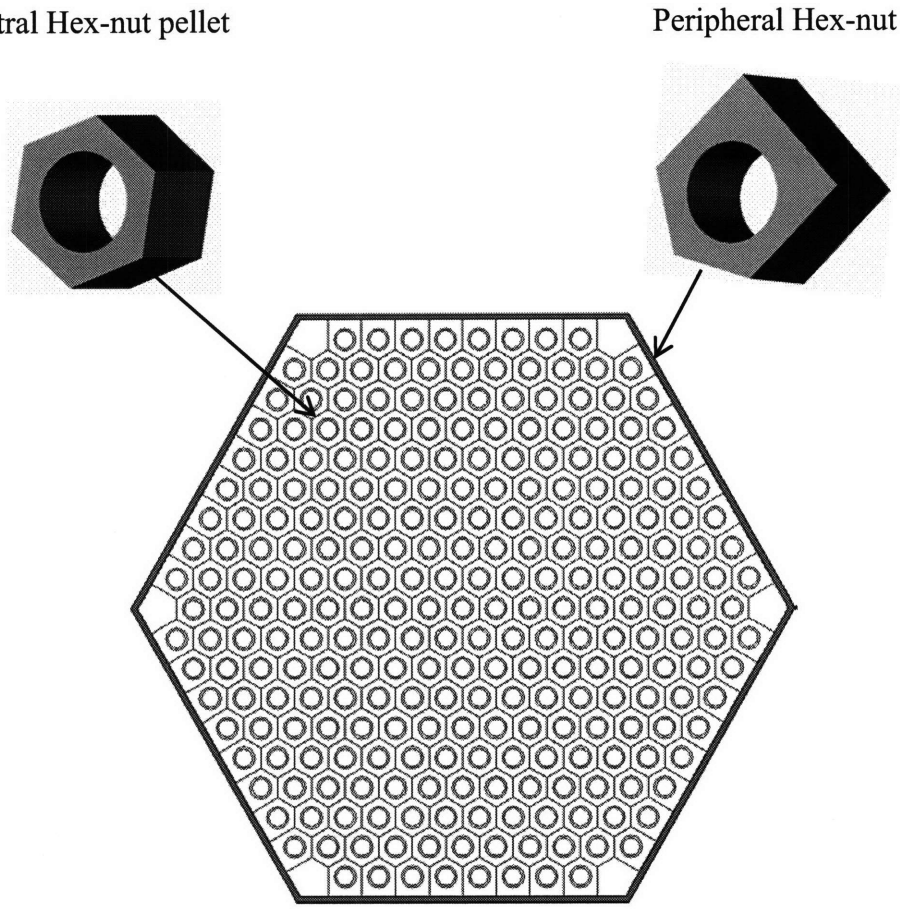

Figure 2.1: Horizontal Cross Section of the TID Fuel Assembly with Hex-nut Pellets [Pope,2006]

Alternatively, it has been suggested that a trefoil shaped pellet be used in place of the hex-nut pellet, as shown in Fig 2.2. The use of such pellets would ease fabrication of fuel, while allowing for the same configuration of the fuel around the coolant tubes, hence affording the same neutronic and thermal hydraulic benefits. The overall effect is simply the relocation of the gaps between pellets.

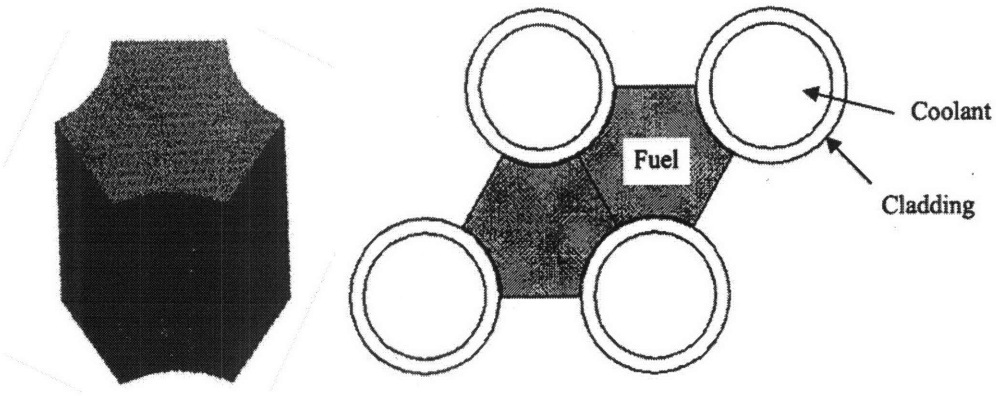

Figure 2.2: Trefoil Fuel Pellet

In either of these cases, the pellets are to be constructed of a mixed oxide consisting of TRU and minor actinides from spent LWR fuel (16.6% by weight), with the balance being natural uranium. The fuel is also diluted by BeO. The core is made up of 378 assemblies, each containing 265 of these fuel pins, and is reflected axially by titanium and radially by S-CO_2. Shielding is provided by a layer of B_4C around the reflectors, and this entire setup is housed by a prestressed cast iron vessel (PCIV). Table 2.1 reproduces the final specifications for the GFR reference design as given by Handwerk's 2007 work. For further information on the reference design, the reader is referred to the 2007 work by Handwerk and Pope.

Table 2.1: Whole Core Parameters, GFR Reference Design [Handwerk, 2007]

Parameter	Value
Whole Core Parameters	
Thermal Power	2400 MW_{th}
Specific Power	20.7 kW/kg_{HM}
Power Density	85.4 kW/l
Reactivity Limited Burnup	1st cycle: 140 MWd/kg, 18.48 EFPY 2nd cycle: 133 MWd/kg, 17.66 EFPY 3rd cycle: 130 MWd/kg, 17.16 EFPY
System Pressure	20 MPa
Core Inlet Temperature	485.5 °C
Core Outlet Temperature	650 °C
Active Core Height	1.54 m
Effective Core Diameter	4.81 m
H/D (Active Core)	0.32
Reflector	S-CO2 (radial), Ti (axial)
Shielding (radial and axial)	99 wt% B_4C
Fuel Assembly Parameters	
Fuel Assembly Description	Tube-In-Duct (TID)
Fuel Enrichment	16.6% TRU
Assembly inner can flat-to-flat distance	22.32 cm (cold), 22.49 (hot)
Assembly outer can thickness	0.2 cm (cold), 0.2015 cm (hot)
Inter-Assembly gap size	0.28 cm (cold), 0.111 (hot)
Cladding thickness	0.07 cm
Coolant hole diameter	0.8 cm
Fuel, volume %	$(U\text{-}TRU)O_2$, 59
Cladding, volume %	ODS MA956, 14
Coolant, volume %	S-CO_2, 27

2.2 Vent System

The innovative design of the reference GFR lends itself particularly well to venting of its fuel. For example, the use of supercritical carbon dioxide as the coolant is important to the success of vented fuel assemblies because the lower diffusion coefficients for gases in CO_2, as compared to the corresponding quantities in He, mean that radioactive nuclei experience greater delay in CO_2 than He when identical path lengths are considered. Additionally, the ability of the two oxygen atoms in CO_2 to react chemically with many fission products contributes to the ability of a CO_2-cooled system to immobilize fission products through deposition of their oxides onto surfaces. This ability is discussed in further detail in chapter 5 of this report.

The GFR's innovative fuel design also lends to the desirability of fuel assembly venting. The tube-in-duct geometry of the fuel allows for the presence of a common upper axial plenum located at the top of the fuel assembly (the presence of such a structure in a pin-type assembly would impede coolant flow). In order to reach this plenum, diffusing nuclides must pass through the upper axial reflector. Additionally, adsorptive materials may be placed between the reflector and plenum to further impede the transport of radionuclides and volatile fission products. Also, while this single plenum is effective at slowing the transport of the diffusing fission products, the extension of the vent path through the addition of vent tubes and more plena can be easily accommodated by the reference GFR assembly design. These additional vent tubes, shown in Fig. 2.3, are of the same dimensions as a standard coolant channel (0.8 cm) and allow transport of the diffusing species through one of three downflow tubes to a lower axial plenum and debris trap, and then through one of three upflow tubes to a third plenum on top of the first. Depending upon the desired reduction in activity of the diffusing radionuclides, the contents of the vent could be released into the primary coolant at the outlet of any of the vent tubes. Further discussion on the benefits of fission product holdup by one, two, or three plena can be found in Chapters 4 and 7.

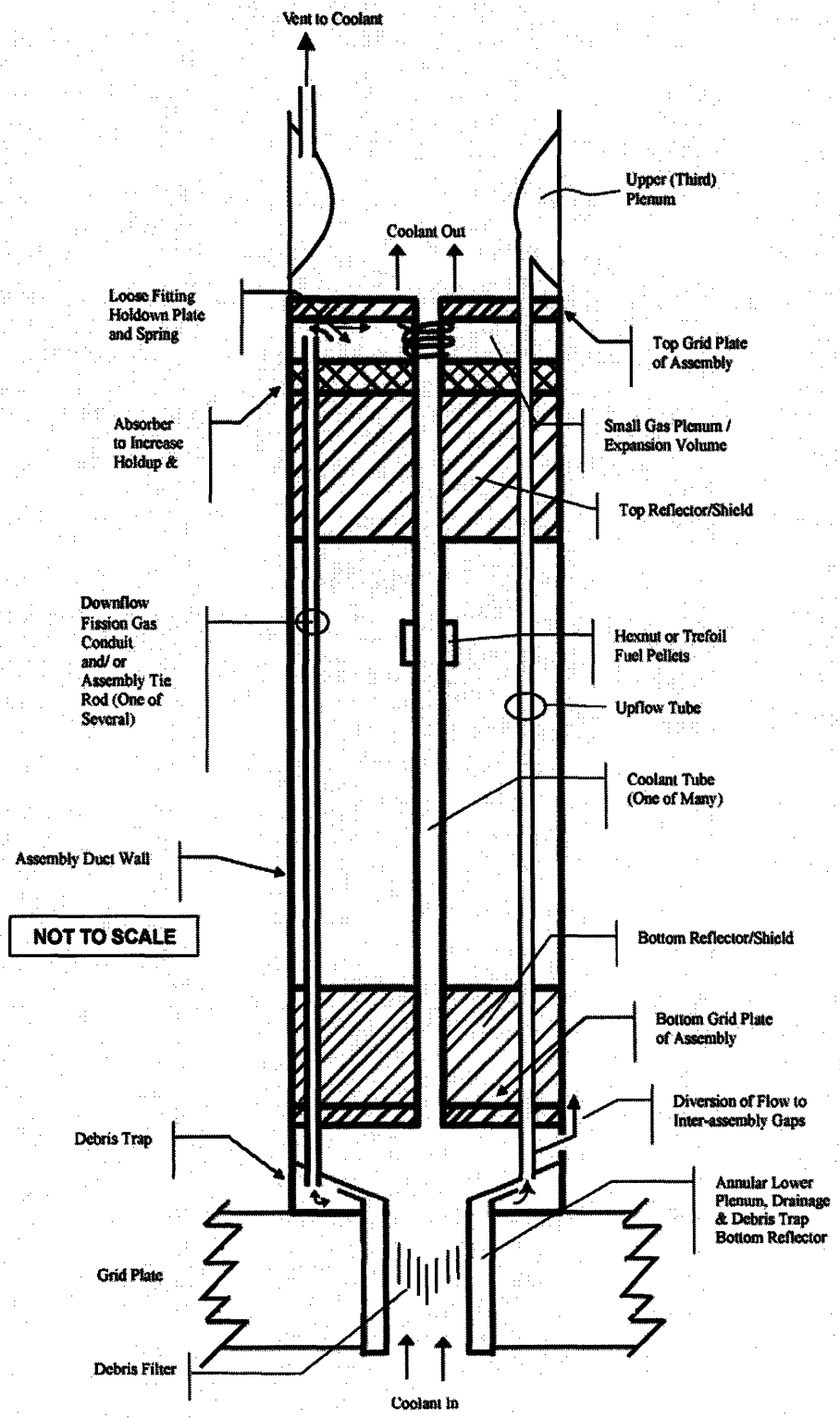

Figure 2.3: Vent-to-Coolant TID Fuel Assembly with Three Plena

Alternatively, the diffusing species can be swept from the vent path after holdup by one plenum and vent tube, and transported to a grid-plate collection system rather than released directly to the primary coolant. The sequestered gases would then be processed, with the fission products separated for holdup and disposal, while the CO_2 would be separated from the rest of the stream and returned to the primary coolant via the makeup system. While this venting configuration, shown in Fig 2.4, might appear attractive, prior analysis has shown coolant inventories of radionuclides to be low enough to allow venting directly to the primary coolant system when a few constraints are imposed on the design of the primary coolant purification system [McKee, 2007]. Because the collection and sequestration approach to fuel venting requires the presence of additional support equipment, while the vent-to-coolant approach requires only modification of existing systems, the vent-to-coolant approach is selected as the area of primary focus of the present work. It should be noted here that such a design has not previously been submitted to the U.S. Nuclear Regulatory Commission for evaluation, and that difficulties would certainly exist in satisfying the regulator that this configuration maintains defense in depth. Nevertheless, it is believed that the vent-to-coolant configuration is the more straightforward of the two approaches of venting, and would in the long run prove more favorable to regulators because of the greater assurance that assembly internal overpressure will be avoided. The development of the configuration which uses a grid-plate collection system is left to future work as an alternative to venting to the primary coolant.

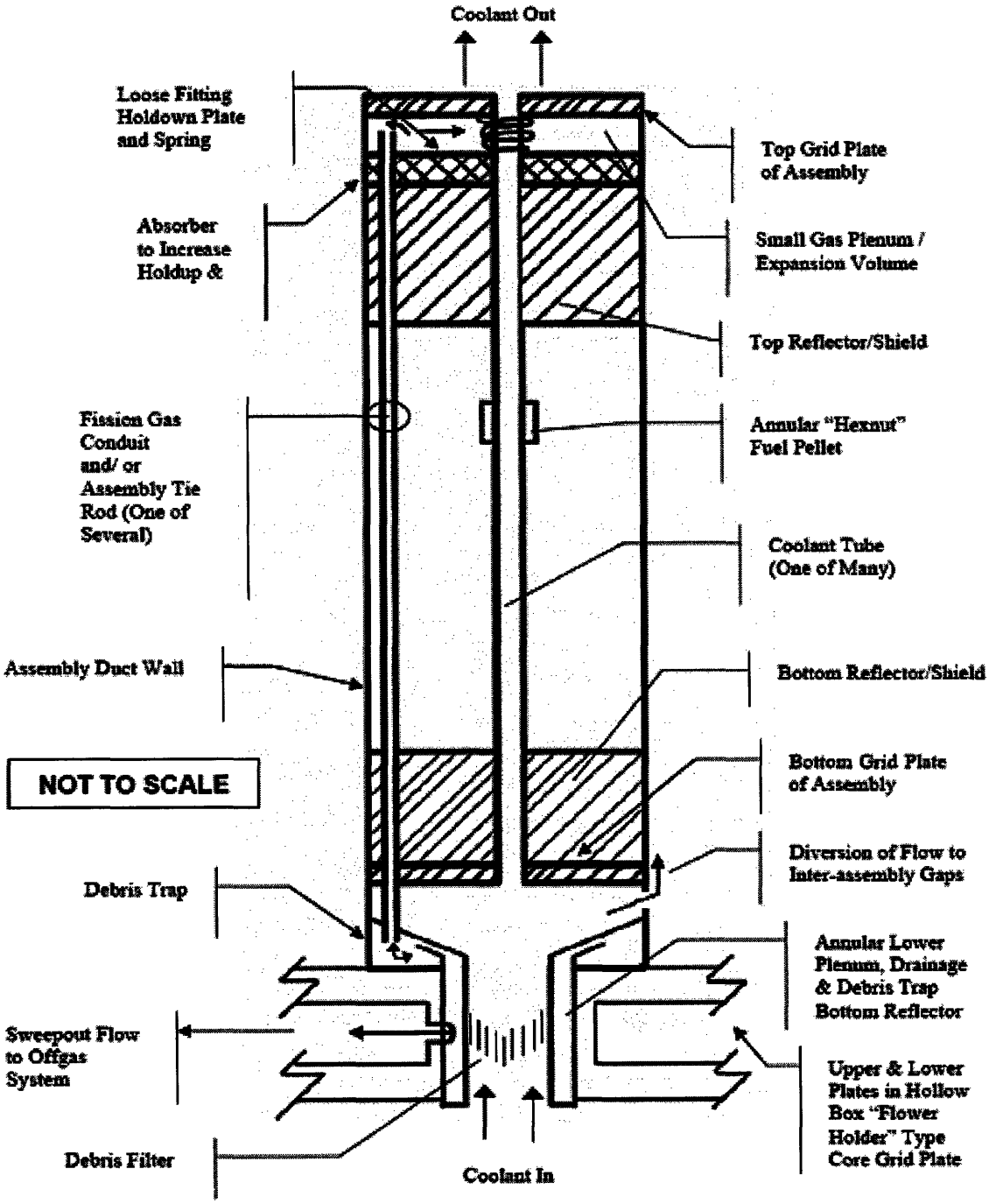

Figure 2.4: Fuel Assembly Vented to Grid-Plate Collection System

2.3 Integration into Reference Design

In order to implement vented fuel assemblies in the reference design of the GFR, a few changes must be made to the support systems, as outlined by previous work [Freas, 2007]. One of the most important contributions of the present work is in more detailed description of a system only vaguely described in the previous body of work: the primary

coolant purification system. Coolant purification systems are traditionally present even in reactors which do not employ venting, due to the presence of both small amounts of fission products which enter the coolant through breaches in cladding, and the products of reactions between the coolant and the reactor environment. Purification systems become much more important, however, in systems utilizing vented fuel due to the presence of large quantities of radioactive fission gases and volatile fission products. In order to maintain safety of day-to-day operation, the coolant purification system must be capable of continually removing significant quantities of both radioactive and volatile fission products. Previous work in this area identified the need for desiccants to remove water, oxygen getters to reduce the likelihood of oxidation, and cryogenic distillation to remove hydrocarbons which may form during day-to-day operation. The use of robust forms of each of these separation techniques, in addition to others not described in the previous body of work, will be required in order to keep up with the higher levels of coolant impurities which occur in vented systems. Specific strategies for separation of undesirable isotopes from the coolant, as well as requirements on the fraction of coolant which must be purified each day, are outlined in detail in chapter 6.

Another system which has been described in significant detail [Freas, 2007] is the coolant leak detection system. While detection of leaks on both a local and general scale is important even in non-vented systems, the monitoring of containment activity levels in the containment of a system using vented fuel is crucial due to the higher activity levels of the coolant. Because it is expected that some leakage will occur on a daily basis, knowledge of containment activity levels is also key to ensuring that the containment atmosphere purification system, which must similarly be more robust than is traditionally common, is functioning properly. The predicted rate of leakage into the containment air, as well as methodology for purification of the containment atmosphere, is discussed in chapter 6.

2.4 Summary

This chapter discussed the reference design of the GFR, and described why this system, with its tube-in-duct fuel assemblies, is well suited to venting of fission products from fuel. The differences between two approaches, venting to coolant, and venting to a grid-plate collection and sequestration system, were also addressed. The emphasis of the

present work is on venting directly to the coolant. Also discussed were modifications to support systems necessary to allow implementation of vented fuel in the GFR reference design. More specific constraints on these modifications are dealt with in later chapters.

Chapter 3: Production and Transport

3.0 Introduction

This chapter introduces the mechanisms by which fission products undergo transport through the vent system. Computational modeling is discussed for each stage of the process, and the appropriate models are selected for later use. The end result is a generalized computational approach which can be used to predict the amount of each fission product in the vent system and in the coolant at any point in time.

Nuclides arrive in the vent tube after a succession of steps. First, a particular isotope is created as a product of the fission reaction or of radioactive decay of another isotope. Next, the atoms diffuse within the fuel material and go on to coalesce into bubbles with other atoms [Olander,1974]. These bubbles then migrate toward grain boundaries in the fuel, as well as edges and corners. The gas is then released when the saturation condition is reached along the grain boundary [Long,2002]. Once the gas is released from the fuel into the gap between the fuel surface and the cladding, the atoms diffuse upward to the expansion volume, and then downward through the vent tube for collection. The individual processes which make up this production and transport sequence are discussed in further detail in the following sections.

3.1 Production of Radionuclides

The change in quantity of any radioactive isotope can be described by the equation

$$\frac{dN}{dt} = \gamma\Sigma_f\varphi(z) + (\lambda N)_{precursor} - \Sigma_a\varphi(z) - \lambda N, \qquad (3.1)$$

Where N = quantity of isotope in question, atoms/cm^3

γ = fission yield of isotope, atoms/fission

Σ_f= macroscopic fission cross section, cm^{-1}

ϕ = neutron flux at height z in fuel, cm^{-2}s^{-1}

λ = decay constant of isotope, s^{-1}

Σ_a= macroscopic absorption cross section, cm^{-1}.

From this equation, the quantity of any isotope can be derived by using or neglecting the appropriate portions of the equation. For example, stable nuclides essentially have a decay constant equal to zero, and so the final term in the rate equation may be neglected; some isotopes are produced only in fission, with no precursors, and so the second term may be neglected. In the present work, production of species through absorption of neutrons is neglected because those species with large enough yields to be considered problematic do not, in general, have a large cross section for fast neutrons. This simplification is considered conservative because the capture of a neutron by one of the species under study would tend to result in the production of either a stable nucleus, another radioactive nucleus of similar decay constant, or a nucleus with a very short half life, which would tend to decay away before reaching the end of the vent path. In short, the capture of neutrons by fission products would have the overall effect of decreasing the radiological hazard of the fission products.

3.2 Diffusion to Gap

The representation of the motion of gas atoms through the fuel and into the gap between the fuel and the cladding is the most difficult concept in the modeling of vented fuel. This diffusion relies on a number of complex and interacting mechanisms relying on fuel composition, temperature, irradiation history, and gas atom identity. While the treatment of fission gas migration originally relied upon classical diffusion theory, it was eventually discovered that the polycrystalline structure of fuel causes gases to move in a non-classical manner through the microstructure of the fuel. Also, though it was originally believed that gases moved through the fuel as individual atoms, it was later found that clusters or bubbles of like atoms actually dominate gas transport [Olander,1974]. This occurs because of the insolubility of the gas atoms in the fuel matrix. These bubbles migrate to the grain boundaries, corners and edges of the fuel, because of the lower stresses in these areas. The gas is released from these bubbles when a saturation condition has been reached [Long, 2002]. This saturation condition is given by

$$N_s = \left(\frac{4rF(\theta)V_c}{3k_B T \sin^2 \theta} \right) \left(\frac{2\gamma}{r} + P_{ext} \right), \qquad (3.2)$$

where θ = dihedral half angle, radians

k_B = Boltzmann constant, J/K

γ = surface tension, N/m

V_c = critical area coverage fraction

r = bubble radius, m

$F(\theta) = 1\text{-}1.5\cos\theta + 0.5\cos^3\theta$

P_{ext} = external pressure on bubbles, atm

T = temperature, K.

However, as this calculation is somewhat cumbersome, engineers generally rely on one of a few approximations for the fraction of gas released from the fuel. The first [Turnbull, 1982] is given by

$$R/B = \left(s/v \right) \left(\frac{\bar{D}}{\lambda} \right)^{1/2}, \qquad (3.3)$$

where R/B = release rate/birth rate, dimensionless

s/v = equivalent sphere size, relating surface area to volume for non-spherical fuel grain, cm

D = diffusion coefficient, averaged over radius of fuel, cm^2/s

λ = decay constant of isotope, s^{-1}.

While this equation would otherwise be very useful, it is problematic because the quantity s/v is strongly dependent not only on fuel makeup, but on burnup. To date, there is little experimental data relating grain size to burnup for TRU-O_2. Therefore, it was deemed advantageous to proceed with another approximation of release fraction, which also incorporates burnup dependence, but in a different manner. This approximation [Waltar, 1981] is given as

$$F_r = 1 - \frac{4.7}{B}\left(1 - e^{-B/5.9}\right), \qquad (3.4)$$

for restructured fuel, and

$$F_u = 1 - \frac{25.6}{B-3.5}\left[1 - e^{-(B/3.5-1)}\right]e^{-0.0125x}F'(B),$$
$$F'(B) = 1 (B < 49.2) \qquad (3.5)$$
$$F'(B) = e^{-0.3(B-49.2)} (B > 49.2)$$

for unrestructured fuel. In these equations, B represents burnup in MWD/kg and x represents the local linear power density in kW/m. At the high power density and high burnup at which the GFR operates, the ultimate release fractions are essentially equal to unity, as shown in figure 1. Therefore, in the present work, for conservatism, all fission gases are assumed to escape from the fuel instantaneously.

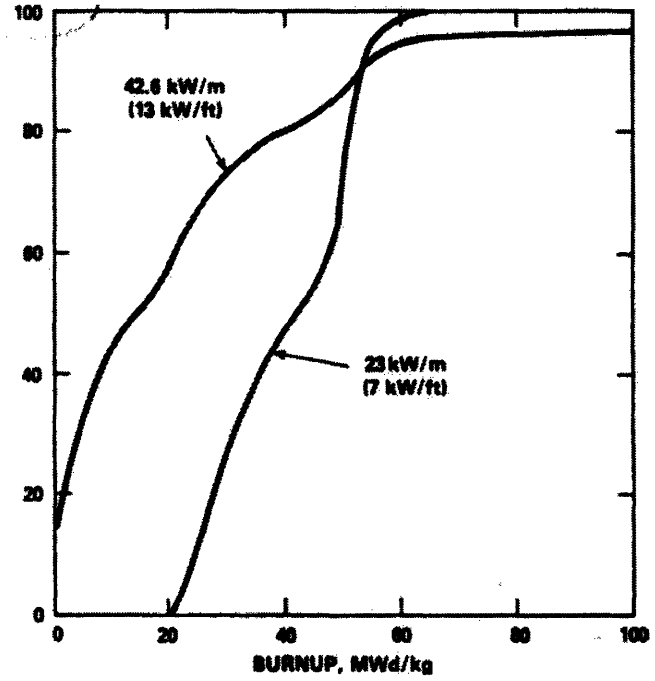

Figure 3.1: Fission Gas Release vs. Burnup [Waltar,1981]

3.2.1 Recoil and Knockout

While gaseous fission products tend to arrive in the fuel-cladding gap by the processes described in the previous section, there are other means by which fission products, gaseous and otherwise, may leave the fuel. The first, recoil, pertains mostly to gas atoms, but may also result in the release of small quantities of other species. Recoil describes the direct flight of an atom from the fuel surface while it is still an energetic fission fragment. Because fission fragments tend to lose energy quickly through interaction with their surroundings, recoil generally only causes release of fission

products from the fuel when the fission event takes place within a few microns of the fuel surface. Another means by which fission products escape from fuel is knockout. In knockout, a stationary atom near the surface of the fuel is imparted energy by either interaction with an energetic fission fragment, a neutron, or by a fission spike. Because the release fraction of fission gases is assumed to be equal to unity due to the high burnup of the fuel, no corrective addition has been made for release by recoil and knockout, as such a correction would clearly be bounded by the assumption of 100% instantaneous gas release.

3.3 Transport to Plenum

After their escape from the fuel, the fission products undergo diffusion governed by both concentration gradients and the temperature gradients of their surroundings. While classical diffusion, in which concentration gradients dictate the motion of the particles, tends to dominate transport in this situation, both modes of diffusion are discussed here for completeness. It should be noted that although the fission products must diffuse through the titanium upper axial reflector and boron carbide shield in order to reach the upper axial plenum, the presence of both materials is at present neglected for the sake of conservatism in estimates of fission product release.

3.3.1 Atomic Diffusion

Diffusion along a concentration gradient is often expressed in terms of the concentration at a particular location and time after a pulse injection of the species of interest. The relationship commonly used for this pulse insertion of atoms is [Cussler, 1984]

$$C(x,t) = \frac{1}{2}\frac{e^{-x^2/4Dt-\lambda t}}{\sqrt{4\pi Dt}}(M/A), \qquad (3.6)$$

where C(x,t) = concentration at location x and time t, g/cm^3

M/A= initial mass injected over area, g/cm^2

D = diffusion coefficient of host material, cm^2/s

λ = decay constant, s^{-1}.

The factor of ½ is present because when the pulse is introduced to the gap, the diffusing species can travel either up to the plenum or down towards the lower axial reflector. If mirror boundary conditions are put into effect at the lower axial reflector, the end result is

that all stable or long-lived products will eventually diffuse to the plenum, albeit after undergoing some additional decay due to the effective extension of the vent path. In the present work, this contribution is neglected in favor of the assumption that all products diffuse immediately upward to the upper axial plenum, effectively changing the ½ coefficient to unity. This modification is in the interest of conservatism.

As steady state power generation continually increases the amount of product available for diffusion and injects these atoms at a variety of distances from the plenum, this relationship must be modified to account for what is essentially an infinite number of pulses distributed over a range of locations.

As the concentration at each point in space within the assembly is of little interest in this problem, the rearrangement of the previous equations can be simplified by "counting" the atoms which arrive in the plenum at each step in time. The best way to do this is to simply determine how much product is inserted into the diffusion path, calculate its contribution to the plenum inlet current, J (which is found using Fick's law), at each point in time subsequent to emission of the gas from the fuel, and sum these values for each point in time. This can be expressed as

$$J_{plenum}(x,\tau) = \frac{1}{4\sqrt{\pi D}} \int_0^{\tau} \frac{x e^{-z^2-\lambda t}}{t^{3/2}} R dt \quad \text{in which} \qquad (3.7)$$

$$z = \frac{x}{2\sqrt{Dt}},$$

Where x = distance from production site to plenum

R=nuclide production rate, atoms/s

D = diffusion coefficient of vent gas, cm^2/s

t = time after release from fuel, s

τ = operating time of reactor, s.

This integral is then effectively the sum of contributions from each possible time after emission. The equation cannot be solved analytically, but can be easily adapted into a computer program which can approximate the sum. Alternatively, the integral can be evaluated as t approaches infinity, yielding an effective upper limit on the current at any particular location. The resulting equation

$$J_{\infty}(x) = \frac{1}{2} e^{-\sqrt{\frac{\lambda}{D}}x} \cdot R \qquad (3.8)$$

is highly useful as an estimate of steady state current over long operating cycles. Its importance becomes apparent when it is used to derive an equation describing steady state fission product population in the coolant.

3.3.2 Thermal Diffusion

An additional influence on the transport of radionuclides along the vent path is thermal diffusion, which in liquids is known as the Ludwig-Soret effect. As temperature of the fuel assembly varies with axial position, so too does temperature inside the vent tube. This imposed temperature gradient gives rise to a diffusion current which can be either parallel or anti-parallel to the gradient. For gases, the effect is generally described by the equation [Cussler, 1984]

$$-j_1 = Dc\left(\alpha x_1 x_2 \frac{\nabla T}{T}\right), \qquad (3.9)$$

Where j = flux, #/cm^2·s,

D = diffusion coefficient, cm^2/s

x = mole fraction of species

α = thermal diffusion factor

T = temperature, K.

As can be seen from the equation, the resulting flux is very small for dilute solutions of the diffusing species, that is, when x_1 is small compared with x_2. It is assumed that most species present in the vent system will be very dilute due to their short half lives and the presence of large quantities of CO_2. This prediction will be further discussed in later chapters. For the majority of species, thermal diffusion is expected to provide only a small contribution to the overall rate of flow of radionuclides [Satterfield, 1970]. Thus, in the present work, thermal diffusion is neglected.

3.4 Diffusion to Primary Coolant

After arrival in the plenum, the gas atoms then diffuse through a long vent tube, in order to increase the holdup time, and hence reduce the activity of the material, before it

is vented to the coolant. It is possible, after calculating the plenum influx at each point in time, to determine the amount of product reaching the end of the diffusion path at any time. The current at the end of the diffusion path is determined by using equation 3.7, but replacing the production rate with the rate of influx into the plenum: in essence, the rate at which nuclides enter the second stage of the diffusion path. It is, however, also important to know the cumulative quantity of each product which reaches the end of the diffusion path, especially in the case of venting directly to coolant, where this quantity will represent the total coolant inventory of the nuclide in question. This quantity is determined using the formula

$$C_{out}(t) = \int_0^t J_{out}(\tau) \cdot e^{-\lambda(t-\tau)} dt \qquad (3.10)$$

Where τ = time of arrival at outlet, s

t = time of measurement, s

$J_{out}(\tau)$ = outlet current, atoms/cm^2·s.

It is important to note when using these equations that the equations defining current at each time do not take into account holdup outside the vent tube. This means that because the equations do not include holdup time within the plena or within the upper axial reflector, they provide a conservative estimate of the activity present at the end of the vent tube.

3.4.1 Plenum Holdup

Because of the relatively large volume of the plena relative to the volumes of the vent tubes, and their unusual geometry, it is difficult to mathematically describe transport of radionuclides through them. However, it is possible to use the same expressions developed above to describe the current of fission products exiting a plenum when a simple correction factor is applied. This correction factor stems from the fact that when previous analysis neglected the plena, the population of fission products was effectively restricted to a small fraction of the true available volume. For example, if an assembly has two 2000 cc plena and six 100 cc vent tubes (three downflow, three upflow), the true volume available to the diffusing fission products is 4600/600, or 7.7 times that of the vent tubes alone. This same factor, or a similar factor taking into account differences in

geometry, can be multiplied by the length of the vent path (when plena are neglected) to obtain a longer "effective" path length which takes into account holdup in the plena. The equivalent "length" of each of the plena is then found by multiplying the total effective path length by the fraction of the total volume taken up by the plenum. For example, a single 1000 cc plenum results in a total effective path length of 667 cm. By multiplying this by 1000/1300, the ratio of the plenum volume to the total volume, an equivalent plenum path length is calculated as 513 cm. By performing a similar calculation for a 2000 cc plenum, the equivalent plenum length is found to be twice the value for a 1000 cc plenum, 1026 cm.

The knowledge of the equivalent length of each plenum is important because it allows the determination of the contents of each plenum. By recognizing that the difference between the flow into the plenum's entrance and flow out of the plenum's exit is stored in the plenum, less the quantity of nuclides which decay during transit across the plenum, it is possible to write the change in the plenum inventory as

$$\frac{dN}{dt} = J(x_{in}) - J(x_{out}) - \lambda N, \qquad (3.11)$$

Where $J(x_{in})$ = the current into the plenum at its entrance, atoms/s

$J(x_{out})$ = the current out of the plenum, atoms/s

λ = decay constant, s^{-1}

N = plenum inventory, atoms.

By using this relationship in an iterative computational approach, the amount of a nuclide in residence in each plenum can be calculated with time. This calculation will become of great importance in chapter 7, where the consequences of a vent system blowdown to atmospheric pressure will be addressed.

It should be noted that this correction assumes slug flow of the diffusing species instead of perfect mixing in the plena. Laminar/slug flow through the plena is fostered by filling the plena with steel or ceramic wool, which takes up only 2% of the plenum volume but forces the enclosed gas to follow a restricted flow path. It is recommended that the validity of this assumption be tested during irradiation of a mock fuel assembly.

3.5 Modeling of Diffusion Coefficients

Because of the low concentrations of fission products in the background CO_2, the influence of one fission product on the transport of another is minimal. For this reason, the transport of fission products is treated as diffusion in a binary mixture. In addition, the transport is treated as laminar flow rather than turbulent mixing. It has been suggested that mechanical vibration of the fuel assemblies could lead to mixing of the gases, increasing the diffusion velocity of many fission products. However, because great effort is generally taken to avoid mechanical vibration of the assemblies, thereby reducing the likelihood of fretting or other serious problems, the effect of mechanical vibration on the diffusion coefficients of fission gases is neglected.

Traditionally, the values for diffusion coefficients in a binary mixture are given at standard temperature and pressure, and are determined at other conditions through the relation

$$D_{AB} = D_o\left(\frac{T}{T_o}\right)^{3/2}\left(\frac{P_o}{P}\right), \qquad (3.12)$$

Where D_o = the value of the diffusion coefficient for the pair of gases in reference state (typically STP),

T_o = reference temperature, K

T = temperature of interest, K

P_o = reference pressure, Pa

P = pressure of interest, Pa.

This simple equation demonstrates a particularly strong effect of pressure in reducing diffusion in binary gases, which is especially important in the present application. However, the true value of the diffusion coefficient for a particular species in the vent tube is unlikely to actually obey this rule. First, this equation is based on the classical kinetic theory of gases. Experimental measurements actually show that the exponent on the temperature ratio should be closer to 1.75 than 1.5. Second, some sources describe a breakdown in the application of this equation near the critical point of the gas. Since the GFR operates with supercritical CO_2, it is reasonable to question whether the equation given above may not satisfactorily describe diffusion under the conditions present in the

reactor. Cussler gives another equation intended to describe the change in the diffusion coefficient above the critical point

$$\rho D = \rho_o D_o, \qquad (3.13)$$

Where ρ_o and D_o are the reference density and diffusion coefficient, and ρ and D are the density and diffusion coefficient at the desired pressure, and same temperature as in the reference case. If supercritical CO_2 is taken to obey the ideal gas law, then for $D_o = 0.043$ cm^2/s, the diffusion coefficient at 650 degrees C and 20 MPa is calculated as approximately 0.00068 cm^2/s.

This result is much lower than estimates from other sources, and so for the sake of conservatism, a different model for D has been selected. The Lennard-Jones model [Satterfield, 1970] gives the diffusion coefficient for a binary gas as

$$D = \frac{0.00158T^{3/2}\left[(M_1 + M_2)/M_1M_2\right]^{1/2}}{P\sigma_{12}{}^2\Omega_p}, \qquad (3.14)$$

where T = Kelvin temperature of gas

M_1, M_2 = Molar mass of constituent, 44 for CO2 and 85 for 85Kr

P = pressure of gas, atm

σ_{12}= Lennard-Jones force constant, 3.941 Angstrom, from tabulated data

Ω = collision integral, 0.8530, from tabulated data.

This formula gives a value of 0.0037 cm^2/s as the diffusion coefficient for a binary mixture of CO_2 and ^{85}Kr (the next most dominant component in the mixture, as established in later chapters) at 650 degrees C and 20 MPa. Because this value is the highest, and therefore most conservative, this value will be used in all of the calculations which follow. The value also corresponds most closely with the experimental value of 0.001522 cm^2/s at 35 °C and 5.789 MPa [Durbin, 1962]. When this experimental data is used in conjunction with the pressure-temperature relation, the resulting value for the diffusion coefficient is 0.0030 cm^2/s. For the sake of comparison, the values calculated using each of the models described are summarized below.

Table 3.2: Summary of Diffusion Coefficient Calculation

Method	Diffusion Coefficient (cm^2/s)
Temperature-Pressure Relation	0.0020
Proportional Density	0.00068
Lennard-Jones	0.0037

The selected value of the diffusion coefficient, while chosen to be conservatively large, is still a great deal smaller than diffusion coefficients for systems which have previously used vented fuels. For example, the GA GCFR released fission products to helium at 7 MPa, and accordingly allowed the diffusion of fission products at a much higher rate.

3.6 Summary

This chapter has summarized the models selected to describe the production and transport of radionuclides through the vent system and into the primary coolant. In the next chapter, these relationships will be important in determining which fission products will be present outside the assembly in large quantities. In a later chapter, this information will be used in the establishment of requirements for coolant purification.

It should be recalled that this chapter has outlined conservative models for each step of the fission product transport process. Transmutation of radionuclides through neutron absorption has been neglected, and 100% of the nuclides produced in the fuel are assumed to be released to the fuel-clad gap instantaneously, even at low burnup. Thermal diffusion, which causes an overall reduction in the forward motion of the diffusing species, has been neglected. Finally, a variety of models for the diffusion coefficient of the mixture present in the vent system have been analyzed, with the largest predicted value being used in the calculations in the following chapters.

Chapter 4: Identification of Potentially Troublesome Nuclides

4.0 Introduction

This chapter introduces the nuclides which were selected as problematic due to their high yields in fission, radioactivity, or volatility. Additionally, the presence of daughter and granddaughter nuclides through radioactive decay of fission products is addressed. Methods for elimination of species from the list of isotopes of concern are addressed, and a final set of nuclides is identified which must be handled by the coolant purification system.

4.1 Preliminary Criteria

In order to determine both the positive aspects and risks associated with venting of fuel in a nuclear power system, it was first necessary to determine which species would make their way into the vent tube, and which will have to be handled carefully due to their radioactive or volatile nature. Figure 4.1 identifies the chemical species of concern, based on their chemical properties and significant yield in fission, as shown in figure 4.2. Of particular interest in venting are the noble gases, which tend in non-vented fuel assemblies to accumulate in fuel pins in large quantities, increasing the strain on the fuel's cladding and degrading heat transfer to the coolant. The noble gases have also historically been analyzed in vented fuel studies due to the activity levels which they induce by virtue of their yields and great mobility within the fuel matrix [Gee,1969]. A group of similar concern is the halogens, Br and I, which also diffuse easily into the vent path due to the mobility lent by their gaseous form, and may beta decay to form additional noble gas atoms. Other groups which must be considered are the alkali metals, Rb and Cs, and the alkali earth metals, Sr and Ba. The transport of both cesium and iodine in vented fuel reactors has been investigated in depth due to the large yields of many isotopes of each [Campana, 1974]. Although these metals are far less mobile than the gas species under study, they are chemically volatile, and must be handled with caution should any quantity of them migrate into the vent system. In addition, Se and Te

are both considered because they have historically been found to attack cladding and structural materials [Hofmann, 1981].

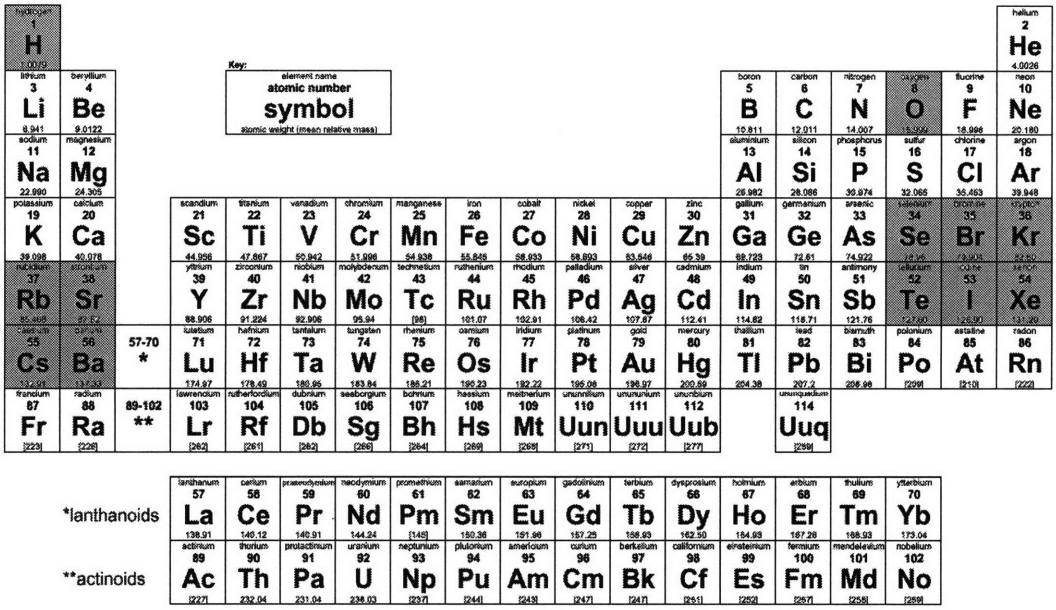

Figure 4.1: Periodic Table of the Elements, Showing Elements Included in Study (shaded)

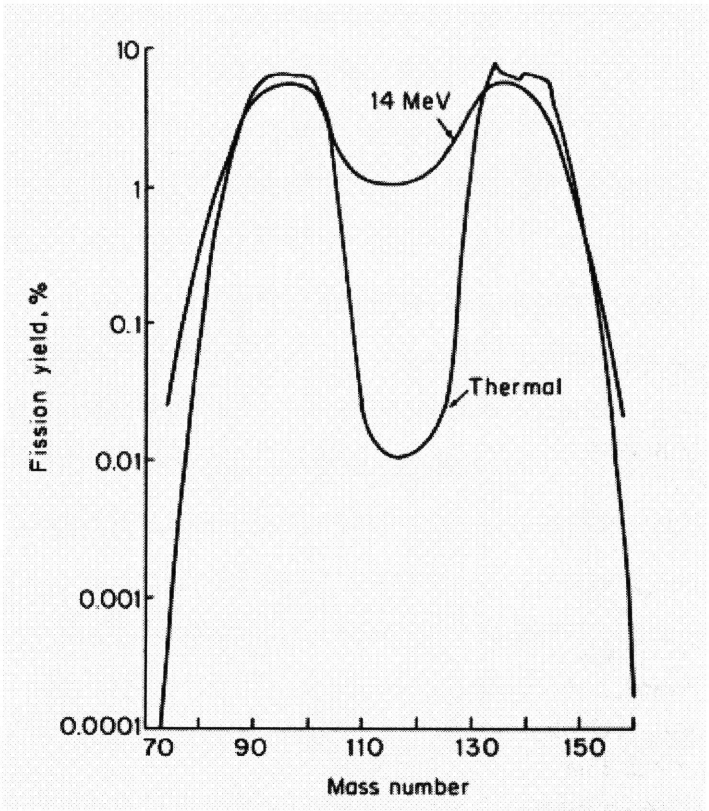

Figure 4.2:Fission Yield vs. Mass Number [Lamarsh,1966]

Only two additional elements, oxygen and hydrogen, were added to the study with these other groups. These are the only elements not included in the previously listed groups which are present in a gaseous state under most conditions. Oxygen is also included because it is present in UO_2 fuel and CO_2 coolant and reacts with many other species which have been included in the study, leading to questions about the formation of solid product in the vent tube. It is also the source of ^{16}N, which has been shown in prior studies to dominate coolant activity at full power [Wang, 2005].

Hydrogen, in the form of tritium, is in particular interest in this study because it is the byproduct of ternary fission. It is also produced by boron in control rods. In addition, it is known to diffuse through steels, making it less likely to be held up by the vent system [Chen, 1998]. However, experience has shown that this diffusion is strongly dependent on the nature of the steel's surface, and that treatment of the steel's surface can result in greatly retarded transport of tritium [Kalin, 1998]. For this reason, it is assumed that the tritium produced in the assemblies can be handled by the same venting process as that used for other nuclides. Even if a significant amount of the tritium produced in fission does diffuse through the fuel's cladding and directly into the primary coolant, rather than experiencing holdup in the vent path, it is expected that it will quickly react with CO_2 to form tritiated water, which allows for the tritium to be quite simply removed from the gas stream by the primary coolant purification system. This occurrence will be discussed in further detail in chapter 5.

Except in the event of failed fuel pins, experiments have shown that rarely do species other than those listed above diffuse out of fuel elements. In fact, it has been demonstrated that the majority of the gas molecules of interest remain frozen in place in the fuel matrix at temperatures lower than 1300 K [Olander, 1974], and so a study of the motion of less mobile species is outside the scope of the current work. Still, even discounting the many nuclides which are unlikely to enter the vent system, a long list of isotopes are left to be individually studied. However, many of these isotopes have half-lives short enough that they would be unlikely to leave the fuel before decay, let alone survive the lengthy holdup time induced by the vent tube. In this light, a rough estimation of holdup time was calculated, assuming that a pulse of nuclides would diffuse to the

opposite end of the vent tube to reach a peak concentration at a time approximately equal to the "holdup time" necessary to diffuse from one end of the tube to the other. This approximation was done using ^{133}Xe, because the results of prior experiments have documented that this nuclide generally survives the venting process [Campana, 1974]. From equation 3.6, the time of peak concentration during diffusion can be derived as

$$\hat{t} = \frac{x}{2\sqrt{\lambda D}}, \qquad (4.1)$$

where

x = length of diffusion path, here taken as the minimum likely value, 200 cm

λ = decay constant of nuclide, 5.508×10^{-3} h^{-1}

D = diffusion coefficient in CO_2 at 20 MPa, 0.0037 cm^2/s, from Chapter 3,

The resulting peak concentration for a pulse of ^{133}Xe occurs at 385 hours. This time also corresponds to the time of the peak current at location x due to the original pulse.

After this calculation was made, several hundred short-lived isotopes were eliminated from the study. As a result, no isotope with a half life shorter than nine hours was included, as it is usually acceptable when dealing with radioactive isotopes to neglect quantities of isotopes which have undergone ten or more half lives before assessment. In addition, the nine-hour mark represented a significant break in the half lives, i.e. the half lives of the eliminated species were on the order of only a few minutes or seconds, and would thus decay on a much shorter time scale than that of the nuclides under study. Also neglected are nuclides which would appear only due to (n,γ), (n,p), (n,α) or (n,2n) reactions, as the majority of the fission products of present interest have low cross sections for neutron absorption.

In previous assessments of the quantity of fission gases removed by the vent pathway, researchers have traditionally neglected the quantities of stable or very long-lived nuclides, citing their lack of radiological consequence. However, because it is within the scope of this project to determine the total quantity of gases vented, and especially to quantify the amount of chemically volatile species present, numerous stable and near-stable species will be included in the study. All of the isotopes of interest are listed in tables 4.1-4.4. Half-life values cited are from the Chart of the Nuclides [KAPL, 2002].

Table 4.1: Medium Half-life Nuclides of Present Interest

Nuclide	Half Life	Nuclide	Half Life
^{3}H	12.32 y	^{129m}Te	33.6 d
^{75}Se	119.79 d	^{131m}Te	30 h
^{82}Br	35.3 h	^{132}Te	3.204 d
^{85}Kr	10.76 y	^{125}Xe	16.9 h
^{83}Rb	86.2 d	^{127}Xe	36.4 d
^{84}Rb	32.9 d	^{133}Xe	5.243 d
^{86}Rb	18.65 d	^{135}Xe	9.1 h
^{83}Sr	32.41 h	^{129}Cs	1.336 d
^{85}Sr	64.84 d	^{131}Cs	9.69 d
^{123}I	13.2 h	^{132}Cs	6.48 d
^{124}I	4.176 d	^{134}Cs	2.065 y
^{125}I	59.4 d	^{136}Cs	13.16 d
^{126}I	13.0 d	^{137}Cs	30.07 y
^{130}I	12.36 h	^{131}Ba	11.5 d
^{131}I	8.02 d	^{133}Ba	10.51 y
^{133}I	20.8 h	^{140}Ba	12.75 d

Table 4.2:Long Lived Nuclides of Present Interest

Nuclide	Half Life (y)
^{81}Kr	$2.3x10^{5}$
^{129}I	$1.57x10^{7}$
^{135}Cs	$2.3x10^{6}$

Table 4.3:Stable Volatile Species of Present Interest

^{78}Se	^{128}Te
^{79}Se	^{130}Te
^{80}Se	^{136}Xe
^{82}Se	^{132}Ba
^{81}Br	^{134}Ba
^{84}Sr	^{135}Ba
^{86}Sr	^{136}Ba
^{123}Te	^{137}Ba
^{124}Te	^{138}Ba
^{125}Te	^{133}Cs
^{126}Te	

Table 4.4: Noble Gas Daughters of Fission Product Chains*

Isotope	Half life	Reason for Concern
^{75}As	Stable	Daughter of ^{75}Se (β)
^{82}Kr	Stable	Daughter of ^{82}Br(ε)
^{83}Kr	Stable	Daughter of ^{83}Rb (ε)
^{84}Kr	Stable	Daughter of ^{84}Rb (ε)
^{86}Kr	Stable	Daughter of ^{86}Rb (ε)
^{126}Xe	Stable	Daughter of ^{126}I (β)
^{129}Xe	Stable	Daughter of ^{129}I (β)
^{130}Xe	Stable	Daughter of ^{130}I (β)
^{131}Xe	Stable	Daughter of ^{131}I (β)
^{132}Xe	Stable	Daughter of ^{132}Cs (ε)

β indicates decay by β- emission, ε indicates decay by electron capture.

4.1.1 Decay Chains

All of the nuclides included in the study are either the stable product of a long radioactive decay chain, or are otherwise an integral part of such a chain. For this reason, it was deemed prudent to include daughters of the nuclides listed above which are stable. This list of additional isotopes turns out to be quite short, as many of the isotopes have parents and daughters which are already included in one of the previously named groups for study. In the case of those isotopes which are produced through decay in a near-instantaneous fashion, their quantities were approximated by using accumulated fission yields rather than the independent fission yields typically used. The usual method of accounting for production by decay of a parent would be to include a term for the activity of the parent in the differential equation describing change in quantity of the nuclide with time. This results in a lengthy equation which can be easily approximated by the technique described above when the daughter has a much longer half life than the parent. However, those parent and daughter nuclides which do survive the time necessary to diffuse through the vent tube should be included in the study, as the parents significantly influence the quantities of the other nuclides of interest which are present, and the daughters must be added to the list of long-lived isotopes to be handled upon collection from the vent tube.

4.1.2 Code Outputs

In order to confirm that all species which could potentially be problematic due to radioactivity or volatility were included in the list of isotopes for investigation, the list generated to this point was checked against the output of a previously run depletion analysis. This analysis was performed using the state-of-the-art code BGCore, for a fast spectrum TRU-O_2 fueled reactor with similar burnup characteristics to the GFR reference core [Shwageraus, 2006]. Because BGCore combines Monte Carlo analysis with decay chain data, it is has been used at MIT to determine the core inventories of roughly 1700 individual fission products produced through fission, decay, and capture reactions. While the code output cannot exactly reflect the post-irradiation makeup of the GFR core, it can serve as a rough check to make sure that all nuclides of concern have been included. Comparison between this code output and the previously listed species revealed only one significant omission: the metastable states of several nuclides. Thus these metastable states, ^{125m}Te, ^{129m}Te, and ^{131m}Te were included in the present investigation for the sake of completeness.

In addition to identifying these species for analysis, the output of BGCore was also used to predict the end of lifetime quantity of ^{85}Kr which would be present in a 2400 MW^{th} reactor at the end of a 6700 day irradiation period, in hopes of using this as a check on the output of the MATLAB code and all further hand calculations. The BGCore output of ^{85}Kr from the above mentioned TRU-O_2 core was predicted to be 4.139×10^{25} atoms at the end of the 1800 EFPD operating cycle. When corrected for differences in burnup and fuel composition, this corresponded to a predicted value of 2.86×10^{26} atoms for the GFR after 6700 EFPD.

4.2 Preliminary Elimination

4.2.1 Methodology for Preliminary Elimination

Using the models developed for fission gas transport in Chapter 3, a MATLAB script and functions (see Appendix B) were developed which predicted the rate at which quantities of a chain of fission products made it to a single plenum located in the top of the assembly (as shown in fig. 2.4), and the cumulative quantities of a chain of fission products which arrived at the end of the diffusion path, represented as a tube leading

away from the top of the assembly. Because the MATLAB code does not allow for direct modeling of holdup within a plenum, a simple correction is made. The vent tubes each have an interior volume of 100 cc, much smaller than the total volume presented to the gas by the combination of vent tubes and plena. The corrective step is therefore to represent the plena as vent tubes of equivalent volume. This correction can be expressed as

$$x_{eff} = \frac{V_p + V_t}{V_t} x \qquad (4.1)$$

Where x = the path length of the vent tubes alone, cm

V_p = the total volume of all plena in the system, cc

V_t = the total volume of all vent tubes in the system, cc

x_{eff} = the effective path length of the configuration, cm.

For the preliminary run of the code, the system is treated as a single 1000 cc plenum attached to three vent tubes. Because the total volume available is 1300 cc (representing plenum and three downflow tubes), the 154 cm path length of a single tube is multiplied by 4.33, the ratio of the available volume to the volume represented in MATLAB. The resulting effective vent path length is about 667 cm.

The inputs for the code included data about the nuclide chain under study, as well as the power rating of the reactor and the duration of its full power operation, the combination of which is enough to fully determine the yields of the isotopes in this simple calculation. For the results presented here, the power rating used was 2400 MWth, and the lifetime of the fuel was 6700 days, corresponding to 18.36 effective full power years [Handwerk, 2006]. The probability of release of all isotopes from the fuel itself was assumed to be 1, as discussed in Chapter 3. For the present investigation, the JEFF 3.1 fast fission yields from 235U were used for each nuclide, as these gave the most conservative estimates of noble gas production, particularly in the case of ^{85}Kr.

The MATLAB script and functions may be found in Appendix B. As a result of the calculations performed using this code, the maximum activity release for the entire core due to each radionuclide was determined. In all cases, this time of maximum activity occurred at the end of the fuel lifetime. An example plot of cumulative isotopic outputs is

shown in Figure 4.1. The vertical axis of the plot gives the total number of atoms present at time t.

4.2.2 Hand Calculation of ^{85}Kr Production

In order to confirm the validity of the computer model in calculating coolant inventories of radionuclides, a simple hand calculation was performed. This was most easily done by computing the number of nuclides produced during a long irradiation period:

$$N(t) = \frac{R}{\lambda}\left(1 - e^{-\lambda t}\right), \qquad (4.2)$$

Where R = radionuclide production rate, fission rate multiplied by yield, s^{-1}.
This equation represents the total primary coolant inventory without purification and with a vent path length of zero. This hand calculation is best performed with ^{85}Kr because it has been shown in previous work to survive the venting process. Using the 10.76 year half life, the JEFF-3.1 yield in fission of 0.013 and a reaction rate of 6.48×10^{24} fissions per day for a 2400 MWth reactor, the ^{85}Kr inventory at the end of the 6700 day operating cycle is 3.2×10^{26} atoms (a difference of 11% from the value predicted by BGCore), or approximately 17.7 MCi. This figure is nearly twice the coolant inventory activity calculated by the MATLAB code, but this can be attributed to the slow transport of the gas atoms along the vent path; many of the atoms produced do not reach the primary coolant until long after the reactor has been shut down. This hypothesis was confirmed by modifying the MATLAB code to record the portion of each pulse which did not leave the fuel element by the end of the 6700 day operating cycle. When the total end-of-lifetime fuel inventory was summed with the total end-of-lifetime primary coolant inventory, the resulting value deviated from the expected activity of 17.7 MCi by less than 1%. This error is likely the result of inaccuracies in the calculational techniques.

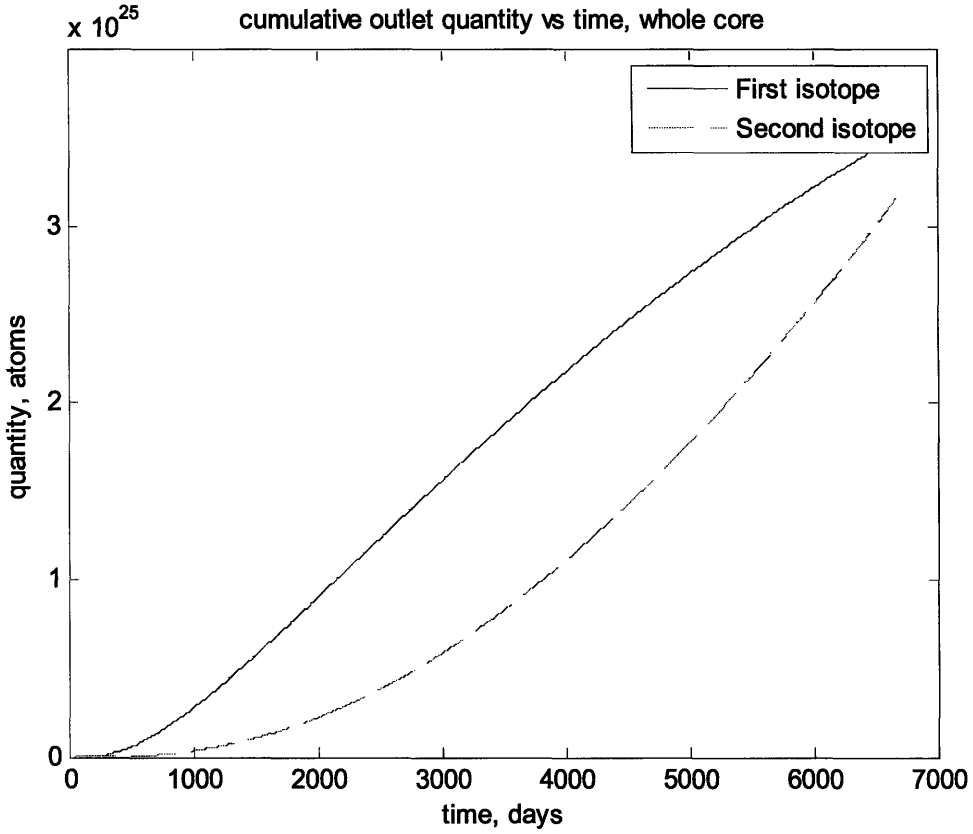

Figure 4.3:Cumulative Output Levels due to Kr-85 (first isotope)and Rb-85 (second isotope) Over Lifetime of Reactor for Full Core

4.2.3 Results of Initial Elimination

Upon calculation of the output quantities of the isotopes studied, it became clear that many would not yield even a single atom at the outlet of the 667 cm vent path. These isotopes are shaded in dark gray in table 4.5. Many others demonstrated high yields, but were stable and thus did not present a radiation hazard. These isotopes are shaded in light gray in table 4.5. As can be seen in table 4.6, those radioactive isotopes which did survive the venting process in significant quantities often resulted in only small activities by virtue of their lengthy half lives, by which they survived the vent tube in the first place. Note that some of the nuclides will be immobilized by formation of non-volatile chemical species, or by deposition onto steel surfaces, as discussed further in chapter 5.

Table 4.5: Quantities of Products Accumulated at End of 667 cm Vent Path at End of Fuel Lifetime

Isotope	Output (atoms)	Isotope	Output (atoms)
^{3}H	1.434×10^{24}	^{127}Xe	1.321×10^{15}
^{75}Se	2.165×10^{11}	^{127}I	2.575×10^{19}
^{75}As	4.448×10^{17}	^{128}Te	1.128×10^{26}
^{78}Se	4.681×10^{24}	^{129m}Te	3.819×10^{21}
^{79}Se	1.053×10^{25}	^{129}I	1.105×10^{26}
^{80}Se	2.317×10^{25}	^{129}Xe	1.417×10^{19}
^{82}Se	8.895×10^{25}	^{130}I	0
^{79}Br	5.852×10^{21}	^{130}Xe	3.394×10^{22}
^{81}Kr	1.475×10^{17}	^{130}Te	5.150×10^{26}
^{81}Br	3.113×10^{21}	^{131}I	1.857×10^{19}
^{82}Br	1.114×10^{8}	^{131}Xe	7.958×10^{26}
^{82}Kr	1.014×10^{23}	^{131}Ba	1.613×10^{10}
^{83}Sr	220	^{131}Cs	1.973×10^{10}
^{83}Rb	6.541×10^{14}	^{131m}Te	5.919×10^{10}
^{83}Kr	1.188×10^{21}	^{132}Te	1.345×10^{16}
^{84}Rb	6.329×10^{5}	^{132}Cs	1.190×10^{16}
^{84}Kr	6.554×10^{22}	^{132}Xe	1.084×10^{27}
^{84}Sr	4.891×10^{18}	^{133}I	4.033×10^{8}
^{85}Kr	1.540×10^{26}	^{133}Xe	1.563×10^{18}
^{85}Rb	3.168×10^{25}	^{133}Cs	1.700×10^{27}
^{86}Rb	5.183×10^{16}	^{134}Cs	5.654×10^{20}
^{86}Sr	1.779×10^{22}	^{134}Ba	5.989×10^{21}
^{86}Kr	1.780×10^{19}	^{135}Xe	0
^{123}Te	1.779×10^{17}	^{135}Cs	1.475×10^{27}
^{124}Te	3.160×10^{22}	^{135}Ba	1.409×10^{21}
^{125}Xe	0	^{136}Cs	1.254×10^{18}
^{125}I	4.848×10^{13}	^{136}Ba	2.575×10^{24}
^{125}Te	1.359×10^{20}	^{137}Cs	1.084×10^{27}
^{126}I	1.586×10^{12}	^{137}Ba	2.952×10^{26}
^{126}Te	2.313×10^{22}	^{138}Ba	1.521×10^{27}
^{126}Xe	3.504×10^{18}	^{140}Ba	6.670×10^{20}

The remaining radioactive nuclides introduce the coolant activities shown in table 4.6.

Table 4.6: End of Lifetime Output Activities, 667 cm

Isotope	Activity (Ci)
^{3}H	68900
^{75}Se	3.92×10^{-7}
^{81}Kr	3.81×10^{-7}
^{82}Br	1.64×10^{-8}
^{83}Rb	1.65×10^{-3}
^{84}Rb	4.19×10^{-12}
^{85}Kr	8.50×10^{6}
^{86}Rb	0.603
^{125}I	1.77×10^{-4}
^{126}I	2.64×10^{-5}
^{127}Xe	7.86×10^{-3}
^{129}I	4.18
^{129m}Te	2.16×10^{4}
^{131m}Te	1.03×10^{-5}
^{131}I	502
^{131}Ba	3.04×10^{-7}
^{131}Cs	4.41×10^{-7}
^{132}Cs	0.399
^{132}Te	2.53×10^{-4}
^{133}I	1.01×10^{-7}
^{133}Xe	64.6
^{134}Cs	160
^{135}Cs	381
^{136}Cs	20.6
^{137}Cs	2.14×10^{7}
^{140}Ba	1.13×10^{4}

4.3 Methodology for Secondary Elimination

This list is still quite lengthy, and many of its members do not contribute a significant level of activity over the lifetime of the reactor. In order to determine which nuclides would present small enough activity levels to justify their exclusion, the end-of-lifetime coolant activity levels in table 4.6 were converted into the activity concentrations which would result if the entire coolant inventory were released into the 70,000 m^3 free volume of the containment structure [Pope, 2006] during a severe accident. These levels were then compared to the DAC limits prescribed by 10CFR20. Those nuclides which did not exceed their DAC limit at the end of lifetime, the time of maximum activity, and under this assumption of total release to the containment without purification, were deemed safe for exclusion from the study.

4.3.1 Results of Secondary Elimination

The containment activity concentrations and the DAC limits are shown in table 4.7 for comparison. The eliminated species are shaded. As can be seen, only fourteen nuclides remain for study: ^{3}H, ^{85}Kr, ^{86}Rb, ^{129}I, ^{131}I, ^{129m}Te, ^{131}Ba, ^{133}Xe, ^{132}Cs, ^{134}Cs, ^{135}Cs, ^{136}Cs, ^{137}Cs, and ^{140}Ba.

Table 4.7: Comparison of Containment Activities and DAC Limits for Hypothetical LOCA

Isotope	Specific Activity, μCi/mL	DAC Limit, μCi/mL
^{3}H	0.984	2×10^{-5}
^{75}Se	5.60×10^{-12}	3×10^{-7}
^{81}Kr	5.44×10^{-12}	7×10^{-4}
^{82}Br	2.34×10^{-13}	2×10^{-6}
^{83}Rb	2.36×10^{-8}	4×10^{-7}
^{84}Rb	5.99×10^{-17}	3×10^{-7}
^{85}Kr	27.7	1×10^{-4}
^{86}Rb	8.61×10^{-6}	3×10^{-7}
^{125}I	2.25×10^{-9}	3×10^{-8}
^{126}I	3.77×10^{-10}	1×10^{-8}
^{127}Xe	1.12×10^{-7}	1×10^{-5}
^{129}I	5.97×10^{-5}	4×10^{-9}
^{129m}Te	0.309	3×10^{-7}
^{131m}Te	1.47×10^{-10}	2×10^{-7}
^{131}I	7.17×10^{-3}	2×10^{-8}
^{131}Ba	4.34×10^{-12}	3×10^{-6}
^{132}Te	3.61×10^{-9}	9×10^{-8}
^{131}Cs	6.30×10^{-12}	1×10^{-5}
^{132}Cs	5.70×10^{-6}	2×10^{-6}
^{134}Cs	2.29×10^{-3}	4×10^{-8}
^{133}Xe	9.23×10^{-4}	1×10^{-4}
^{133}I	1.44×10^{-12}	1×10^{-7}
^{135}Cs	5.44×10^{-3}	5×10^{-7}
^{136}Cs	2.94×10^{-4}	3×10^{-7}
^{137}Cs	306	6×10^{-8}
^{140}Ba	0.161	6×10^{-7}

With this shorter list of nuclides in hand, the next step in the analysis was to calculate outlet quantities of the remaining nuclides for a range of potential vent paths. Six additional cases were set up for the purpose of comparison:

1. Single plenum, with a volume of 2000 cc
2. Two plena, both 1000 cc in volume
3. Two plena, with one 2000 cc in volume and one 1000 cc in volume

4. Three plena, all 1000 cc in volume
5. Three plena, with one 2000 cc in volume and two 1000 cc in volume
6. Three plena, with two 2000 cc in volume and one 1000 cc in volume.

These cases were investigated using the same approach described above for the 667 cm vent path. The coolant inventory levels of radioactive species determined as a result of these calculations are shown in the tables 4.8-4.13. For comparison, they are shown as total output quantities, and as activities.

Table 4.8: End-of-Life Radioisotope Coolant Inventory for 2000 cc plenum, x=1180 cm

Isotope	Coolant inventory, a	Activity (Ci)
^{3}H	8.518×10^{23}	40927
^{85}Kr	9.045×10^{25}	4.99×10^{6}
^{86}Rb	2.048×10^{14}	0.00238
^{129}I	1.468×10^{26}	5.55
^{131}I	4.037×10^{15}	0.109
^{129m}Te	5.708×10^{19}	368
^{131}Ba	1.478×10^{7}	2.79×10^{-10}
^{133}Xe	4.599×10^{13}	0.00190
^{132}Cs	1.516×10^{5}	5.08×10^{-12}
^{134}Cs	2.328×10^{20}	66.9
^{135}Cs	9.246×10^{26}	239
^{136}Cs	1.713×10^{17}	2.82
^{137}Cs	6.660×10^{26}	1.32×10^{7}
^{140}Ba	7.314×10^{17}	12.4

Table 4.9: End-of-Life Radioisotope Coolant Inventory for Two 1000 cc Plena, x=1333 cm

Isotope	Coolant inventory, a	Activity (Ci)
^{3}H	7.244×10^{23}	34849
^{85}Kr	7.669×10^{25}	4.23×10^{6}
^{86}Rb	3.931×10^{13}	4.57×10^{-4}
^{129}I	1.267×10^{25}	4.79
^{131}I	3.263×10^{14}	0.00882
^{129m}Te	1.669×10^{19}	108
^{131}Ba	1.817×10^{6}	3.44×10^{-11}
^{133}Xe	2.047×10^{12}	8.30×10^{-5}
^{132}Cs	9220	2.99×10^{-13}
^{134}Cs	1.793×10^{20}	51.4
^{135}Cs	7.984×10^{26}	207
^{136}Cs	2.408×10^{14}	0.00396
^{137}Cs	5.717×10^{26}	1.13×10^{7}
^{140}Ba	9.987×10^{16}	1.69

Table 4.10: End-of-Life Radioisotope Coolant Inventory for One 1000 cc Plenum and One 2000 cc Plenum, x=1848 cm

Isotope	Coolant inventory, a	Activity (Ci)
^{3}H	4.109×10^{23}	19768
^{85}Kr	4.317×10^{25}	2.38×10^{5}
^{86}Rb	1.520×10^{11}	1.77×10^{-6}
^{129}I	7.535×10^{25}	2.85
^{131}I	6.866×10^{10}	1.86×10^{-6}
^{129m}Te	2.663×10^{17}	1.73
^{131}Ba	1570	2.97×10^{-14}
^{133}Xe	5.784×10^{7}	2.34×10^{-9}
^{132}Cs	0	0
^{134}Cs	7.413×10^{19}	21.2
^{135}Cs	4.747×10^{26}	123
^{136}Cs	3.264×10^{11}	5.37×10^{-6}
^{137}Cs	3.338×10^{26}	6.59×10^{6}
^{140}Ba	1.227×10^{14}	0.00208

Table 4.11: End-of-Life Radioisotope Coolant inventory for Three 1000 cc Plena, x=2002 cm

Isotope	Coolant inventory, a	Activity (Ci)
^{3}H	3.445×10^{23}	16573
^{85}Kr	3.612×10^{25}	1.99×10^{6}
^{86}Rb	2.886×10^{10}	3.35×10^{-7}
^{129}I	6.398×10^{25}	2.42
^{131}I	5.460×10^{9}	1.48×10^{-7}
^{129m}Te	7.727×10^{16}	0.501
^{131}Ba	190	3.59×10^{-15}
^{133}Xe	2.520×10^{6}	1.02×10^{-10}
^{134}Cs	5.687×10^{19}	16.3
^{135}Cs	4.031×10^{26}	104
^{136}Cs	4.531×10^{10}	7.45×10^{-7}
^{137}Cs	2.820×10^{26}	5.57×10^{6}
^{140}Ba	1.653×10^{13}	2.80×10^{-4}

Table 4.12: End-of-Life Radioisotope Coolant Inventory for Two 1000 cc Plena and One 2000 cc Plenum, x=2513 cm

Isotope	Coolant inventory, a	Activity (Ci)
^{3}H	1.875×10^{23}	9020
^{85}Kr	1.953×10^{25}	1.08×10^{6}
^{86}Rb	1.165×10^{8}	1.35×10^{-9}
^{129}I	3.618×10^{25}	1.37
^{131}I	1.227×10^{6}	3.32×10^{-11}
^{129m}Te	1.273×10^{15}	0.00826
^{131}Ba	0	0
^{133}Xe	77	3.12×10^{-15}
^{134}Cs	2.349×10^{19}	6.73
^{135}Cs	2.279×10^{26}	59.1
^{136}Cs	6.465×10^{7}	1.06×10^{-9}
^{137}Cs	1.571×10^{26}	3.10×10^{6}
^{140}Ba	2.139×10^{10}	3.62×10^{-7}

Table 4.13: End-of-Life Radioisotope Coolant inventory for One 1000 cc Plenum and Two 2000 cc Plena, x=3026

Isotope	Coolant inventory, a	Activity (Ci)
^{3}H	9.759×10^{22}	4695
^{85}Kr	1.014×10^{25}	5.56×10^{5}
^{86}Rb	4.602×10^{5}	5.35×10^{-12}
^{129}I	1.954×10^{25}	0.739
^{131}I	267	7.22×10^{-15}
^{129m}Te	2.064×10^{13}	1.34×10^{-4}
^{133}Xe	0	0
^{134}Cs	9.579×10^{18}	2.74
^{135}Cs	1.231×10^{26}	31.9
^{136}Cs	8.990×10^{4}	1.48×10^{-12}
^{137}Cs	8.376×10^{25}	1.65×10^{6}
^{140}Ba	2.697×10^{7}	4.57×10^{-10}

As can be seen in the tables, the extension of the vent path through the addition of tubes and plena is highly effective at reducing the output quantities of the isotopes of interest. This extension is important in both the reduction of the overall activity of the coolant and, because many of the shorter lived species are volatile, decreased probability of chemical reactions between fission products and their surroundings. The potential for such chemical reactions to occur will be discussed in detail in chapter 5.

Another trend identified in the output data is the relatively weak dependence of output quantities of isotopes with longer half lives on vent path length. The output

quantities and activities of species such as ^{85}Kr and ^{137}Cs vary by roughly an order of magnitude over the range of potential venting setups; over this same range the output quantities and activities of many other species vary by several orders of magnitude. What is interesting about these two isotopes is that despite their long half lives, they remain the sources of the highest activity over the range of potential venting setups. This means that while the total list of nuclides of concern includes the fourteen radioactive isotopes shown in Table 4.14, ^{85}Kr and ^{137}Cs can be used as conservative bounding cases for other radioactive isotopes. Table 4.15 adds on the volatile species of interest.

Table 4.14: Final List of Radioactive Isotopes of Concern

Isotope	Half Life
^{3}H	12.33 y
^{85}Kr	10.76 y
^{86}Rb	18.63 d
^{129}I	1.57×10^{7} y
^{131}I	8.02 d
^{129m}Te	33.6 d
^{131}Ba	11.5 d
^{133}Xe	5.24 d
^{132}Cs	6.48 d
^{134}Cs	2.0648 y
^{135}Cs	2.30×10^{6} y
^{136}Cs	13.16 d
^{137}Cs	30.07 y
^{140}Ba	12.75 d

Table 4.15: Final List of Volatile Nuclides of Concern

Isotope	Half Life	Isotope	Half Life
^{3}H	12.33 y	^{136}Cs	13.2 d
^{78}Se	Stable	^{137}Cs	30.1 y
^{79}Se	Stable	^{134}Ba	Stable
^{80}Se	Stable	^{135}Ba	Stable
^{82}Se	Stable	^{136}Ba	Stable
^{79}Br	Stable	^{137}Ba	Stable
^{81}Br	Stable	^{138}Ba	Stable
^{82}Br	35.3 h	^{140}Ba	12.8 d
^{85}Rb	Stable	^{124}Te	Stable
^{127}I	Stable	^{125}Te	Stable
^{129}I	1.57×10^{7} y	^{126}Te	Stable
^{131}I	8.02 d	^{128}Te	Stable
^{133}Cs	Stable	^{129m}Te	33.6 d
^{135}Cs	2.30×10^{6} y	^{130}Te	Stable

4.4 Summary

This chapter identified nuclides of particular concern in venting due to their radioactivity and/or volatile chemical nature. The primary coolant activity levels, under the assumption of no purification, for each of the species under study were determined using a MATLAB simulation developed from the models for fission gas transport developed in chapter 3. As a results of these calculations, it was determined that the fourteen radioactive isotopes present at the end of the vent path in significant quantities can be bounded by the isotopes ^{85}Kr and ^{137}Cs due to the fact that their yields and activity levels are much higher than those of other species. In addition, a number of volatile species were identified which could potentially undergo chemical reaction in the vent tube or following their release to the primary coolant. Such chemical reactions will be discussed in detail in chapter 5, where it will be shown that many of the nuclides in tables 4.14 and 4.15 are immobilized through deposition onto surfaces and are therefore unavailable for escape. Discussion on the special case of tritium production and release can also be found in chapter 5. Techniques for removal from the primary coolant of both the volatile and radioactive species identified in this chapter will be discussed in chapter 6. The MATLAB code and the results developed through its use will be adapted and used further in chapter 7, which will address both the physics and consequences of pressure transients in the vented fuel assembly and primary coolant.

Chapter 5 – Chemical Interactions

5.0 Introduction

An understanding of the potential reactions between fission products and coolant is important in systems utilizing vented fuel. For example, it is desired that the coolant be of low activity so that incidental leakage of coolant into the containment results in low enough activity levels that routine maintenance may be performed inside the containment structure without increased risk to workers. Therefore, investigation of immobilization of radioactive fission products through formation and deposition of stable compounds is clearly in order. In addition, study of the potential effects of volatile species on structural materials is necessary in order to ensure that venting does not result in degradation of structures vital to the safe and efficient operation of the plant.

5.1 Reactions of Interest

The most important of the potential reactions are the reactions of volatile fission products with other fission products, and the reactions of fission products with the carbon dioxide coolant. In addition, the reactions between fission products and radiolytically produced oxygen must be considered. These reactions are particularly important because while many fission products are present as gases or liquids at reactor operating temperatures, their compounds are generally solid at the temperatures encountered in the vent system, purification system and heat exchangers. The very stable nature of these compounds means that a significant amount of the fission products could be removed from the vent path through filtration or through deposition onto reactor surfaces.

The many potential reactions of fission products with cladding, coolant, structural materials, and other species of fission products were investigated using the chemistry code HSC 6.1. The program allows for the modeling of multi-step chemical processes, enabling the user to calculate the reaction potential for any reaction of interest, and the corresponding quantity of products which would be formed under fixed operating conditions. The program is also capable of converting mineralogical information into

chemical composition, an important feature in determining the potential of naturally-occurring minerals as adsorbents [Roine, 2006].

The first step in the analysis was to determine the likelihood of the potential reactions between the fission products and their surroundings. In this light, the change in Gibbs free energy was calculated for each reaction at a range of temperatures. Gibbs free energy is defined as the sum

$$G = H - TS, \tag{5.1}$$

where H = enthalpy, kJ/kg

T = absolute temperature, K

S = enthalpy, kJ/K.

When reactants and products are in their standard forms, the change in Gibbs free energy can be calculated as

$$\Delta G^o = -RT \ln K, \tag{5.2}$$

Where R = universal gas constant, 8.314 J/mol·K

K = equilibrium constant for the reaction.

For a given reaction

$$aA + bB \leftrightarrow cC + dD, \tag{5.3}$$

the equilibrium constant is given as

$$K = \frac{[C]^c[D]^d}{[A]^a[B]^b} = e^{\frac{-\Delta G}{RT}}. \tag{5.4}$$

In this equation, the quantities inside the brackets denote chemical activities, which can be effectively replaced by the applicable concentrations in the case of dilute reactants and products.

In general, reactions which have negative values of ΔG at a given temperature preferentially proceed forward. As can be seen in the above equation, when ΔG is negative, the equilibrium constant is greater than unity, favoring the concentrations in the numerator of the equilibrium equation. Similarly, reactions which have ΔG which is positive but small can also result in K being greater than unity. These reactions will also tend to proceed forward. Those reactions with large, positive ΔG, however, will favor the

reverse reaction, resulting in a large quantity of the initial reactants being present at equilibrium.

HSC was used to investigate the tendency for a number of potential reactions to occur: the generation of water through reaction of tritium with CO_2; the formation of oxides, carbonates and bicarbonates through reaction of volatile species with CO_2 and ^3H; and formation of ionic compounds through reaction of fission products with other fission products. In addition, the reactions of volatile species with the products of radiolysis of the CO_2 were investigated. The results of these calculations are shown in Tables 5.1 through 5.10 on the following pages. It should be noted that comparison of these results with tabular data from the CRC Handbook of Chemistry shows strong agreement. Some key results can be derived from this data. First, as seen in Table 5.1, the formation of water from the tritium produced in ternary fission is unlikely, as the reaction proceeds spontaneously only at very low temperatures. Next, as seen in Table 5.2, the alkali metals preferentially form carbonates and bicarbonates, rather than oxides. The alkaline earth metals, as seen in Table 5.3, spontaneously form both oxides and carbonates through a range of possible reactions. The Chalcogens, as seen in Table 5.4, do not react easily to form any of the compounds investigated. However, the fission products investigated react strongly with products of the opposite valence state to form ionic compounds, as seen in both Tables 5.5 and 5.6.

Investigation of reactions between fission products and radiolytic oxygen, however, reveals that fission products in the presence of free oxygen tend to form oxides spontaneously. This is especially apparent in table 5.9, where it can be observed that the 2^+ valence state of the alkali earth metals leads to strongly negative values of ΔG for the formation of oxides.

Reactions between fission products and the structural materials which make up the reactor were also considered, and investigated using HSC. Because no spontaneous chemical reactions of fission products with any structural material were identified, the results are not presented here.

Table 5.1: Water Produced through Reaction of Tritium with CO2

Reaction	Temperature (Celsius)	ΔG (kJ)
$CO_2(g) + 2H_2(g) \rightarrow C + 2H_2O$	0	-21.086
	300	0.946
	600	18.854
	900	33.169
	1200	44.902
	1500	54.635
$CO2(g) + H_2(g) \rightarrow CO + H_2O$	0	4.321
	300	8.952
	600	11.529
	900	12.409
	1200	12.095
	1500	10.867

Table 5.2: Compounds Produced through Interaction of Alkali Metals with CO2

Reaction	Temperature (Celsius)	ΔG (kJ)
$2CO_2(g) + Rb \rightarrow RbO_2 + 2CO(g)$	0	67.168
	300	65.382
	600	62.262
	900	57.039
	1200	51.389
	1500	45.498
$CO_2(g) + Rb \rightarrow RbO_2 + C$	0	37.439
	300	48.423
	600	58.057
	900	65.391
	1200	72.101
	1500	78.399
$3CO_2(g) + 4Rb \rightarrow 2Rb_2CO_3 + C$	0	-221.382
	300	-178.661
	600	-138.183
	900	-100.140
	1200	-67.640
	1500	-36.741
$2CO_2(g) + 2Rb \rightarrow Rb_2CO_3 + CO(g)$	0	-95.827
	300	-80.851
	600	-66.989
	900	-54.246
	1200	-44.176
	1500	-34.821
$2CO_2(g) + 2\,Cs \rightarrow Cs_2O_2 + 2CO(g)$	0	31.574
	300	33.830
	600	35.642
	900	35.069
	1200	34.025
	1500	32.849
$CO_2(g) + 2Cs \rightarrow 2Cs_2O_2 + C$	0	163.186
	300	167.060
	600	170.255
	900	170.854
	1200	170.819
	1500	170.521

$CO_2(g)+ Cs \rightarrow CsO_2 + C$	0	35.503
	300	46.308
	600	56.138
	900	65.093
	1200	73.309
	1500	80.922
$2CO_2(g)+ Cs \rightarrow CsO_2 + 2CO(g)$	0	65.232
	300	63.266
	600	60.342
	900	56.741
	1200	52.597
	1500	48.022
$2CO_2(g)+ 2 Cs \rightarrow Cs_2O_2 + 2CO(g)$	0	31.574
	300	33.830
	600	35.642
	900	35.069
	1200	34.025
	1500	32.849
$CO_2(g)+ 2Cs \rightarrow 2Cs_2O_2 + C$	0	163.186
	300	167.060
	600	170.255
	900	170.854
	1200	170.819
	1500	170.521
$3CO_2(g)+ 4Cs \rightarrow 2Cs_2CO_3 + C$	0	-223.298
	300	-181.617
	600	-142.349
	900	-107.329
	1200	-77.394
	1500	-48.953
$2CO_2(g)+ 2Cs \rightarrow Cs_2CO_3 + CO(g)$	0	-96.785
	300	-82.329
	600	-69.072
	900	-57.840
	1200	-49.053
	1500	-40.927
$2CO_2(g)+ 2Cs +2H(g) \rightarrow 2CsHCO_3 + C$	0	-233.145
	300	-171.508
	600	-100.938
	900	-24.415
	1200	56.771
	1500	141.942
$2CO_2 (g)+ Cs + H(g) \rightarrow CsHCO_3 + CO(g)$	0	-101.708
	300	-77.275
	600	-48.367
	900	-16.383
	1200	18.029
	1500	54.521

Table 5.3: Compounds Produced through Interactions of Alkaline Earth Metals with CO2

Reaction	Temperature (Celsius)	ΔG (kJ)
$CO_2(g)+ Sr \rightarrow SrO_2 + C$	0	-46.058
	300	-34.307
	600	-23.652
	900	-13.422
	1200	-3.380
	1500	6.236
$2CO_2(g)+ Sr \rightarrow SrO_2 + 2CO(g)$	0	-16.330
	300	-17.348
	600	-19.447
	900	-21.774
	1200	-24.093
	1500	-26.664
$CO_2(g) + Sr \rightarrow SrO + CO(g)$	0	-72.850
	300	-71.941
	600	-71.242
	900	-70.277
	1200	-68.907
	1500	-67.436
$CO_2(g)+ 2Sr \rightarrow 2SrO_2 + C$	0	-175.430
	300	-160.840
	600	-146.689
	900	-132.202
	1200	-117.102
	1500	-101.972
$CO_2(g)+ 2Ba \rightarrow 2BaO + C$	0	-155.562
	300	-142.233
	600	-129.146
	900	-115.376
	1200	-101.025
	1500	-86.684
$CO_2(g)+ Ba \rightarrow BaO + CO(g)$	0	-62.917
	300	-62.637
	600	-62.471
	900	-61.864
	1200	-60.869
	1500	-59.792
$2CO_2(g)+ Ba \rightarrow BaO_2 + 2CO(g)$	0	-16.241
	300	-16.623
	600	-17.584
	900	-18.478
	1200	-19.359
	1500	-20.513
$CO_2(g)+ Ba \rightarrow BaO_2 + C$	0	-45.970
	300	-33.581
	600	-21.788
	900	-10.126
	1200	1.353
	1500	12.388

$3CO_2(g)+2Ba \rightarrow 2BaCO_3+C$	0	-263.142
	300	-225.263
	600	-188.596
	900	-153.223
	1200	-120.775
	1500	-89.743
$2CO_2(g)+ Ba \rightarrow BaCO_3 + CO(g)$	0	-116.707
	300	-104.152
	600	-92.196
	900	-80.707
	1200	-70.743
	1500	-61.322

Table 5.4: Compounds Produced through Interactions of Chalcogens with CO_2

Reactions	Temperature (Celsius)	ΔG (kJ)
$CO_2(g)+ Se \rightarrow SeO_2 + C$	0	52.152
	300	65.373
	600	77.040
	900	87.342
	1200	96.952
	1500	106.043
$2CO_2(g)+ Se \rightarrow SeO_2 + 2CO(g)$	0	81.881
	300	82.331
	600	81.244
	900	78.991
	1200	76.240
	1500	73.143
$3CO_2(g)+ 2Se \rightarrow 2SeO_3 + 3C$	0	117.233
	300	134.534
	600	150.249
	900	164.860
	1200	178.708
	1500	191.987
$3CO_2(g)+ Se \rightarrow SeO_3 + 3\ CO(g)$	0	161.826
	300	159.972
	600	156.556
	900	152.333
	1200	147.639
	1500	142.636
$2CO_2(g)+ Te \rightarrow TeO_2 + 2CO(g)$	0	59.255
	300	59.600
	600	60.257
	900	60.463
	1200	59.189
	1500	57.432
$CO_2(g)+ Te \rightarrow TeO_2 + C$	0	29.527
	300	42.642
	600	56.052
	900	68.815
	1200	79.901
	1500	90.333

$CO_2(g)+ 2Te \rightarrow 2TeO + C$	0	-5.046
	300	8.884
	600	23.989
	900	38.202
	1200	49.887
	1500	61.127
$CO_2(g)+ Te \rightarrow TeO + CO(g)$	0	12.341
	300	12.921
	600	14.097
	900	14.925
	1200	14.587
	1500	14.113

Table 5.5: Bromides Produced through Interaction of Fission Products

Reaction	Temperature (Celsius)	ΔG (kJ)
$2Rb + Br_2 \rightarrow 2RbBr$	0	-183.111
	300	-175.400
	600	-166.604
	900	-159.900
	1200	-154.314
	1500	-148.655
$Se + Br_2 \rightarrow SeBr_2$	0	-167.435
	300	-162.288
	600	-156.242
	900	-151.098
	1200	-146.028
	1500	-141.017
$2Cs + Br_2 \rightarrow 2CsBr$	0	-187.554
	300	-178.969
	600	-169.344
	900	-162.873
	1200	-157.028
	1500	-151.121
$Ba + Br_2 \rightarrow BaBr_2$	0	-176.767
	300	-171.496
	600	-165.208
	900	-158.319
	1200	-152.683
	1500	-146.912

Table 5.6: Iodides Produced through Interactions of Fission Products

Reaction	Temperature (Celsius)	ΔG (kJ)
$2Rb + I_2 \rightarrow 2RbI$	0	-157.367
	300	-151.881
	600	-144.155
	900	-138.896
	1200	-134.242
	1500	-129.432
$Sr + I_2 \rightarrow SrI_2$	0	-133.415
	300	-130.431
	600	-125.868
	900	-122.185
	1200	-118.095
	1500	-113.908
$2Cs + I_2 \rightarrow 2CsI$	0	-163.638
	300	-157.334
	600	-148.790
	900	-143.726
	1200	-139.053
	1500	-134.137
$Ba + I_2 \rightarrow BaI_2$	0	-143.818
	300	-140.660
	600	-135.339
	900	-130.310
	1200	-125.623
	1500	-120.857

Table 5.7: Selenides Produced through Interaction of Fission Products

Reaction	Temperature (Celsius)	ΔG (kJ)
$2Rb + Se \rightarrow Rb_2Se$	0	-95.770
	300	-88.715
	600	-77.205
	900	-63.290
	1200	-47.519
	1500	-30.122
$Sr + Se \rightarrow SrSe$	0	-91.051
	300	-88.283
	600	-82.453
	900	-74.699
	1200	-65.339
	1500	-54.914
$Ba + Se \rightarrow BaSe$	0	-85.064
	300	-80.534
	600	-74.917
	900	-68.551
	1200	-61.579
	1500	-54.297

Table 5.8: Compounds Formed through Interaction of Alkali Metals with Radiolytic Oxygen

Reaction	Temperature (Celsius)	ΔG (kJ)
$Rb + O_2(g) \rightarrow RbO_2$	0	-237.647
	300	-192.488
	600	-152.764
	900	-122.444
	1200	-94.572
	1500	-68.295
$2Cs + O_2(g) \rightarrow Cs_2O_2$	0	-386.572
	300	-324.499
	600	-264.141
	900	-214.367
	1200	-167.220
	1500	-121.219
$Cs + O_2(g) \rightarrow CsO_2$	0	-245.745
	300	-201.340
	600	-160.794
	900	-123.691
	1200	-89.516
	1500	-57.738
$2Cs + CO(g) + O_2(g) \rightarrow Cs_2CO_3$	0	-923.623
	300	-810.509
	600	-702.264
	900	-603.101
	1200	-514.821
	1500	-429.897
$Cs + H(g) + CO(g) + O_2(g) \rightarrow CsHCO_3$	0	-944.221
	300	-789.362
	600	-615.632
	900	-429.644
	1200	-234.148
	1500	-30.546

Table 5.9: Compounds Formed through Interaction of Alkaline Earth Metals with Radiolytic Oxygen

Reaction	Temperature (Celsius)	ΔG (kJ)
$Sr + O_2(g) \rightarrow SrO_2$	0	-586.999
	300	-538.630
	600	-494.634
	900	-452.197
	1200	-410.385
	1500	-370.224
$Ba + O_2(g) \rightarrow BaO_2$	0	-586.628
	300	-535.593
	600	-486.837
	900	-438.407
	1200	-390.582
	1500	-344.485
$Ba + CO(g) + O_2(g) \rightarrow BaCO_3$	0	-1006.976
	300	-901.817
	600	-799.013
	900	-699.110
	1200	-605.573
	1500	-515.230

$Sr + O(g) \rightarrow SrO$	0	-797.334
	300	-749.020
	600	-700.610
	900	-650.968
	1200	-599.722
	1500	-548.188
$Ba + O(g) \rightarrow BaO$	0	-755.772
	300	-710.094
	600	-663.910
	900	-615.769
	1200	-566.089
	1500	-516.205

Table 5.10: Compounds Formed through Interaction of Chalcogens with Radiolytic Oxygen

Reaction	Temperature (Celsius)	ΔG (kJ)
$Se + O_2(g) \rightarrow SeO_2$	0	-176.088
	300	-121.570
	600	-73.340
	900	-30.599
	1200	9.405
	1500	47.368
$Se + O(g) + O_2(g) \rightarrow SeO_3$	0	-334.123
	300	-244.744
	600	-160.769
	900	-80.668
	1200	-3.276
	1500	72.095
$Te + O_2(g) \rightarrow TeO_2$	0	-270.752
	300	-216.677
	600	-161.153
	900	-108.119
	1200	-61.938
	1500	-18.364
$Te + O(g) \rightarrow TeO$	0	-440.892
	300	-393.958
	600	-343.552
	900	-294.484
	1200	-250.382
	1500	-206.985

When the results of these calculations are combined with information about the fission products available for reaction, some key predictions can be made. For example, cesium is produced in fission in large quantities, as shown in figure 5.1, and reacts strongly with other fission products and with coolant. But because iodine and bromine, the two fission products most likely to react with cesium, have lower yields and shorter half lives, a large amount of cesium can be predicted to either react with coolant or

remain unreacted. In addition, because cesium reacts so preferentially with iodine and bromine, while barium, rubidium and strontium have slightly lower reaction potentials with the halogens, one can predict that these species will tend to react with CO_2 in the absence of halogen atoms. In addition, due to the presence of unreacted tritium, it can be inferred that these species might also tend to form bicarbonates. This prediction is supported by the very negative values of ΔG for formation of bicarbonates from these species. Finally, it can be predicted that the formation of oxides will be limited by the amount of radiolytic oxygen present in the system, since oxide formation through reaction with radiolytic oxygen has extremely high values for ΔG across the range of fission products investigated. It is crucial to note that these statements are simply predictions, and that only through complex chemical equilibrium calculations can it be determined what products are formed and in what quantities.

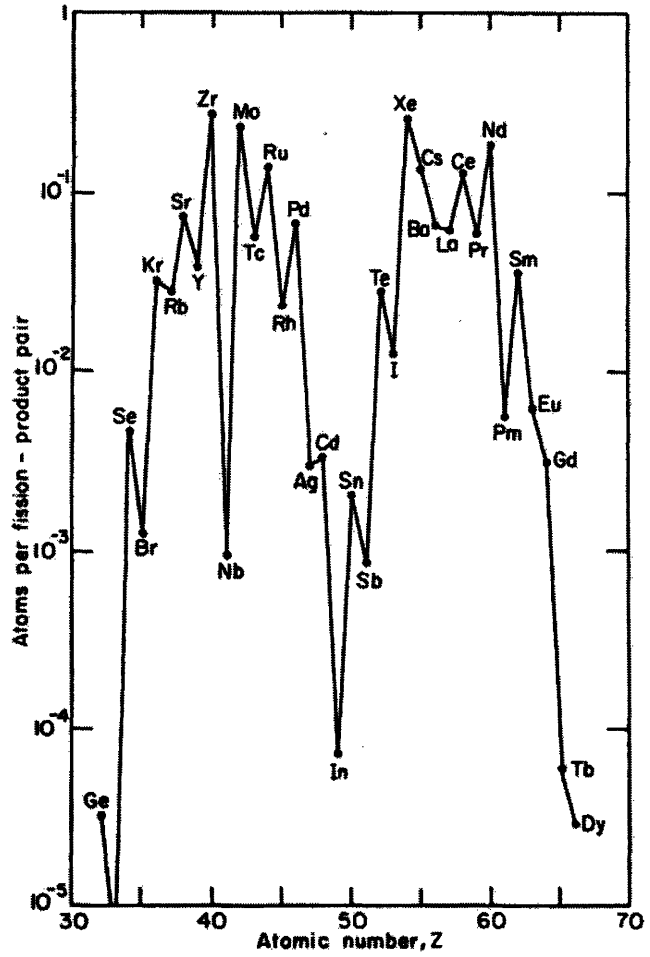

Figure 5.1: Chemical Composition of Fission Products [Benedict, 1981]

5.2 Equilibrium Quantities in Primary Coolant

Also of particular interest in analyzing the potential interactions of fission products with the reactor environment is calculation of the equilibrium quantities of reactants and products. Since the entire volume of the coolant circulates through the system in a short period of time (roughly thirty seconds [Freas, 2007]), it can be assumed that the system is essentially a well-mixed pot of reactants. The first step then, in determining the equilibrium state of the volatile species present was to determine the amounts of reactants present at steady state. The rate of change of the quantity of reactant present can be expressed as

$$\frac{dN}{dt} = J - \lambda N - fN, \qquad (5.5)$$

Where N = quantity of reactant present, mol

J = influx of reactant at time t, from eq. 3.7, mol/s

λ = decay constant of reactant, s^{-1}

f = fraction of reactant removed by purification system per second

Using this relation and equation 3.7, which was derived in the section on nuclide production in order to describe diffusion of radionuclides, the equation describing the steady state concentration of any radioactive fission product in the coolant is

$$N_{eq} = \frac{\gamma\varphi\Sigma_f e^{-\sqrt{\frac{\lambda}{D}}x}}{(\lambda + f)}. \qquad (5.6)$$

Stable species can be assumed to be present in the total quantities produced over the reactor's lifetime. Similarly, long-lived species are best represented as total quantities produced over the lifetime of the reactor because their small decay constants result in unreasonable calculated values for N_{eq}. As expected, few of the volatile species selected for study were found to be present in significant quantities at steady state. These species and their quantities, calculated using equation 5.6, are shown in Table 5.11. For this calculation, zero purification was assumed for conservatism and prior immobilization by chemical reaction was neglected. The half lives for this calculation are those found in Chapter 4; fission yields used are accumulated yields from JEFF 3.1. Note that many of the volatile isotopes under study are present only in minute quantities; those which have

equilibrium coolant inventories of less than 10^{-10} gram moles were neglected. The end result is that significant contamination could result unless we take credit for immobilization of species by chemical reactions inside the assembly.

Table 5.11: Steady State Quantities of Volatile Species in Coolant, Assuming Zero Purification

Isotope	Quantity, gram moles	Total elemental quantity, gram moles
^{3}H	0.04493	0.04493
^{78}Se	14.4239	180.3
^{79}Se	28.8478	
^{80}Se	64.9076	
^{82}Se	72.1196	
^{83}Rb	1.15×10^{-5}	937.6
^{84}Rb	2.5×10^{-5}	
^{85}Rb	937.555	
^{86}Rb	0.00580	
^{84}Sr	4.8×10^{-7}	0.05500
^{86}Sr	0.0550	
^{127}I	1.9170	9.177
^{129}I	5.2940	
^{131}I	1.8467	
^{133}I	0.119	
^{132}Cs	4774.6	8689
^{133}Cs	23.8983	
^{134}Cs	3833.9	
^{135}Cs	25.8295	
^{136}Cs	7.7889	
^{137}Cs	22.5293	
^{81}Br	0.4925	145.2
^{79}Br	0.0181	
^{81}Br	144.7	
^{82}Br	2.43×10^{-10}	
^{123}Te	5.498	1997
^{124}Te	0.09377	
^{125}Te	48.3201	
^{126}Te	8.6544	
^{128}Te	347.6165	
^{129m}Te	0.0137	
^{130}Te	1586.6312	
^{132}Te	8.22×10^{-8}	
^{134}Ba	0.02019	8997
^{135}Ba	23.6236	
^{136}Ba	10.0967	
^{137}Ba	21.1252	
^{138}Ba	4687.7741	
^{140}Ba	4255.0565	

5.2.1 Steady State Quantities of Radiolytic Gases

Radiolysis, or the chemical alteration of a molecule during exposure to radiation, is a complex process. In CO_2-bearing systems such as the GFR, the area of primary concern with respect to radiolysis is the breaking of chemical bonds by β- and γ-radiation, resulting in production of C, O, and CO radicals. This phenomenon has been the focus of a great deal of prior research [Anbar,1966; Haissinsky,1961], which has allowed the use of a simple rule to describe the total production of radiolytic gas. The capability of radiation to decompose a material is often given as a G-value: the number of bonds broken per 100 eV of a specific type of radiation absorbed. Thus, with knowledge of the energy deposited in the coolant by β- and γ- radiation, one can determine the rate of radiolytic gas production [Rigual, 2004].

According to Duderstadt, gamma radiation is far more dominant than beta radiation in deposition of energy in the coolant. Therefore, the influence of beta radiation on coolant radiolysis is neglected here. Duderstadt also lists the gamma energy in the reactor as 4% of the energy produced in fission, or about 96 MW. If the G value for the destruction of CO_2 is taken to be 0.5/100 eV absorbed, the best available value for the temperature and pressure of interest [Haissinsky, 1961], and the purification of the radiolytic products occurs once per hour, the same rate assumed for the rest of the coolant, equation 5.5 can be used to derive a steady state coolant inventory of 91.7 moles of each CO and O radical, ignoring recombination.

5.2.2 Equilibrium Reaction Products

With this information on the quantities of reactants available, it was possible to use HSC to calculate the equilibrium quantities of these chemical species, their oxides, and products of their reactions with each other. Each potential product was input into an HSC calculation, which revealed the final equilibrium amount of each reactant and product at 20 MPa, the system's operating pressure. Many of the potential products were not produced in any quantity, and have not been included in the results tabulated in Table 10. As can be seen, the majority of the potentially volatile species only appear in the table as compounds. This is because the volatile species react fully with the carbon dioxide or each other, leaving almost no free metallic or hydrogen nuclei. The major exceptions to this are selenium, which is predicted to remain almost totally unreacted, and tellurium,

which is present in smaller quantities. For this reason it will be important that the coolant purification system be capable of removal of a significant quantity of selenium, tellurium, and any other species which may remain unreacted.

Table 5.12: Equilibrium Quantities at 20 MPa in Primary Coolant

Species	Equilibrium Quantity, gram moles
CH_4	1.819×10^{-15}
H_2	3.648×10^{-10}
HCOOH	3.785×10^{-15}
HI	5.358×10^{-21}
$BaBr_2$	1.072×10^{-20}
CsBr	142.48
RbBr	2.7153
CsI	9.1399
RbI	3.7049×10^{-2}
$BaCO_3$	8997
Cs_2CO_3	4269
CsOH	2.120×10^{-14}
H_2O	2.059×10^{-2}
Rb_2CO_3	467.42
RbOH	7.289×10^{-14}
$SrCO_3$	0.05500
TeO_2	2.750×10^{-17}
I	2.1387×10^{-14}
Se	180.3
Te	1997

5.2.3 Physical Form of Products

In order to fully determine the impact of these reactions on the reactor environment and on the mobility of radioactive species, more information is required. For example, both the mobility of the fission products and the impact of these products on the reactor (i.e. plateout and other phenomena) depend upon their state at the temperatures encountered within the fuel, vent system, and primary system. In this light, the melting and boiling points for each spontaneously produced compound or element were considered.

Table 5.13: Melting and Boiling Points of Equilibrium Products [CRC Handbook, 2007]

Species	Melting Point, C	Boiling Point, C
CH_4	-182.47	-161.48
H_2	-259.198	-252.762
HCOOH	8.3	101
HI	-50.76	-35.55
$BaBr_2$	857	1835
CsBr	636	1300
RbBr	692	1340
CsI	632	1280
RbI	656	1300
$BaCO_3$	decomp. 1555	---
Cs_2CO_3	793	---
CsOH	342.3	---
H_2O	0	100
Rb_2CO_3	837	---
RbOH	385	---
$SrCO_3$	1494	---
TeO_2	733	1245
I	113.7	184.4
Se	220.8	685
Te	449.51	988

This data has some important implications. Solid reaction products which have melting points well in excess of operating temperatures, would likely be deposited near where they are formed, with any remaining suspended particles settling out quickly or being filtered out by the coolant purification system. A few other products, such as CsI and CsBr, with melting points slightly lower than operating temperatures, would most likely be mobile within the core but would solidify and deposit in cooler areas of the plant, including the debris trap at the lower end of the assembly which is at roughly 500 °C. It is assumed at present that all metals and free compounds with melting points greater than 500 °C will deposit on the debris trap and be rendered immobile. These species are shaded in table 5.7. Note that any species which are liquid or gaseous above 500 °C will remained suspended in the coolant transiting the core, but may deposit onto surfaces after entering the power conversion system, where temperatures down to 35 °C are encountered.

5.3 Removal of Species from Vent Path through Deposition

As stated in the introduction to this work, one important metric in the assessment of venting directly to the coolant is an estimation of surface contamination in the primary system. This information is vital in determining whether hands-on maintenance of primary system components can be performed, and also provides insight into whether certain fission products are released to the containment facility as a result of leakage or primary system depressurization. Prior experimentation [Chapman, 1982] has demonstrated that the highest rate of deposition occurs at locations where the impurity concentration in the gas is the highest, and this would imply that the most deposition occurs within the fuel assembly, as the radionuclide concentrations drop off due to decay by holdup. However, hands-on maintenance of the assembly interior is irrelevant, and so the estimate of surface contamination is reserved for the vent tube outlet into the primary. This should be considered a very conservative estimate since high levels of deposition within the assembly can be expected to reduce the population of radionuclides available for deposition in the primary.

As discussed in Chapters 3 and 4, the MATLAB simulation of radionuclide transport through the vent system showed that only a few isotopes survive the vent tube. Of these, several are isotopes of krypton and are unlikely to undergo deposition. Others react to form stable compounds which have high melting points and are assumed to deposit on the debris trap within the assembly. Due to the lower temperatures of regions of the primary system (25 °C in some places), it can be expected that all free atoms of Se, Te, and I will plate onto surfaces. Note that because no radioactive isotopes of Se are expected to survive the venting process, no Se surface contamination occurs. The remaining species in table 5.13 are unlikely to deposit in the same fashion because all but H_2O remain gaseous at the full range of primary system temperatures.

The EOL surface contamination level of the two species of interest, then, can be found by first determining the fraction of the EOL activity of each species which has not already been immobilized through formation of products which are caught in the assembly debris trap (as determined using tables 5.12-5.13). Next, this quantity can be assumed to be uniformly dispersed over the primary system surface area, estimated as

800,000 m^2 [Gezelius, 2004]. In all likelihood, this is not physically correct, as plateout will tend to occur most quickly in the cooler regions of the plant. However, an in-depth modeling of temperature-dependent deposition is outside the scope of the present work. The results of the calculations are shown in table 5.14.

Table 5.14: EOL Primary Surface Contamination Estimates

Element	EOL Contamination Estimate (dps/cm^2)
Te	99900
I	19.3

For comparison, the regulatory limit for hands-on maintenance is 1 dps/cm^2. As can be seen in the table, activity from two isotopes exceeds this value, and so hands-on post-shutdown maintenance of primary system components may not be allowable under the present conservative estimates. Some refinement of this estimate may indicate that the regulatory limit is not breached, and so further work in this area should be pursued. In any case, most direct cycle systems pose other barriers to hands-on maintenance, and so the restriction due to fission product contamination levels is of no great consequence. In fact, the plateout of Te onto surfaces can be viewed as beneficial, since plated Te cannot easily leak from the purification system or be released during an accident.

5.3.2 Decontamination of Surfaces

Because a significant amount of free atoms are likely to be adsorbed by structural materials and because most compounds of fission products are expected to deposit in small quantities on primary surfaces, decontamination of primary system components becomes a significant issue. While atoms which have been adsorbed by steel surfaces remain fixed in place, most solid products of chemical reactions in the vent system and primary coolant system are highly soluble in water and can thus be removed from the surface by washing with water and detergent. The solubilities of these common reaction products are shown in table 5.8.

Table 5.15: Solubility of Reaction Products in Water [CRC Handbook, 2007]

Species	Solubility, g/100 g H2O
SeTe	N/A
TeI_2	N/A
$BaBr_2$	100
CsBr	123
RbBr	116
CsI	84.8
RbI_2	165
RbIO	N/A
$BaCO_3$	0.0014
Cs_2CO_3	261
$CsHCO_3$	209
CsOH	300
Rb_2CO_3	223
$RbHCO_3$	116
RbOH	173
$SrCO_3$	0.00034
TeO	N/A
TeO_2	N/A

5.4 Summary

This chapter investigated the effects of diffusing fission products on their surroundings. Volatile chemical species, of concern due to their potential to react with cladding and structural materials, were for the most part found to react strongly with coolant and with other fission products to form stable compounds. These compounds are important in both preventing negative impacts on reactor operation and in causing additional holdup of radioactive species. Several chemical species were found to remain unreacted in significant quantities, namely Se and Te. For this reason, it is recommended that the coolant purification system include some form of chalcogen "getter" which will remove these species from the waste stream before they can participate in attack on structural materials. The titanium upper axial reflector is one option for removal of these species from the waste stream. However, there is a lack of experimental data available on the use of titanium in retention of fission products, and so investigation of this is left to future work. The use of TeO_2, in particular, should be considered.

Deposition of a number of species onto steels was also investigated, and conservative estimates of surface contamination levels were derived. From this information it is predicted that hands-on maintenance of primary system components will not be possible. This result is not unusual in direct cycle systems, even in those which do not utilize vented fuel assemblies. In any case, the information developed in this chapter will prove important; the next chapter sets requirements for purification of the primary coolant based on knowledge of the immobilization of chemical species through reaction and/or deposition.

Chapter 6: Purification of Primary Coolant

6.0 Introduction

Coolant purification systems are incorporated into the designs of most nuclear reactors. Even in reactors which do not employ venting, impurities often make their way into coolant through the failure of fuel, reaction of the coolant with structural materials, or irradiation of coolant atoms. For this reason, great care is taken to remove this contamination in order to prevent the problems associated with impure coolant, such as increased damage to structural materials, fouling of heat transfer surfaces, and transport and deposition of activated corrosion products. In the case of a reactor which vents fission products directly to coolant, this problem is exacerbated, particularly in that the coolant receives a significant amount of radioactive fission gas. It is planned that a purification system will be implemented which can remove the bulk of the fission gas impurities from the coolant. In addition, the system must also be capable of the removal of a number of other contaminants, including water vapor, dust, oil, and any additional fission products which survive the venting process.

6.1 Common Purification Systems

The majority of coolant purification systems in gas cooled reactors follow very similar philosophies in removal of impurity atoms, despite the differences in the reactors which they serve [Gee,1969; Yao, 2002; Olson, 1980]. Typically, a high-temperature absorber is used to capture dusts and large particles, which are particularly problematic in gas-cooled systems containing graphite reflectors. Following this step, the coolant is chilled by water, and water vapor is condensed out of the gas stream. Helium-cooled systems generally follow this by reducing the temperature of the stream still further in order to condense and remove CO_2 from the gas. A molecular sieve is often employed to remove any water and carbon dioxide still remaining as vapor. After this, a number of troublesome gases (Kr, Xe, CO, N, CH_4, and H) are removed from the stream through deposition on an activated carbon absorber. In systems where particularly aggressive removal of these species is desired, cryogenic distillation may alternatively be used to

purify the gas stream. In either case, the stream is usually passed through a final filter, intended to remove charcoal dust from the gas, and is then reheated and returned to the primary coolant stream.

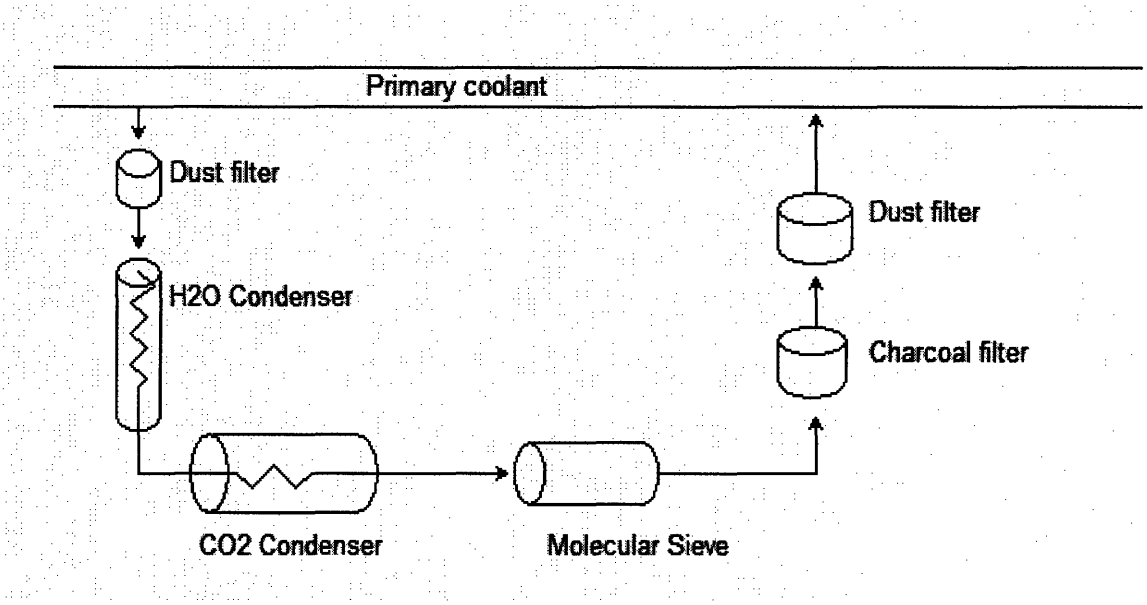

Figure 6.1: Traditional Gas-Coolant Purification Scheme

6.2 Requirements for Purification

Any purification system selected for use with the GFR must satisfy two major requirements: the removal of a significant fraction of the coolant's impurities, and the ability to maintain low pressure losses. One attractive option in removing impurities from the primary coolant is directing a portion of the flow through a packed bed of desiccant and molecular sieves. A number of simple purification beds are commercially available, and it is quite possible that one of these beds or a larger scale version of the same concept could be implemented with success in the CO_2 purification system. One such commercially available gas purifier allows a flow rate of 300 L/hr, through a flow area of 28.3 cm^2 [Drierite, 2007]. Knowing that the density of CO_2 is about 0.0120 g/cm^3 at 0.67 MPa, the maximum inlet pressure for this device, one can calculate the mass flow rate as 0.035 $g/cm^2 \cdot s$. The pressure loss through the packed bed is given approximately by

$$\Delta P \approx \frac{G^2}{\rho}, \qquad (6.1)$$

Where G = mass flux, $g/cm^2 \cdot s$

ρ= density, g/cm^3.

Usually this equation would include friction and form loss terms, but to calculate these terms would require a number of questionable assumptions about the particles which make up the packed bed. In any case, these terms are expected to be small, and so the pressure drop across the purifier is approximated by Eq. 6.1. The pressure loss through this small packed bed is then roughly 10 Pa, which is about 15% of the inlet pressure. It is desirable to keep pressure losses of similarly low fraction, and preferably lower, even when such a packed bed is scaled up for use in purification of the 330,000 kg coolant inventory [Pope, 2006]. If it is assumed that the entire primary coolant volume is purified once per hour as stated in Freas' 2007 work, then the flow rate through each bed must be 22.9 kg/s. If the scaled up bed has a diameter of 0.5 m, and the density of the coolant is 0.4 g/cc (the density as the gas exits the precooler), the pressure loss across the bed is approximately 29.2 Pa. This represents only 0.0004% of the inlet pressure, making purification by filtration appear to be feasible.

One major question which arises, however, is whether this rate of purification is really sufficient to achieve a tolerable level of radionuclides in the primary coolant. The greatest concern for everyday operation is the activity of the containment air. It is desired that activity levels within containment remain as low as reasonably achievable, but at the minimum, the levels must remain below the regulatory limits set in 10CFR50, with a reasonable margin of safety. As has been established previously in this report, ^{85}Kr is by far the most likely isotope to leak into the containment, due to its high yield in fission, lengthy half life, high mobility, and chemical stability. It therefore makes a suitable bounding case for determination of the necessary purification rate. 10CFR50 gives a Derived Air Concentration (DAC) limit of 1×10^{-4} μCi/mL. For the 70,000 m^3 containment volume, this means that the maximum allowable activity in the containment volume is 7 Ci. Assuming a conservative leak rate of 1% of the primary volume per day (Previous analysis postulated only 0.5% per day [Freas, 2007]), this means that no more than 700 Ci of ^{85}Kr may be present in the primary coolant at any time. Using the equation describing steady state fission product inventories,

$$N_{eq} = \frac{\gamma \varphi \Sigma_f e^{-\sqrt{\frac{\lambda}{D}}x}}{(\lambda + f)}, \qquad (6.2)$$

Where f = fraction of coolant purified, s^{-1}

one can derive a required purification rate of 3.88 primary coolant volumes per day. This is clearly feasible, as the purification system can handle such flow rates without unacceptable loss of pressure or other complications. In fact, there is a factor of six between this minimum value and the purification rate specified in the packed bed analysis. Hence, under the conservative leak rate assumption above, the primary coolant can be controlled to contain less than 20% of the maximum ^{85}Kr activity.

In order to assure that this rate of purification is truly satisfactory, the impact of this rate on the steady state inventories of the other species of interest must be determined. By altering the MATLAB script used to calculate coolant inventories of radionuclides to reduce the coolant inventory of each nuclide by 1% per day, the maximum coolant activity levels for each of the radioactive nuclei of concern were found. These results, along with the regulatory limits on containment activity, are reproduced in table 6.1.

Table 6.1: EOL Coolant Inventories of Radioactive Species Under Hourly Purification

Species	Coolant Activity (Ci)	Containment Specific Activity of 1% (μCi/ml)	DAC Limit
^{3}H	0.755	1.1×10^{-7}	2×10^{-5}
^{85}Kr	97.667	1.4×10^{-5}	1×10^{-4}
^{86}Rb	7.807×10^{-4}	1.1×10^{-10}	3×10^{-7}
^{129}I	6322	9.0×10^{-4}	4×10^{-9}
^{131}I	1.188	1.7×10^{-7}	2×10^{-8}
^{129m}Te	17.691	2.5×10^{-6}	3×10^{-7}
^{131m}Te	9.467×10^{-9}	1.4×10^{-15}	2×10^{-7}
^{131}Ba	5.778×10^{-10}	8.3×10^{-17}	3×10^{-6}
^{132}Cs	1.659×10^{-10}	2.4×10^{-15}	2×10^{-6}
^{134}Cs	0.00615	8.8×10^{-10}	4×10^{-8}
^{135}Cs	0.00273	3.9×10^{-10}	5×10^{-7}
^{136}Cs	0.0351	5.0×10^{-9}	3×10^{-7}
^{137}Cs	187.95	2.7×10^{-7}	6×10^{-8}
^{140}Ba	17.504	2.5×10^{-6}	6×10^{-7}

As can be seen in the table, the purification of 1% of the coolant inventory each day renders all but ^{129}I, ^{129m}Te, ^{137}Cs and ^{140}Ba below DAC limits for a 1% daily leak rate. It should be recalled from the discussion on chemical reactions of fission products that these species are unlikely to be present in the primary system as free atoms, and that

the compounds formed by these species will be deposited in significant quantities on surfaces within the fuel assembly of origin and primary coolant surfaces in the reactor. While this tendency causes high enough surface activity to preclude hands-on maintenance of the primary system, it also reduces the potential for these species to escape from the primary and into the containment environment. The proposed purification rate is therefore deemed sufficient for maintaining containment facility access.

6.3 Cryogenic Distillation

Cryogenic distillation refers to the use of the differing solubilities of gases in the liquid and vapor forms of either N_2 or O_2 for the purpose of separation of a mixture of gases. The technique is widely used in the production of industrial gases through air separation, and has been evaluated favorably for use in separation of noble gases from helium. This is because helium remains gaseous at cryogenic temperatures, while the impurities which it contains condense at the surface of the cryogenic fluid. There are, however, some serious challenges in the use of cryogenic distillation. Early cryogenic decontamination systems were known for having somewhat erratic efficiency in purification, leading to some uncertainty about their ability to purify the coolant at an acceptable rate. In addition, the systems often require a large input of energy and have very high startup costs [Stern, 1978; Ianovski, 2002].

Most unfortunately, this approach does not appear attractive for use with carbon dioxide, which freezes well above cryogenic temperatures, and tends to clog equipment in the process. In systems which use cryogenic distillation as a purification technique, CO_2 is usually removed from the stream prior to the cryogenic process, by means of molecular sieving or a similar sorbent process. Under the correct circumstances, it might be possible to purify coolant by allowing the CO_2 to freeze on a structure held slightly above cryogenic temperatures, while permitting the remainder of the waste gas to exit. However, there are significant technical challenges involved in the implementation of such a strategy, and the process would remain, at best, a batch-type operation rather than a continuously operating means of purification.

Table 6.2: Thermal Properties of Pure Substances

Species	Freezing Point, °C	Boiling Point, °C
O_2	-218.3	-182.9
N_2	-210.1	-195.75
He	-272.2	-268.93
CO_2	-78	-56.5
Xe	-111.7	-108
Kr	-157.36	-153.22

6.4 Sorbent Materials

The numerous difficulties in the practical use of cryogenic distillation for separation of waste gases have led to interest in the use of solid adsorbents as getters of noble gas atoms. Such adsorbents also show promise in the removal of other impurities, including particulate matter, volatile species, and compounds of these species. The adsorbents traditionally come in one of two forms, though more exotic varieties also exist.

6.4.1 Charcoal

Activated charcoal is a popular material in removal of impurities from gas streams, and is an essential part of purification systems such as those for the high temperature gas-cooled reactor (HTGR). The material is inexpensive when compared to other sorbents, and has an extremely high pore surface area per unit volume (300-4000 m^2/g [Yang,2003]), making it capable of long periods of service prior to regeneration. When regeneration is eventually needed, only a low energy input is required due to charcoal's low heat of adsorption. Charcoal also has an added benefit over other materials, in that it is not hydrophobic, and therefore does not require a preceding desiccation of the waste stream. In addition, because charcoal is not a strongly polar material, it is capable of the attraction of more nonpolar and weakly polar molecules than other sorbent materials. This characteristic contributes to the excellence of charcoal as an adsorber of noble gases like krypton and xenon, two of the largest contributors to the activity level of the coolant.

Prior experimentation on recovery of radioactive tracers from exhaled gases during lung function testing [Bolmsjö, 1978] has demonstrated the feasibility of using activated charcoals to draw xenon out of a carbon dioxide waste stream. This work was particularly insightful because the xenon was removed from the filter by regeneration,

enabling its reuse, and indicating that filtration of noble gases followed by regeneration enables the sequestration or eventual release of the captured species.

As stated in Monson's work, activated charcoal is capable of sorption of Kr up to a level of 11 cc_{STP}/g. This means that if all of the ^{85}Kr purified from the coolant were adsorbed by charcoal without regeneration of the sorbent, 520 kg of charcoal would be required. Since ^{85}Kr represents roughly a quarter of the total amount of Kr produced, 2080 kg of charcoal, would be required to handle the full burden of krypton removal without regeneration of the sorbent.

6.4.2 Molecular Sieves

Charcoal is one of the most commonly used adsorptive materials for a wide variety of purposes, and is good at removing both Kr and Xe from waste streams. However, there is some concern that charcoal may be oxidized in an environment which contains oxygen, as occurs in the GFR due to radiolysis of the coolant. For this reason, a great deal of research has been conducted into the use of molecular sieves. Molecular sieves are materials which have a standard pore size which allows the material to selectively adsorb molecules which are smaller than that standard pore size. Such sieves are commonly one of two classes of materials: alumina (Al_2O_3), and zeolites. While alumina is commonly available and is an excellent candidate for removal of certain impurities from waste streams, zeolites are of greater interest due to their better adsorptive properties. Zeolites are minerals which can be either found in nature or synthetically produced. The synthetically produced form is an excellent candidate for adsorption of undesirable chemical species because the materials can be engineered to select the most useful pore size for adsorption of the desired chemical species [Yang,2003].

Early experiments with zeolite adsorbers demonstrated that silver mordenite (AgZ) had the highest dynamic adsorption coefficient among a number of mordenites and other candidate materials [Monson,1982]. This dynamic adsorption coefficient is defined as

$$K_d = T_m F / M,$$

Where Tm = residence time of adsorbate on adsorbent, min

F = total gas flow, cc/min

M= mass of adsorbent, g.

While this high dynamic adsorption coefficient would seem to establish AgZ as the best choice for a solid adsorber, its high cost has spurred research into other, more economical adsorber materials.

In the 1982 study conducted by P.R. Monson, hydrogen mordenite, also referred to as H-mordenite or HZ, was demonstrated to be a stronger adsorber of Kr than all materials except AgZ. At the time of the study, HZ cost only one sixtieth of the price of AgZ, meaning that although larger quantities of HZ would be required to achieve the same purification goals, the overall cost would be greatly reduced. To deal with the total GFR coolant inventory of krypton, roughly 3,300 kg of HZ would be required without regeneration of the sorbent. For comparison, the same task would require 1200 kg of AgZ or 23,000 kg of alumina. It should be noted that Monson's study used N_2 as a carrier gas for the krypton, and that no records have been found of any experiments involving CO_2 as a carrier gas. However, the similar sizes of these molecules, coupled with their non-polarity imply that they would behave similarly as carrier gases. Therefore, this approach to stripping of krypton from the gas stream appears attractive, and it is recommended that experimentation be conducted in order to determine its feasibility.

6.4.3 Desiccants

Desiccants are a special class of molecular sieves used in the selective adsorption of water. Of these, silica gel is most often selected due to its ability to adsorb 40% of its weight in water. In addition, it can be regenerated at low temperatures, and is inexpensive to replace [Yang, 2003]. Gels can be produced with a variety of surface areas, pore volumes, and strengths, depending on the specifics of the manufacturing process. In addition to silica gel, activated alumina, already mentioned as a candidate for selective adsorption of other chemical species, can be specially tailored for use as a desiccant.

Both silica gels and alumina are subjected to heat treatments which enhance their adsorptive properties. The heat treatment changes the crystal structure of the material to a form which is better at retention of water molecules. In addition to this, the manufacturing of alumina also usually includes an acid treatment step. The increase in surface acidity afforded by this method causes the polar water molecules to be more strongly attracted to the material. Unfortunately, this treatment adds to the expense of the

alumina. While alumina remains an attractive option for adsorption of other chemical species, the removal of water is best served by silica gel, which has the highest total water capacity, adsorbs a great deal of water at low humidity and is inexpensive and simple to regenerate.

6.5 Separation by Permeation

The method of separation of species through their differing abilities to permeate a material has been widely used in the nuclear industry. The gaseous diffusion approach to uranium enrichment is one such process. In recent decades, the use of semi-permeable membranes and capillary tubes has been investigated as a passive means of removing impurities from off-gas streams [Stern, 1978].

6.5.1 Membrane Separation

The use of non-porous polymeric membranes has been strongly considered as a technique for the separation of Xe and Kr from gas streams due to the safety of the process. The safety issues, expense, and lack of feasibility of cryogenic distillation have already been addressed. The use of passive membrane separation avoids these obstacles. Unfortunately, membrane separation has a number of drawbacks of its own which discourage its use in a system like the GFR. Fortunately, the concept of selective permeation through a non-porous membrane can be applied through another approach.

6.5.2 Capillary Tubes

While permeation through membranes is a highly attractive technique for separation of species such as Kr and Xe from a waste stream, capillary tubes constructed of the same or similar materials have significant advantages over membranes. First, thin membranes require extensive support systems to prevent rupture, and often cannot be used at high pressures because they are so easily torn. Capillary tubes do not require such support. Their small surface area, coupled with the fact that flow occurs along the surface of the rubber tube, rather than normal to it, reduces the probability of rupture and therefore the need for maintenance. All of these characteristics make capillary tubes better suited than membranes for passive separation of nuclides. In addition to these

benefits, the use of capillary tubes allows for the packing of a great deal of permeation surface into a relatively small volume.

Prior experimentation [Stern, 1978] investigated the separation of Xe and Kr from both air, the usual environment in a containment facility, and argon, which was to represent the cover gas present in a liquid metal fast breeder reactor. While CO_2 was not used as a carrier gas in this experiment, the molecular weights of Ar and CO_2 are similar, and so it can be expected that the ability of capillary tubes to separate the heavier noble gases from argon should be comparable to the ability of the same tubes to separate these gases from CO_2.

The permeation of gases through elastic capillaries is governed by the equation

$$G = \bar{P}\frac{2\pi L(p_o - p_I)}{\ln(R_o / R_I)}, \qquad (6.3)$$

Where G = steady state rate of permeation of pure gas, kg/s

P = mean permeability coefficient for gas-capillary system, s

L = length of capillary,m

R_o, R_I = outer and inner radii, mm

P_o, P_I = external and internal pressures, Pa.

This same equation can be used for a mixture of gases, provided that the partial pressures of the components are used in place of the total pressures, and that the mean permeability coefficient for the component in question is used. Stern's experiment allowed the modeling of the permeability coefficients with temperature. These results are reproduced below, with P given in seconds and T in Kelvin.

Nitrogen: $P \times 10^{-15} = 221 \exp[-1410/T]$

Oxygen: $P \times 10^{-15} = 198 \exp[-1111/T]$

Argon: $P \times 10^{-15} = 250 \exp[-1107/T]$

Krypton: $P \times 10^{-15} = 318 \exp[-771/T]$

Xenon: $P \times 10^{-15} = 340 \exp[-432/T]$

At the temperatures likely to be encountered in a reactor containment facility, this indicates a xenon permeability coefficient approximately an order of magnitude greater than that of argon, and a krypton permeability coefficient approximately five times that of argon. This indicates the high degree of selectivity in the removal of heavy noble gases

from the primary coolant feed stream. In addition, the very low permeability coefficients of nitrogen and oxygen indicate that selective permeation techniques could be quite useful in purification of an air-containing environment such as the containment facility.

The ultimate test of the worth of the capillary tube approach rests on the quantity of gas which such a system can purify each day, because while capillary tubes have been shown to be successful in separation of Kr and Xe from a waste stream, they frequently suffer from low throughput. This would appear to make them unattractive for use in daily purification of the primary coolant due to the requirement that 19,800 kg of CO_2 be purified by each purification loop per day, corresponding to 1×10^{12} cc/day (STP). However, Stern's experiment used a 0.91 m long apparatus containing 263 capillaries (6.35×10^{-4} m OD) with a maximum throughput of about 10^5 cc/s (STP). This corresponds to 8.64×10^9 cc/day (STP), implying that a scaled up permeator would require roughly 30,000 capillaries, with a total cross sectional area of 0.01 m^2. It remains to be seen whether capillary tubes could withstand the high operating pressures of the GFR, and whether CO_2 really behaves similarly to other light gases in the presence of the capillary tubes. In the future, experimentation should be undertaken in order to answer these questions. Even if the capillaries can not be favorably evaluated for service in a high pressure CO_2 environment, this approach could be used favorably for a situation where lower pressure is required, such as in purification of the containment facility, which would likely contain low levels of radioactive noble gases due to minor leakage of the primary coolant.

6.6 Experiment: Effectiveness of a Commercially-Produced Packed Column in CO_2 Purification

6.6.1 Motivation and Objectives

As discussed in section 6.3, both desiccants and molecular sieves appear attractive as tools for purification of CO_2. The subject of the experiment was therefore to investigate the ability of a packed column constructed of common and inexpensive materials to strip low-grade CO_2 of water vapor, noble gases, hydrocarbons, and any additional impurities in the gas sample. The final result is a qualitative assessment of the efficiency of the packed bed, as well as a scaled estimate of the physical size of a similar packed column for use in the GFR. In addition, these results were compared with the

results of prior experimentation with molecular sieving of fission products in order to determine the attractiveness of using a packed column of this type.

6.6.2 Experimental Apparatus

The complete experimental apparatus was a setup using both a gas purifier and aresidual gas analyzer, along with a set of supporting equipment. A cylinder of compressed CO_2, in some cases supplemented with argon or an N_2-O_2 mixture, provided the feed material for the experiment. Following its inlet into the experimental setup, the gas was next swept through a flask which contained air, deionized water, or ethanol. The gas then flowed up through the desiccant and molecular sieve.

After filtration, the gas made its way to the RGA through a capillary tube, which caused the decrease in pressure necessary for operation of the RGA. The RGA itself operated under vacuum conditions, which were maintained by vacuum pumps. The signals produced by the RGA were transmitted to a computer for data analysis. The entire apparatus is shown in fig. 6.1.

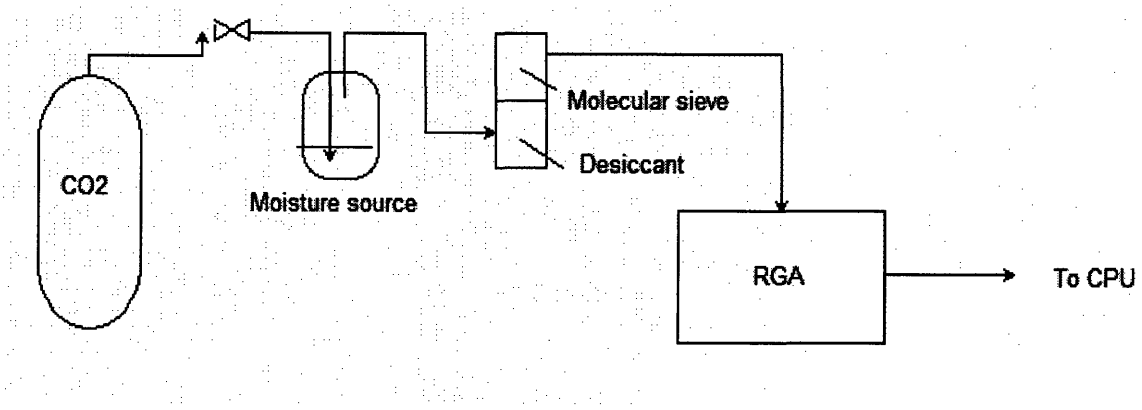

Figure 6.2: Diagram of Purification Experimental Setup

6.6.3 The commercial gas purifier

The commercial gas purifier selected for the experiment (Drierite model # 27068) was a packed column, 28.4 cm tall by 6.45 cm in diameter, as shown in figure 6.1. The entering gas was directed first through a desiccating region, containing 250 cc of anhydrous $CaSO_4$ under the brand name "Drierite", and then passed through a molecular sieve made of 250 cc of Al_2O_3 beads. The Drierite desiccant is capable of drying gases to a water vapor concentration of 0.005 mg/l, and the amount of desiccant present in the column can hold a total of 25 g of water before regeneration or replacement is required.

The alumina, which was subjected to a special surface treatment under a proprietary process by its manufacturer, Union Carbide, had a pore size of 5 Å, and thus was capable of the removal of impurities which have molecular dimensions smaller than this. It should be noted that because the CO_2 molecule is slightly smaller than 4 Å, it was possible that the adsorbed species would include some CO_2.

For the purposes of investigating the effectiveness of such a packed bed device in purification of the CO_2 coolant of the GFR, the experiment compared the compositions of CO_2 prior to and after purification. To accomplish this, a sample of impure CO_2 (containing water vapor, oxygen, hydrocarbons, argon, and potentially other chemical species), was sent to a residual gas analyzer (discussed further in section 6.6.4), which used mass spectroscopy to determine the makeup of the gas sample. This simple procedure acted as a control case for a second case, where the CO_2 was channeled through the gas purifier before being analyzed by the RGA.

Figure 6.3: Commercial Packed Column [Drierite, 2007]

In order to best ascertain the effects of the individual components of the sample gas, a series of gas samples were analyzed:

- Instrument grade CO_2, bubbled through deionized water with and without purification
- Industrial grade CO_2 with and without purification.
- Industrial grade CO_2, bubbled through ethanol with and without purification
- Industrial grade CO_2 and Ar-O_2 mixture, with and without purification

This combined approach to the investigation of gas purification is important because prior experimentation has demonstrated that the adsorption of impurities from a mixed stream of gases is generally dominated by one or two of the species of interest rather than being simply the sum of the adsorptions of the independent impurities [Yang, 2003].

6.6.4 The Residual Gas Analyzer (Dycor LC)

After reaching the vacuum that surrounds the mass spectroscopy hardware, the molecules of the incoming gas sample are ionized. The filament releases electrons after an electrical current heats it to the point of incandescence; these electrons then flow in the direction of the ionizer body due to the potential difference between the two components. Collisions between these electrons and the molecules of the gas sample cause the production of ions. Because the energy of the incoming electrons is greater than the bond strength of the molecules, the collisions often result in the breakage of these bonds. This complicated the analysis of the incoming gas, as is discussed later.

After the ions are formed, they are focused in the direction of the mass filter by a difference in potential. The quadrupole mass filter is made up of four parallel cylindrical rods of differing polarities onto which a constant DC current and a radio frequency alternating current are both applied. The oscillations induced by the poles caused the ions to either strike one of the rods, and escape detection, or to pass through the rods and proceed in the direction of the detector. A negative voltage applied to the exit lens attracts the positive ions and ensures their passage toward the detector. This application of constant current allowed the mass filter to select a single mass-to-charge ratio for detection. In order to obtain a spectrum which shows peaks for difference mass-to-charge ratios, the applied currents were periodically changed to allow the selection of a range of mass-to-charge ratios. This process is known as "sweeping" [McLafferty, 1980].

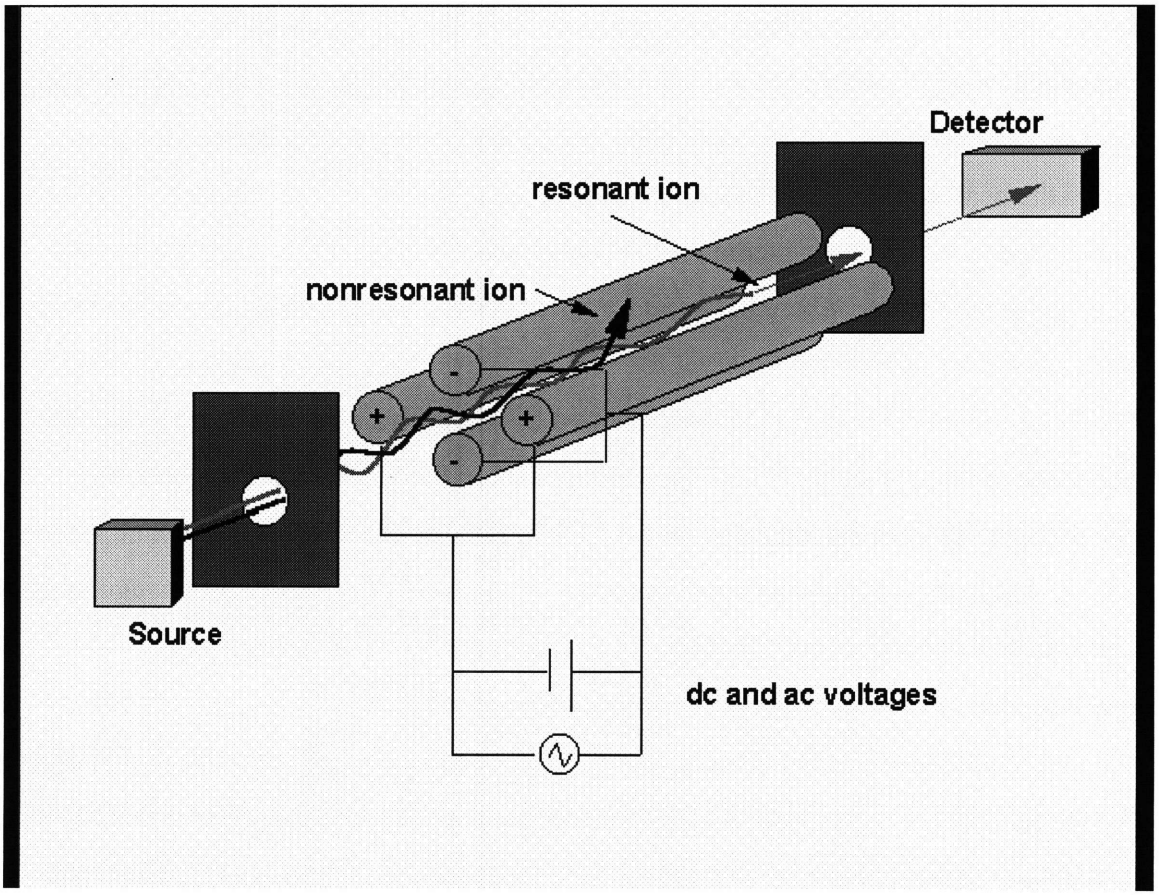

Figure 6.4: Schematic of quadrupole mass filter [Tissue, 1996]

Detection of the selected ions is achieved by a Faraday cup, a plate or cup shaped structure which emits a current (with a gain equal to unity) when ions strike its surface. The signal produced was then amplified and sent to the data acquisition system for processing. Alternatively, an electron multiplier could have been used to increase the sensitivity of the analyzer through the production of an electron cascade for each positive ion that struck the negatively charged multiplier.

6.6.5 Data Acquisition and Analysis

Management and analysis of the data from the RGA was handled by Dycor System 200, a software package provided with the RGA. The software recorded and displayed the partial pressure on the detector cup for each value of the mass-to-charge ratio; these partial pressures added up to the total pressure experienced by the Faraday cup, since the analyzer is evacuated. Each mass-to-charge ratio corresponds to one or more specific chemical species, and species which are detected in significant quantities

are indicated by a peak on the plot generated by the software. The total area under any given peak is the partial pressure for the chemical species in question. While the software was not capable of directly calculating the areas under these peaks, a simple Riemann sum of the peak could be calculated, as has been recommended in much of the literature on mass spectroscopy. This method was made simple by the fact that the software also has a bar-graph feature, where the pressure for each short range of mass-to-charge ratios is placed into the appropriate interval for analysis. When using this method, one must keep in mind that the partial pressures reported by the software cannot be used to derive the total quantities of each chemical species present in the analyzer at any given time. This is due to the fact that the vacuum pumps continually sweep out a significant portion of the gas sample, leaving only small amounts for analysis. As a result, the change in the peak area of a particular constituent of the gas stream after purification is not representative of the actual change in composition of the sample.

It should also be mentioned that additional complications exist in the analysis of the acquired data. For example, it was mentioned earlier that many molecules which enter the RGA are broken into their constituent atoms by collisions with energetic electrons from the filament. This means that the carbon dioxide which enters the RGA could appear at the detector as either CO_2, CO, O, or C. However, with some knowledge of stoichiometry, it was possible to ascertain what fraction of these species originated as CO_2, and which represent impurities. In addition to this complication, there was also the possibility that the gases entering the RGA could undergo fractionation: the change in gas composition due to differences in the flow regimes at the entrance and exit of the analyzer [Blessing, 2007]. It was assumed, for the current analysis, that the flow regimes into and out of the analyzer are the same, and that there is no net fractionation by the RGA. Additionally, each trial was run for a long period of time in the hopes that long-term averaging of the obtained data will reduce any small effects of fractionation.

6.6.5 Results and Conclusions

The most straightforward means by which to assess the ability of the purifier to remove various impurities from the gas stream was by direct comparison of the partial pressures of each species which entered the RGA. The pressures induced by a particular species were found by a simple Riemann sum of the corresponding peak, in some cases

added to the areas of related ionization peaks (e.g. a tall hydrogen peak induced by ionization of H_2O). The changes in pressures of the chemical species identified under the conditions investigated are shown in tables 6.3-6.7. Note that the presence of an air leak during the purification of wet CO_2 confounded the data on the presence of species other than CO_2 and H_2O, as large peaks appeared for N, O_2, and Ar under purification conditions. For this reason, this data has been omitted from table 6.3. Additionally, most of the volatile impurities found in other samples were not detected in the wet CO2 test, and are therefore not reported. It is believed that these impurities, while present in the initial gas stream, dissolved into the moisture source.

Table 6.3: Peak Areas of Wet Instrument Grade CO_2 Before and After Purification*

	Unpurified (torr)	Purified (Pa)	Percent Change
CO_2	1.80×10^{-5}	1.75×10^{-5}	-2.8%
H_2O	9.27×10^{-7}	7.63×10^{-7}	-17.7%
F	4.9×10^{-10}	2.52×10^{-10}	-48.6%

*The levels of other contaminants could not be determined reliably due to an air leak into the system while under purification.

Table 6.4: Peak Areas of Dry Industrial Grade CO_2 Before and After Purification

	Unpurified (torr)	Purified (Pa)	Percent Change
CO_2	4.84×10^{-5}	4.20×10^{-5}	-13.3%
H_2O	9.28×10^{-7}	7.86×10^{-7}	-15.3%
He	9.10×10^{-11}	2.20×10^{-11}	-75.8%
O_2	6.45×10^{-9}	8.45×10^{-9}	+31.0%
F	1.02×10^{-9}	5.00×10^{-10}	-51.0%
Ar	4.50×10^{-10}	2.60×10^{-10}	-42.2%
N	---	---	---
Cl	3.46×10^{-10}	6.10×10^{-11}	-82.4%
Oils and solvents	3.88×10^{-9}	1.59×10^{-9}	-59.0%

Table 6.5: Peak Areas of Ethanol-bearing Industrial Grade CO_2 Before and After Purification

	Unpurified (torr)	Purified (Pa)	Percent Change
CO_2	2.32×10^{-5}	1.81×10^{-5}	-22.0%
H_2O	1.56×10^{-6}	7.60×10^{-7}	-51.3%
He	2.09×10^{-10}	0	-100%
O_2	4.05×10^{-7}	1.08×10^{-8}	-97.3%
F	2.10×10^{-8}	4.00×10^{-10}	-98.1%
Ar	6.67×10^{-9}	2.90×10^{-10}	-95.7%
N	---	---	---
Cl	3.40×10^{-10}	1.52×10^{-10}	-55.3%
Ethanol	3.41×10^{-6}	1.78×10^{-6}	-47.8%
Oils, non-ethanol solvents	1.60×10^{-7}	5.30×10^{-10}	-99.7%

Table 6.6: Peak Areas of Ar-O2 and Industrial CO_2 Mixture Before and After Purification

	Unpurified (torr)	Purified (Pa)	Percent Change
CO_2	1.25×10^{-5}	1.10×10^{-5}	-12.0%
H_2O	7.99×10^{-7}	7.58×10^{-7}	-5.13%
He	1.00×10^{-11}	0	-100%
O_2	1.99×10^{-7}	2.28×10^{-7}	+14.6%
F	---	---	---
Ar	5.74×10^{-6}	6.48×10^{-6}	+12.9%
N	2.00×10^{-10}	9.00×10^{-11}	-55.0%
Cl	---	---	---
Oils and solvents	8.13×10^{-6}	8.11×10^{-6}	-0.246%

When attempting to interpret this data, a few points should be kept in mind. First, the data on the molecular components of each mixture are estimations, as these species were found in the sample as ions, some of which could be attributed to multiple sources. Oxygen radicals, for example, could have originated in O_2, CO_2, H_2O, ethanol, or a number of other compounds. Free radicals like these were assigned compound identities based on the relative fractions of each possible compound in the mixture, e.g. if O could be assigned to either CO_2 or H_2O, and the ratio of CO_2 to H_2O detected was 3:1, then 75% of the O signal would be assigned to CO_2, and 25% to H_2O.

As shown in the tables, the purifier shows significant removal of water from each experimental setup, confirming that a desiccant of this type would be useful in removal of water from the primary system of the GFR. The molecular sieve component of the purifier also appears useful for removal of trace amounts of volatile species such as

chlorine and fluorine; by extension the purifier would also be useful at removal of heavier volatiles like Cs, Rb, and I. The pressures of oils and solvents present were also decreased by a great degree in most of the cases. Unfortunately, the test investigating the ability of the purifier to remove noble gases from the waste stream remains inconclusive. This test was conducted following the trial using ethanol as a moisture source, and due to the unusual color change of the desiccant observed during the ethanol test (dark blue as opposed to the pink color which indicates saturation of the desiccant), it is thought that the purifier may have been damaged. The strange results of the Ar-O_2 test, which indicate an increase in both argon and oxygen, as well as reduction in the ability of the purifier to remove water and solvents, appear to confirm this. Nevertheless, this experiment has shown that a desiccant coupled with a molecular sieve can feasibly be used to passively and cost-effectively remove water and volatile species from a CO_2 stream. Further experimentation would be required to ascertain the effectiveness of such a setup in removal of the heavy noble gases from a CO_2 stream. Such experimentation would be quite simple, as the packed column can probably be disassembled and loaded with different sorbent materials for testing.

6.7 Handling of Krypton

Storage of krypton removed from the primary coolant is an attractive option, because it significantly reduces the probability of radionuclide escape to the atmosphere. The waste krypton could be simply directed into tanks or bottles and allowed to decay until it is safe for release, or could be maintained in on-site storage for an extended period of time. This krypton, however, represents a rather large volume when accumulated over the lifetime of the reactor, especially when it is considered that the waste gas will include not only Kr, but isotopes of Xe and a reasonable amount of CO_2, as the separation process is by no means perfect. For this reason, it may be desirable to perform controlled release of ^{85}Kr and its accompanying gases to the atmosphere. Such procedures, known as infinite dilution, are routinely performed by fuel reprocessing plants (note that future U.S. reprocessing plants are required to prevent the release of 90% of the ^{85}Kr they produce). Current regulations require that the total radioactive material above background released to the atmosphere result in doses of no more than 20 millirem for β emitters and

10 millirem for γ emitters. In addition, the concentrations of radioactive effluents are limited as shown in table 6.7.

Table 6.7: Radioactive Effluent Limits [10CFR50]

Isotope	Effluent Concentration Limits (μCi/ml)
^{3}H	7×10^{-7}
^{85}Kr	1×10^{-7}
^{129}I	4×10^{-11}
^{131}I	2×10^{-10}
^{134}Cs	2×10^{-10}
^{135}Cs	2×10^{-9}
^{136}Cs	9×10^{-10}
^{137}Cs	2×10^{-10}
^{140}Ba	2×10^{-9}

Because the continual purification of the primary coolant ensures that only small amounts of each of these isotopes are available for release to the environment each day, it would probably be rather simple to mix them with air prior to release in order to dilute them down to tolerable effluent concentrations. More important, of course, than this dilution, is the ability of this process to meet annual limits on total effluent. The EPA's standard on gaseous radioactive emissions requires that no more than 50,000 Ci/GWeY of ^{85}Kr be released to the atmosphere by a power plant. Therefore, the 1200 MWe GFR is limited to annual ^{85}Kr releases of 60,000 Ci. However, because the fission reaction results in the production of nearly 2 Ci/MWd_{th}, the GFR can be expected to produce nearly 30 times the regulatory limit. Therefore, onsite storage of ^{85}Kr and other waste gases removed from the primary will certainly be required.

6.8 Selection of Purification Methodology

Some degree of uncertainty remains in the final form of the coolant purification system, due to the lack of experimental data surrounding the use of the described technologies in purification of carbon dioxide. Nonetheless, it is possible to describe a general approach to the removal of impurities from the primary coolant. The first step in the purification process should be the filtration of dusts which accumulate in the gas during its circuit through the primary. The removal of dusts as an initial step will serve to protect the later purification equipment from clogging, and will thereby enhance the

material throughput of the purification system. Following this, desiccation of the stream must take place, in order to remove tritiated water and increase the efficiency of the later purification steps. After this must come the use of a getter to attract unreacted Ba and Cs, potentially a bed of heated titanium or another metal. Following this step, the remaining noble gases, and any other remaining species will be removed from the stream by the use of activated charcoal, zeolite beds, or selective permeation through capillary tubes. Further experimentation will be required to determine which would be more satisfactory, and what pore or capillary sizes would be required to extract the greatest quantity of the species of interest. Finally, before re-entering the primary coolant inventory, the gas must be filtered of dusts yet again, in order to prevent the migration of activated charcoal dusts throughout the primary system.

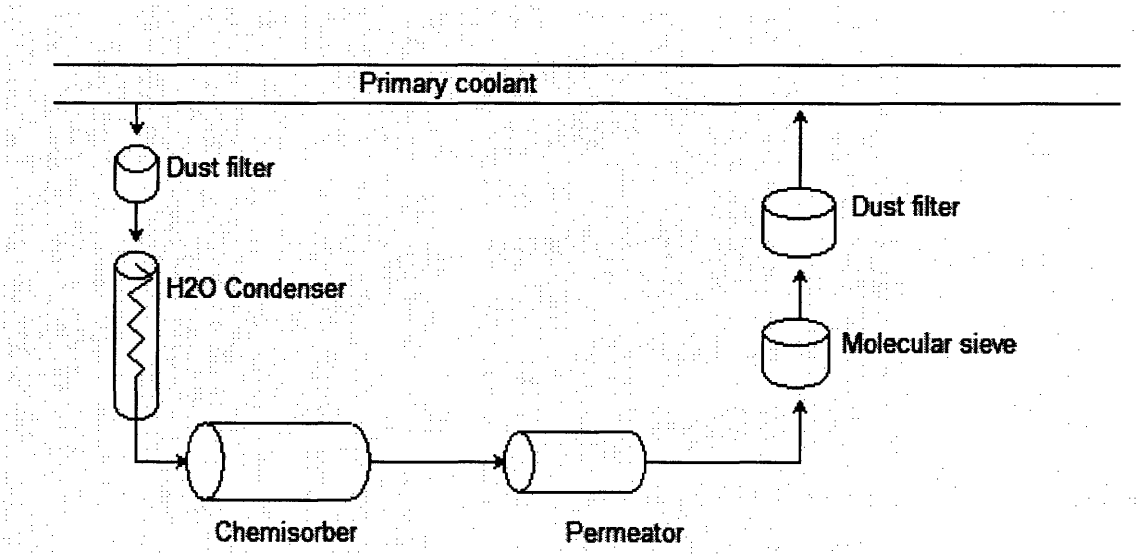

Figure 6.5: Proposed Primary Coolant Purification Setup

6.9 Containment Air Purification

Regardless of the system used to purify the primary coolant of fission products, a small percentage of these fission products will inevitably leak into the containment structure. In addition, there is always some probability that a large volume of radionuclide-bearing coolant will enter containment during a loss of coolant accident. For these reasons, it is important that the containment be equipped with some form of purification system which will keep its air safe for workers and additionally handle an influx of radionuclides during a LOCA. In order to deal with the assumed 1% daily

leakage rate from the primary system, it is recommended that the entire volume of containment air be cycled through a purification system once per day.

The methods described for potential use in purification of the primary coolant system all show promise in their extension to use in the containment structure. However, some appear a great deal more feasible than others. Of the methods discussed, selective permeation through capillary tubes seems most attractive for use in purification of the containment facility because of its passive safety and high level of throughput, as demonstrated through prior experimentation. Purification of the entire containment facility volume would require a flow rate of 8.10×10^6 cc/s, which should be directed through 2130 capillaries in order to retain the same level of performance as in Stern's 1978 tests. Activated charcoal could also be employed for selective adsorption of Kr and other contaminants from containment air, but such a technique could become less effective with time as the charcoal beds become saturated. In addition, the required bed size of such a charcoal trap would be larger than a permeator capable of performing the same task, as shown in table 6.8.

Table 6.8: Required Containment Purifier Volumes

Purification Method	Required volume
Capillary tube permeation	6.46×10^{-4} m^3
Activated charcoal	7.71×10^{-3} m^3
H-mordenite	1.19×10^{-3} m^3

6.10 Summary

This chapter addressed the issues involved in selecting methods for purification of the primary coolant inventory. A calculation involving the most problematic impurity, ^{85}Kr, led to the establishment of a desired purification rate of the primary coolant inventory each hour. Additional calculations confirmed that this rate would be sufficient to reduce the containment facility radiation hazard induced by the other radionuclides of concern. Methods examined for the removal of ^{85}Kr and other impurities included adsorption on solids, use of desiccants, permeation through membranes and capillary tubes, and cryogenic distillation. After an experiment investigated the efficiency of desiccant and solid sorbent in cleaning of CO_2 streams, with mixed results, a general process for purification of the primary coolant, including filtration, moisture separation, chemisorption, and physical adsorption of noble gases was recommended. Using the

information developed in this chapter, recommendations were also made for a system which would purify containment air of the radionuclides which leak into it on a daily basis.

Chapter 7: Pressure Transients

7.0 Introduction

As discussed in the section on fission product transport, the diffusion of radionuclides produced in the fuel occurs very slowly. This means that the bulk of the fission product transport is dominated by the fluctuations in pressure common to direct cycle systems. Knowledge of the effects of small pressure transients is therefore important in determining the potential radiation hazard induced by motion of the gas column. Likewise, an understanding of the large pressure drops which occur during accidents or refueling is necessary to determine the potential for the most radioactive of the fission products to be evacuated from the plena and enter the primary coolant. In this section, the transport of the gas volumes contained by the plena is studied through both simple hand calculation and computer modeling. In addition, the radiological consequences of small and large pressure transients are investigated.

7.1 Theory and Hand Calculation

While the models given in earlier sections describe diffusion of gases at steady state, under normal operating conditions, it is also necessary to consider the quantity of gas which exits the vent tube under transient conditions. While diffusion through the assembly and vent tubes can be expected to proceed in one direction as a result of concentration gradients (as discussed in chapter 4), the gas column will additionally move up and down slightly with changes in primary system pressure, a phenomenon commonly known as breathing. Far more crucial to the success of the vent system, however, is its behavior during the blowdown of the primary system to containment pressure during accidental depressurization.

In the event of blowdown to post-LOCA containment pressure, the maximum flow velocity is equal to the speed of sound for the fluid. In order to determine the speed of sound for a gas, one must first find the gas constant for the gas in question,

$$R = \frac{8314 J/kg \cdot K}{M} \qquad (7.1)$$

where M is the molecular weight of the gas. Next, the effective temperature of the gas entering the low pressure region may be determined using

$$T = (273 + T_{vent}) \cdot \left(\frac{p}{p_o}\right)^{(\gamma-1)/\gamma}$$

$$\gamma = \frac{c_p}{c_v} \qquad (7.2)$$

$$\frac{p}{p_o} = \left(\frac{2}{\gamma+1}\right)^{\gamma/(\gamma-1)}$$

From this, it is possible to calculate the speed of sound in the fluid as

$$v = \sqrt{\gamma RT}. \qquad (7.3)$$

The mass flow rate of gas into the low pressure region is then

$$\dot{m} = \rho A v, \qquad (7.4)$$

where ρ is given by

$$\rho = \frac{p}{RT}. \qquad (7.5)$$

The relevant ideal gas properties for CO_2 at 20 MPa and 650 °C, as well as results of intermediate calculations are given in Table 7.1.

Table 7.1: Summary Results of Blowdown Hand Calculations

M	44 g/mol
R	188.95 J/kg·K
γ	1.22
v	482.0 m/s
ρ	110 kg/m^3

From these formulae [Winterton, 1981] and information about the system under study, the flow rate was determined to be 2.67 kg/s per vent tube, which corresponds to 8.01 kg/s for an entire 3-tube assembly. This value was obtained using an estimated vent tube temperature of 650 °C (given by Pope as the temperature of the reflector and nearby structures), a vent tube inner diameter of 8 mm, the same dimension specified for the GFR coolant tubes [Pope, 2006], and a fluid made entirely of CO_2 fill gas. It is important to note that the flow rate calculated represents primarily fill gas, and not 8.01 kg/s of radionuclides. It is also important to note that this flow rate is only an *initial* flow rate. As

the system loses gas, its pressure drops below the critical pressure, and so the flow rate decreases sharply. This means that the total mass lost by the system is given as

$$M = M_{initial} e^{-t\dot{m}/M_{initial}}, \qquad (7.6)$$

Where $M_{initial}$ = initial mass contained by system, kg

t = time after pressure drop, s

m = initial mass flow rate after pressure drop, kg/s

This relationship also describes the change in system pressure. This means that during a sudden, accidental blowdown, the vent system can achieve a pressure of 0.1 MPa in approximately 0.73 seconds, assuming a volume of 0.01 m^3 of gas per assembly, which includes the vent tubes, plena and gap between cladding and fuel. This time to reduce pressure is far shorter than is plausible for a total primary coolant system depressurization to occur, which Pope calculated as approximately 10 minutes. From this it can be concluded that the vented assembly can quickly follow even large and rapid changes in pressure, thereby reducing the risk of damage to the cladding by differential pressure. A simple criterion for this requirement is that the ratio of vent area to intra-assembly volume is larger than the ratio of primary system break area to primary system volume. In the present example one has

Vent tube area/assembly volume = 0.015 m^{-1}

Primary break area/primary volume=0.000032 m^{-1}

where the primary break area is that of a double-ended guillotine break LOCA scenario [Pope, 2006]. From this comparison it is clear that rupture of the cladding due to overpressure is highly not plausible.

It is important to recall that this calculation assumed that the gas flowing into the low pressure region was made up entirely of CO_2. In addition, this estimate describes the flow rate which would occur given an instantaneous and total depressurization. In practice, depressurizations for refueling and maintenance are usually conducted slowly, often over the course of weeks, and are rare. Far more common are the much smaller fluctuations in pressure due to "breathing", and so this estimate represents a conservative worst-case scenario.

While breathing is of greater concern due to its much greater frequency than total depressurization incidents, it is also of less radiological consequence. While total

depressurization would result in the total release of the contents of the vent system very quickly, the small fluctuations in pressure known as breathing would result in only small momentary "puffs" of activity as the gas column shifts forward for a short period of time. For example, using the ideal gas law,

$$PV = nRT \tag{7.7}$$

Where P = pressure

V = volume

n = quantity of gas

R = universal gas constant

T = absolute temperature

one can derive equations describing the volume fraction of gas expelled from each plenum in terms of the initial and final pressures (P_b and P_a, respectively) and plenum volumes. In what follows, slug flow is assumed, which would imply use of baffles in the plena to avoid turbulent mixing. The plan at present is to fill the plena with steel or ceramic fiber wool, which will promote slug flow while only taking up 2% of the free volume of each plenum. In addition, it is assumed that the breathing process is isothermal.

For one plenum:

$$F_{1,1} = 1 - \left(\frac{P_a}{P_b}\right) \tag{7.8}$$

For two plena in series

$$F_{1,2} = 1 - \left(\frac{P_a}{P_b}\right)\left(\frac{V_1 + V_2}{V_1}\right)$$
$$F_{2,2} = \left[1 - \frac{P_a}{P_b}\right]\left[\frac{V_1 + V_2}{V_2}\right] \tag{7.9}$$

For three plena in series

$$F_{1,3} = 1 - \left(\frac{P_a}{P_b}\right)\left(\frac{V_1 + V_2 + V_3}{V_1}\right)$$

$$F_{2,3} = \left(\frac{V_1 + V_2}{V_2}\right) - \left(\frac{P_a}{P_b}\right)\left(\frac{V_1 + V_2 + V_3}{V_2}\right) \qquad (7.10)$$

$$F_{3,3} = \left[1 - \frac{P_a}{P_b}\right]\left[\frac{V_1 + V_2 + V_3}{V_3}\right]$$

In the above sequence, $F_{i,j}$ is defined as the fraction of the mass contained in plenum i which escapes to the primary coolant by exiting plenum j.

It is anticipated that pressure will drop from 20 MPa to approximately 14 MPa (zero power value) often, due to use of a direct cycle. It is also expected that pressure will decrease to approximately 12 MPa during inventory control at 30% of full power. Assuming that the plena are of equal sizes and that slug flow occurs, the release fractions from each plenum are found in table 7.2.

Table 7.2: Escape Fractions Determined as a Result of Breathing (Hand Calculations, eq. 7.8-7.10)

	14 MPa	12 MPa
1 Plena		
$F_{1,1}$	3/10	2/5
2Plena		
$F_{1,2}$	None; negative F	None; negative F
$F_{2,2}$	3/5	4/5
3 Plena		
$F_{1,3}$	None; negative F	None; negative F
$F_{2,3}$	None; negative F	1/5
$F_{3,3}$	9/10	All, F>1

This clearly indicates the advantage of using multiple plena. When multiple plena are used, the first plena in the series release none of their contents. This is a very important conclusion because the first plena in the series contain the most highly radioactive fission products, having been released from the fuel more recently than the gas further downstream. While the downstream gas is still radioactive, the additional holdup which

has been afforded by the presence of the upstream plenum and vent tubes makes the released gas far lower in activity. As the pressure cycles up and down repeatedly, the non-vented gas will move back and forth along the vent path in accordion fashion, with no net forward progress.

7.2 RELAP Calculations

The next phase in the analysis of pressure transients was to utilize RELAP to confirm the hand calculations outlined previously. In order to simulate LOCA conditions, a set of inputs were created which modeled the vent system as a series of two or three cylindrical volumes and interconnecting tubes, as shown in fig. 7.1-7.4. The final tube in each setup directs flow through a valve and into a large volume (chosen so that the buildup in pressure of this volume would not affect the progression of the transient). A set of eight inputs were run for various numbers and volumes of plena, in order to ascertain the impact of these factors on the speed at which the vent system can follow blowdown. Details of the model, with sample input and output are presented in Appendix B.

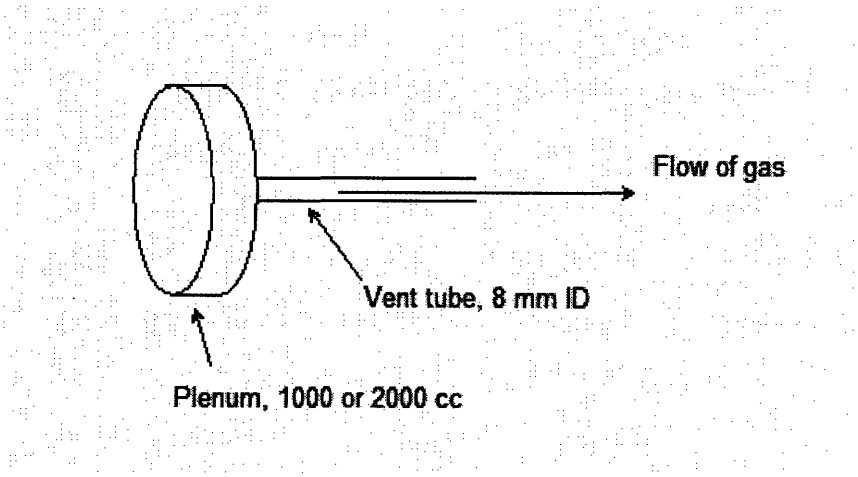

Figure 7.1: RELAP Model Geometry for Single Plenum Cases

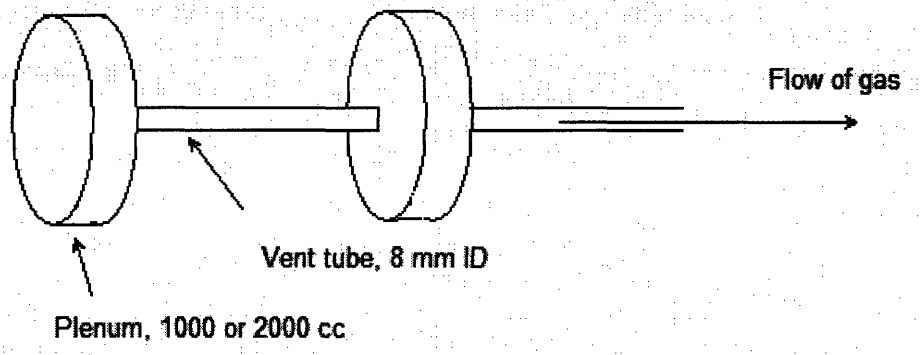

Figure 7.2: RELAP Model Geometry for Two Plenum Cases

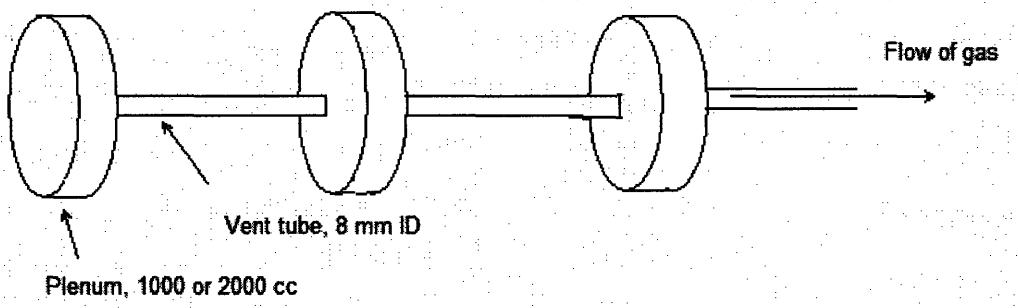

Figure 7.3: RELAP Model Geometry for Three Plenum Cases

In all cases, the system was able to drop to containment post-LOCA design pressure (0.7 MPa) in under three seconds, much faster than would be plausible for a LOCA to decrease the primary pressure. Previous RELAP modeling of the GFR indicated that blowdown to containment pressure during a LOCA (with a 100 cm^2 break of the cold leg) would take approximately 700 s [Pope, 2006]. A summary of the cases investigated and RELAP estimates of their corresponding times to pressure equalization is shown in Table 7.3.

Table 7.3: Summary of Time to Pressure Equalization for Blowdown Scenarios

Case	Plenum Volumes*	Time to 0.7 Mpa
1	2000 cc	0.90 s
2	1000 cc	0.75 s
3	2000 cc	1.15 s
	1000 cc	
4	1000 cc	0.95 s
	1000 cc	
5	2000 cc	1.40 s
	1000 cc	
	1000 cc	
6	2000 cc	1.60 s
	2000 cc	
	1000 cc	
7	1000 cc	1.20 s
	1000 cc	
	1000 cc	
8	1000 cc	1.05 s
	2000 cc	

*For a given case the plena are in series in descending order.

As can be seen in the table, there is a clear correlation between the available plenum volume and the amount of time required to reach 0.7 MPa. In addition, the separation of plena by vent tubes adds a considerable length to the time required. In any case, the time required is of little consequence, since all of these setups are capable of decreasing pressure far more quickly than the overall primary system can depressurize.

Following the investigation of the effects of a LOCA on the venting system, it was necessary to study the increased transport of radionuclides through the small pressure drops known as breathing. In order to gain information about the behavior of the system under smaller transients, the RELAP model constructed for the blowdown case was modified to make the initial pressure at the outlet of the vent system 14 MPa. In each case the mass flow rate of the gas was calculated within each volume (plenum or vent tube). During each test, the largest mass flow rates were experienced by the downstream tubes and plena in series, indicating that the lower activity portions of the gas would be transported the fastest. In addition, within a few seconds, the gas flow dropped the vent system pressure until the vent system reached equilibrium with its surroundings. The results of the mass flow rate calculations are summarized in Tables 7.4-7.10.

Table 7.4: Mass Flow Data for Breathing in One 1000 cc Plenum*

Time (s)	Plenum mass flow (kg/s)	Vent tube mass flow (kg/s)
0	0	0
0.05	0.29003	0.32847
0.1	0.33145	0.37401
0.15	0.21842	0.24559
0.2	7.16363×10^{-2}	8.03248×10^{-2}
0.25	0	0

*Following sudden 20 MPa→14MPa boundary pressure reduction

Table 7.5: Mass Flow Data for Breathing in One 2000 cc Plenum*

Time (s)	Plenum mass flow (kg/s)	Vent tube mass flow (kg/s)
0	0	0
0.05	0.33940	0.36296
0.1	0.48994	0.52259
0.15	0.45830	0.48724
0.2	0.33473	0.35492
0.25	0.18336	0.19403
0.3	2.93428×10^{-2}	3.09150×10^{-2}
0.35	0	0

*Following sudden 20 MPa→14MPa boundary pressure reduction

Table 7.6: Mass Flow Data for Breathing from One 2000 cc plenum (1) and One 1000 cc plenum (2)*

Time (s)	Plenum 1 mass flow (kg/s)	Vent tube 1 mass flow (kg/s)	Plenum 2 mass flow (kg/s)	Vent tube 2 mass flow (kg/s)
0	0	0	0	0
0.05	0.22249	0.23732	0.34989	0.37103
0.1	0.35331	0.37683	0.55714	0.58970
0.25	0.38422	0.40920	0.60074	0.63324
0.2	0.34413	0.36596	0.53325	0.55990
0.25	0.26705	0.28363	0.41068	0.42985
0.3	0.17483	0.18550	0.26723	0.27900
0.35	7.77971×10^{-2}	8.24648×10^{-2}	0.11828	0.12321
0.4	0	0	0	0

*Following sudden 20 MPa→14MPa boundary pressure reduction

Table 7.7: Mass Flow Data for Breathing from Two 1000 cc Plena*

Time (s)	Plenum 1 mass flow (kg/s)	Vent tube 1 mass flow (kg/s)	Plenum 2 mass flow (kg/s)	Vent tube 2 mass flow (kg/s)
0	0	0	0	0
0.05	0.15512	0.17553	0.33333	0.36180
0.1	0.23123	0.26133	0.49280	0.53298
0.15	0.22514	0.25412	0.47675	0.51341
0.2	0.17341	0.19551	0.36518	0.39180
0.25	0.10510	0.11839	0.22038	0.23579
0.3	3.34231×10^{-2}	3.76109×10^{-2}	6.97840×10^{-2}	7.44416×10^{-2}
0.35	0	0	0	0

*Following sudden 20 MPa→14MPa boundary pressure reduction

Table 7.8: Mass Flow Data for Breathing from One 2000 cc Plenum (1) and Two 1000 cc Plena (2,3)*

Time (s)	Plenum 1 mass flow (kg/s)	Vent tube 1 mass flow (kg/s)	Plenum 2 mass flow (kg/s)	Vent tube 2 mass flow (kg/s)	Plenum 3 mass flow (kg/s)	Vent tube 3 mass flow (kg/s)
0	0	0	0	0	0	0
0.05	0.17636	0.18756	0.26692	0.28077	0.35616	0.37120
0.1	0.26392	0.28160	0.41895	0.44373	0.59167	0.61948
0.15	0.31528	0.33587	0.49408	0.52133	0.68171	0.70997
0.2	0.30957	0.32952	0.48289	0.50841	0.65850	0.68311
0.25	0.27197	0.28926	0.42217	0.44354	0.56909	0.58830
0.3	0.21645	0.23006	0.33456	0.35086	0.44661	0.46038
0.35	0.15198	0.16144	0.23402	0.24504	0.30979	0.31859
0.4	8.30785×10^{-2}	8.81953×10^{-2}	0.12749	0.13331	0.16754	0.17195
0.45	1.22954×10^{-2}	1.30254×10^{-2}	1.86662×10^{-2}	1.94183×10^{-2}	2.39422×10^{-2}	2.43777×10^{-2}
0.5	0	0	0	0	0	0

*Following sudden 20 MPa→14MPa boundary pressure reduction

Table 7.9: Mass Flow Data for Breathing from Two 2000 cc Plena (1,2) and One 1000 cc Plenum (3)*

Time (s)	Plenum 1 mass flow (kg/s)	Vent tube 1 mass flow (kg/s)	Plenum 2 mass flow (kg/s)	Vent tube 2 mass flow (kg/s)	Plenum 3 mass flow (kg/s)	Vent tube 3 mass flow (kg/s)
0	0	0	0	0	0	0
0.05	0.14745	0.15673	0.28742	0.29911	0.36153	0.37449
0.1	0.22004	0.23479	0.46515	0.48660	0.61475	0.63965
0.15	0.27321	0.29106	0.56560	0.58980	0.73221	0.75810
0.2	0.27930	0.29739	0.57567	0.59914	0.73726	0.76050
0.25	0.25824	0.27480	0.52960	0.55020	0.67115	0.69000
0.3	0.22052	0.23455	0.45025	0.46704	0.56550	0.57978
0.35	0.17360	0.18455	0.35303	0.36570	0.44000	0.45008
0.4	0.12166	0.12929	0.24651	0.25506	0.30522	0.31162
0.45	6.69518E-02	7.11195E-02	0.13520	0.13974	0.16642	0.16963
0.5	1.09295E-02	1.15934E-02	2.18432E-02	2.24828E-02	2.63587E-02	2.66851E-02
0.55	0	0	0	0	0	0

*Following sudden 20 MPa→14MPa boundary pressure reduction

Table 7.10: Mass Flow Data for Breathing from Three 1000 cc Plena*

Time (s)	Plenum 1 mass flow (kg/s)	Vent tube 1 mass flow (kg/s)	Plenum 2 mass flow (kg/s)	Vent tube 2 mass flow (kg/s)	Plenum 3 mass flow (kg/s)	Vent tube 3 mass flow (kg/s)
0	0	0	0	0	0	0
0.05	0.11450	0.12890	0.23461	0.25234	0.35050	0.36919
0.1	0.16803	0.18995	0.35875	0.38816	0.56181	0.59339
0.15	0.18659	0.21076	0.39700	0.42848	0.61430	0.64602
0.2	0.17103	0.19306	0.36258	0.39051	0.55490	0.58121
0.25	0.13650	0.15400	0.28863	0.31032	0.43793	0.45720
0.3	9.36814E-02	0.10564	0.19762	0.21216	0.29766	0.30996
0.35	4.76953E-02	5.37599E-02	0.10040	0.10765	0.15030	0.15616
0.4	8.79274E-04	9.78279E-04	1.75286E-03	1.80158E-03	2.17301E-03	2.06191E-03
0.45	0	0	0	0	0	0

*Following sudden 20 MPa→14MPa boundary pressure reduction

Table 7.11: Mass Flow Data for Breathing from One 1000 cc Plenum and One 2000 cc Plenum

Time (s)	Plenum 1 mass flow (kg/s)	Vent tube 1 mass flow (kg/s)	Plenum 2 mass flow (kg/s)	Vent tube 2 mass flow (kg/s)
0	0	0	0	0
0.05	0.10524	0.13265	0.34503	0.38169
0.1	0.16981	0.21380	0.55293	0.61081
0.15	0.18415	0.23179	0.59902	0.66072
0.2	0.16430	0.20675	0.53401	0.58820
0.25	0.12777	0.16076	0.41503	0.45667
0.3	8.55793E-02	0.10766	0.27785	0.30550
0.35	4.26327E-02	5.36245E-02	0.13837	0.15204
0.4	3.31371E-04	4.12119E-04	1.04156E-03	1.08014E-03
0.45	0	0	0	0

With this information on mass flow rates in hand, it was possible to determine the mass of CO_2 which is evacuated from each plenum during the transient by integrating over the length of each time step. The results of this calculation are summarized in Table 7.12.

Table 7.12: Total Mass Flow From Plena During Breathing

Case	Plenum	Cumulative mass flow (kg)
1	1000 cc	0.0535
2	2000 cc	0.0975
3	2000 cc	0.0970
	1000 cc	0.1490
4	1000 cc	0.0521
	1000 cc	0.1060
5	2000 cc	0.0958
	2000 cc	0.1473
	1000 cc	0.1974
6	2000 cc	0.0943
	1000 cc	0.1887
	1000 cc	0.2380
7	1000 cc	0.0519
	1000 cc	0.1046
	1000 cc	0.1558
8	1000 cc	0.0440
	2000 cc	0.1432

The total mass contained by each plenum at the start of the transient is 0.133 kg for each 1000 cc plenum and 0.267 kg for each 2000 cc plenum. Knowing this, it was possible to calculate the fractional release from each plenum. The results of this calculation are shown in table 7.12. In cases where the total efflux from a plenum is greater than the initial plenum mass, the difference is applied to the next plenum in succession. It should be noted that although the gases in each plenum expand, often advancing into the next plenum in succession, only a portion of the total reaches the end of the vent path by the end of the transient. The remaining gas is assumed to be contained by the vent system. The fraction of each plenum's mass which exits the vent system and enters the primary system is shown in table 7.13.

Table 7.13: Gas Release During Breathing for Venting Scenarios*

Case	Plenum volume	Fraction released from plenum	Fraction released to primary	Hand calculated fractional release to primary
1	1000 cc	0.401	0.401	0.3
2	2000 cc	0.366	0.366	0.3
3	2000 cc	0.423	0.0592	0
	1000 cc	1	1	0.9
4	1000 cc	0.391	0	0
	1000 cc	0.795	0.795	0.6
5	2000 cc	0.652	0	0
	2000 cc	1	0.481	0.25
	1000 cc	1	1	1
6	2000 cc	0.954	0	0
	1000 cc	1	0.785	0.2
	1000 cc	1	1	1
7	1000 cc	0.389	0	0
	1000 cc	0.953	0.169	0
	1000 cc	1	1	0.9
8	1000 cc	0.331	0	0
	2000 cc	0.536	0.536	0.45

*Following sudden 20 MPa→14MPa boundary pressure reduction

These results, particularly those describing the gas release to the primary coolant, fit reasonably well with the predictions made in table 7.2, which are reproduced in table 7.13 for the purposes of comparison. Unfortunately, it is clear that the original hand calculations cannot be considered conservative. One of the most important results that

can be derived from this table is that the presence of multiple plena effectively guards the earlier plena in the series from large scale gas release. This is important because the earliest plena contain the most highly radioactive gases, as discussed in detail in chapter 4. Another important result is that the presence of large plena early in the series, which is desirable from the standpoint of radionuclide holdup and decay, is apparently counterproductive when viewed in terms of the results of small pressure transients. This can be observed most clearly in the data on case 6, and to a lesser degree in the data on case 5. It can be seen that a drop in pressure in a large plenum leads to the expansion of a large volume of gas, in turn forcing a larger displacement of the gas in the next plenum in sequence. This effect is most pronounced in case 6, where a large plenum is followed immediately by a smaller one, and can be seen to a lesser degree in case 5, where the presence of a second large plenum in the sequence offers significant resistance to the force imposed by the expansion of the gases in the first plenum.

7.3 Release of radionuclides during pressure transients

7.3.1 Release during breathing

As demonstrated in chapter 4, the use of a sequence of large plena is desired because of the ability of such a configuration to reduce fission product activity. On the other hand, the use of fewer numbers of small plena would at first look to be favorable because of the higher rates of gas release, which in the preceding discussion were tied to sequences of large plena. In order to compare the effects of these two conflicting phenomena, it is necessary to compare the total activity releases resulting from the breathing transient in each venting scenario. For each of the seven cases investigated, estimates of fission product inventory were made for each plenum. These estimates were made using a modification to the MATLAB code discussed in chapters 3 and 4. This modified code can be found in appendix A. For each case, the total currents into and out of each plenum were found, and the difference between the two values, less the amount which decayed during each successive time step was assumed to represent the change in activity content of the plenum in question. The plenum entrances and exits were represented as "effective path lengths" as discussed in chapter 4, as the MATLAB code

does not directly take into account the presence of the plena. For reference, the vent path lengths at the entrances and exits of the plena under study are shown in table 7.14.

Table 7.14: Effective Vent Path Lengths for Plenum Activity Calculation

Case	Plenum	Entering Path Length (cm)	Exiting Path Length (cm)
1	1000 cc	1	514
2	2000 cc	1	1025
3	2000 cc	1	1025
	1000 cc	1179	1694
4	1000 cc	1	514
	1000 cc	667	1179
5	2000 cc	1	1025
	2000 cc	1179	2308
	1000 cc	2462	2874
6	2000 cc	1	1025
	1000 cc	1179	1692
	1000 cc	1846	2359
7	1000 cc	1	514
	1000 cc	677	1179
	1000 cc	1333	1846
8	1000 cc	1	514
	2000 cc	677	1692

Using this information, plenum activity levels were calculated for the radioactive isotopes ^{133}Xe and ^{85}Kr. These specific isotopes were selected in order to determine the impact of vent path configuration on both long- and short-lived nuclides. For the sake of completeness, ^{85}Kr is also investigated due to concerns that a significant amount of it is held up in the vent system without decay. The release of these species to the primary coolant during breathing is summarized for each case in tables 7.15-16.

Table 7.15: Xe-133 Activity Release to Primary Coolant During Breathing Transient*

Case	Plenum	Activity Release (Ci)	Total (Ci)
1	1000 cc	52.0	52.0
2	2000 cc	48.3	48.3
3	2000 cc	7.81	7.81
	1000 cc	3.44×10^{-6}	
4	1000 cc	0	9.64
	1000 cc	9.64	
5	2000 cc	0	1.65×10^{-6}
	2000 cc	1.65×10^{-6}	
	1000 cc	0	
6	2000 cc	0	2.70×10^{-6}
	1000 cc	2.70×10^{-6}	
	1000 cc	4.42×10^{-12}	
7	1000 cc	0	0.0158
	1000 cc	0.0158	
	1000 cc	1.50×10^{-7}	
8	1000 cc	0	18.3
	2000 cc	18.3	

*Following sudden 20 MPa→14MPa boundary pressure reduction

Table 7.16: Kr-85 Activity Release to Primary During Breathing Transient*

Case	Plenum	Activity Release (Ci)	Total (Ci)
1	1000 cc	3609	3609
2	2000 cc	9080	9080
3	2000 cc	1467	11094
	1000 cc	9627	
4	1000 cc	0	11221
	1000 cc	11221	
5	2000 cc	0	11440
	2000 cc	7735	
	1000 cc	3705	
6	2000 cc	0	13254
	1000 cc	7556	
	1000 cc	5698	
7	1000 cc	0	10954
	1000 cc	2383	
	1000 cc	8752	
8	1000 cc	0	7494
	2000 cc	7494	

*Following sudden 20 MPa→14MPa boundary pressure reduction

From the data on ^{133}Xe, it is clear that extension of the vent path through the use of plena, particularly large plena, is beneficial in reducing the activity released during a small pressure transient. This same result can be extended to all nuclides of comparable half life. For isotopes with lengthy half-lives, however, extension of the vent path appears to increase the activity released during a small pressure transient. This occurs because the long half-lives of species like ^{85}Kr produce nearly equal activity levels in equal plenum volumes, regardless of the locations or volumes of the individual plena. The increase in plenum volume increases the activity available for expulsion to the primary. However, because the use of a single plenum allows less holdup of other species which decay with greater frequency, more information is needed to ascertain which configuration is better suited to use in the GFR.

7.3.2 Release during blowdown

In the event of a large break LOCA, the most conservative assumption is the total release to containment of the radioactive contents of the primary coolant system and the assembly vent system. The primary system contents can be conservatively predicted as equal to the end-of-lifetime inventories of each radionuclide, as calculated in chapter 4. In total, these nuclides contribute about 10 million Curies (almost entirely of ^{85}Kr) if purification of the primary coolant is not assumed. It should be noted that this activity estimate does not include decay by the N-16 present in the primary coolant. If purification of the primary coolant takes place under the guidelines set in chapter 6, the final primary coolant activity will be on the order of tens or hundreds of Curies instead of millions, as shown in table 7.18. Total activity present in the assembly vent system prior to the transient was predicted using the same methodology as was described in section 7.3.1, and is summarized in tables 7.17 and 7.18. As can be seen, the venting configurations which have the largest plenum volume are those which contain the highest ^{85}Kr activity. This presents a considerable disadvantage to the use of a sequence of large plena.

Table 7.17: EOL Vent system and Unpurified Coolant Kr-85 Activity for 8 Configurations

Case	Vent system activity (Ci)	Coolant Activity (Ci)	Total Activity release (Ci)
1	8576	8.49×10^6	8.49×10^6
2	17800	4.99×10^6	5.01×10^6
3	23577	2.38×10^6	2.40×10^6
4	16994	4.23×10^6	4.25×10^6
5	29713	5.56×10^5	5.59×10^6
6	34001	1.08×10^6	1.11×10^6
7	22110	1.99×10^6	2.01×10^6
8	22557	2.38×10^6	2.40×10^6

Table 7.18: EOL Vent System and Hourly Purification Coolant Kr-85 Activity for 8 Configurations

Case	Vent system activity (Ci)	Coolant Activity (Ci)	Total Activity release (Ci)
1	8576	98.1	8674
2	17800	59.5	17860
3	23577	27.7	23605
4	16994	50.6	17045
5	29713	3.75	29717
6	34001	10.6	34012
7	22110	22.7	22133
8	22557	27.7	22585

7.3.3 Selection of Vent Path Configuration

As demonstrated previously, the selection of a configuration for the vent path (i.e. number and size of plena) is complicated by the presence of several conflicting effects. While any of the seven cases studied could be utilized in the final design, it would be prudent to examine the competing effects in order to determine which configuration best fulfills three goals of venting:

- Low coolant activity levels, by virtue of path length or ability to purify
- Low efflux of activity during breathing transient
- Low efflux of activity during severe depressurization.

First, as shown in detail in chapter 4, the extension of the vent path through the use of a sequence of large plena increases the holdup time of the transported species, resulting in lower levels of primary coolant activity. This effect is most dramatic at the shorter vent path lengths; extension of the effective vent path length beyond roughly 1300 cm does

not result in nearly the reduction in coolant activity that extension to this point does. This is an important result, because the extension of the vent path length through use of additional plenum volume coincides with increased release of highly radioactive plenum contents during both breathing and severe depressurization. In fact, because the bulk of the activity released is due to the long-lived species ^{85}Kr and ^{137}Cs, it would almost seem beneficial to speed the transport of these species through the vent system, allowing them to be purified from the primary coolant sooner, and reducing the consequences of changes in system pressure. Indeed, as shown in table 7.18, the hourly purification of the primary coolant results in a much more massive reduction in coolant radionuclide inventory than does the extension of the vent path. This indicates that the benefits of vent path extension through use of multiple large plena do not nearly outweigh the consequences of large, sudden pressure changes in such a configuration.

In addition, while the use of a short vent path increases the probability that shorter lived species will survive the venting process (especially in the presence of breathing transients), it is clear that the use of a robust purification system can remove these species from the coolant with a great deal of efficiency. Furthermore, shorter vent paths reduce the quantity of long-lived species which exit the plena due to gas expansion during breathing transients. Because these species dominate the activity inventory of both the plena and the primary coolant, their release is deemed to be of greater importance. Furthermore, while each of the venting configurations investigated can respond quickly in the event of a sudden decrease in system pressure, the configurations with the shortest total vent paths respond with the greatest expediency. For this reason, it would appear that a single small plenum should be employed in each assembly for radionuclide holdup. However, such a configuration would likely be complicated to engineer. Instead, as a compromise, it is recommended that two small plena be employed in each assembly in order to compromise between the additional decay time afforded to short-lived nuclides by extension of the vent path and the reduction in plenum inventories available for release during a blowdown situation. Such a configuration allows one of the fastest times to pressure equalization, one of the lowest releases of radionuclides during both breathing (due to the shielding of the upper axial plenum by the large lower annular plenum), and a moderate release of activity during severe drops in system pressure.

This approach is particularly attractive because it could be modified to support either venting directly to the coolant or venting to a grid-plate collection system merely by changing the vent location from the outer to inner periphery of the lower annular plenum. The final configuration of the vent system within the assembly is shown in figure 7.4. Note that this arrangement allows use of six downflow tubes rather than the three previously specified.

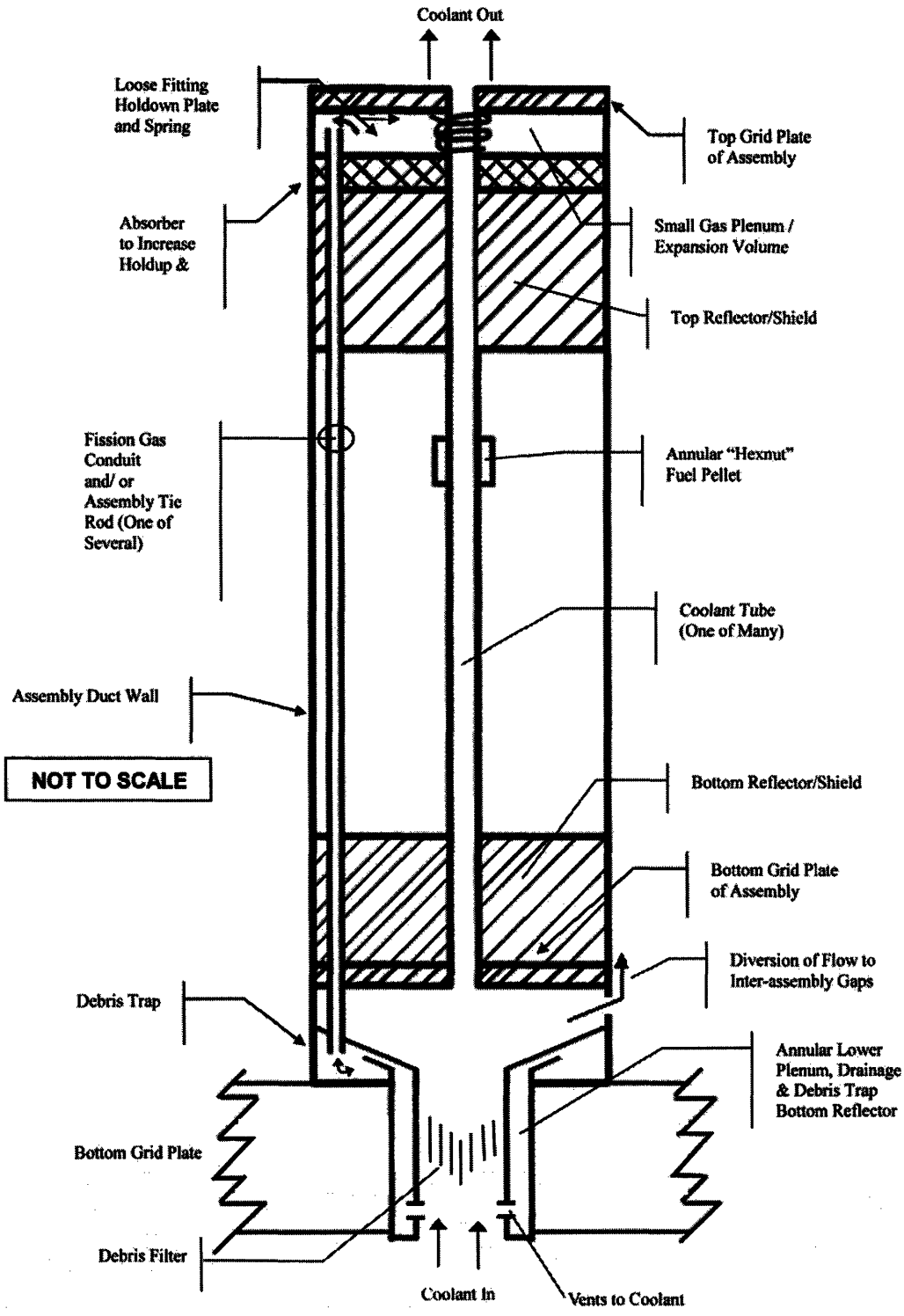

Figure 7.4: Final Assembly Configuration

7.3.4 Mitigating Factors

Even with holdup in the plena and purification of the primary coolant, a significant amount of activity remains to be released into the containment in the event of an accident or change in operating conditions such as refueling. This is because the cladding, one of the earliest defenses against fission product release, has effectively been removed under this analysis, and because a direct cycle power conversion system has been employed. For this reason, it is important to take steps to reduce the probability of leakage of the primary coolant. Engineering of tight-clearance turbomachinery shaft seals and proper maintenance of primary system components are important in maintaining a low daily leak rate. However, the most important goal in preventing escape of radionuclides from the primary is a reduction of the need to perform low-pressure operations, especially refueling, which also breaches the primary system boundary. To this end, it is recommended that the GFR refuel at or near operating pressures, in order to reduce the potential for leakage of radionuclide-bearing coolant into the containment structure. Additionally, it will be necessary to utilize a robust system for purification of the containment air, as discussed in chapter 6.

The performance of refueling at operating pressure has been achieved in the British AGR [Gallie, 1982], though at significantly lower pressures than the GFR operating pressure of 20 MPa. Refueling at pressure in AGRs has met with some technical challenges, including abnormal vibration of fuel assemblies, but with additional effort, it may be possible to adapt the refueling method for use in the GFR. The adaptation of such a technique is left to future research. As an alternative, it is recommended that, at the time of scheduled maintenance, the system be shut down for several days prior to the performance of the maintenance task. This hold time will allow for additional delay and decay of the coolant radionuclide inventory, purification of the primary coolant, and a very gradual reduction in system pressure. This gradual reduction in system pressure will, in turn, allow for the residual inventories of the plena to be handled by the coolant purification system, or by the containment purification system, if leakage into the containment does occur.

7.4 Summary

This chapter discussed the pressure transients which can occur in the direct cycle system and examined their impact on the venting process. Hand calculational methods and computer modeling were employed in investigating the vent system's ability to deal with both the small pressure transients known as breathing and large, sudden decreases in system pressure during an accident. It was demonstrated that under accident conditions, the vent system can decrease in pressure at least as quickly as the overall primary coolant system, meaning that the fuel assembly will not burst due to overpressure. It was also shown that a vent system using a sequence of large plena provides the greatest defense against short-lived species, while the use of a single small plenum would be most effective against the release of long-lived species during small pressure transients. Similarly, it was demonstrated that the use of a single small plenum would result in the smallest radiation hazard following a sudden large pressure transient. A compromise between the two approaches was identified, which used a small upper axial plenum and large lower annular plenum with six downflow tubes instead of the original three. Assessment of this approach confirmed its ability to equalize pressure quickly, and defend against release of radionuclides during small and large pressure transients. This configuration was selected as the final configuration of the vented fuel assembly.

Chapter 8: Summary, Conclusions, and Recommended Future Work

8.1 Introduction

The objective of the present work was to investigate the implementation of vented fuel assemblies in the reference design of the MIT Gas-Cooled Fast Reactor (GFR). A number of factors motivated the present assessment of vented fuel performance, including the desire to either extend fuel lifetime by reduction of cladding strain, or to reduce the required thickness of the cladding. The latter would have a number of potentially beneficial effects, including enhanced neutronic performance of the fuel, and decreased resistance to heat transfer. Additionally, the efflux of fission gases from the interior of the cladding stands to further improve heat transfer from the fuel, as the fission product gases in question have lower thermal conductivities than CO_2.

While the present effort focuses on the application of a vent-to-coolant fuel assembly in a newly completed reactor design, vented fuels have in fact had a long history in both the United States and the United Kingdom. The earliest efforts in venting of fuel were performed in conjunction with sodium-cooled fast reactor development, and were primarily undertaken by General Electric. Roughly contemporary to this design work, two reactors actually operated with vented fuel: the sodium-cooled Dounreay test reactor, and the helium-cooled Peach Bottom Unit 1. Review of available data on the operating experiences of these reactors has lent considerable weight to the analyses performed here.

Specific tasks tied to the analysis of vented fuel implementation included an identification of the nuclides (radioactive and volatile) of interest in the venting process, in addition to estimates of the primary coolant inventories of these species without purification of the primary coolant. Investigation of the reactions between fission products and their surroundings was also performed, as the study of chemical reactions and plateout onto surfaces is crucial to determining the impact of the vented species on the reactor environment. Such an effort is also important in determining the best methods by which to purify the primary coolant inventory of undesirable nuclides. In addition, the

effect of pressure transients on the vent system was examined, as were the radiological consequences of such transients. The potential processes by which fission products may reach their various fates are summarized in Fig. 8.1. During investigation of all of these processes, emphasis was placed on the potential for licensability of vented fuel assemblies under the current Nuclear Regulatory Commission regulations.

The analysis performed in each of these areas enabled the selection of the final form of the vented fuel assembly. The selected configuration, shown in Fig. 8.2, directs fission products first to a small (~1000 cc) upper axial plenum, and then downward through six vent tubes to a larger (~2000 cc) lower annular plenum. From this point, the fission products are released directly to the primary coolant, though this configuration could be easily modified to allow venting to a grid-plate sequestration system by moving the vent outlet to the exterior edge of the fuel assembly rather than its interior.

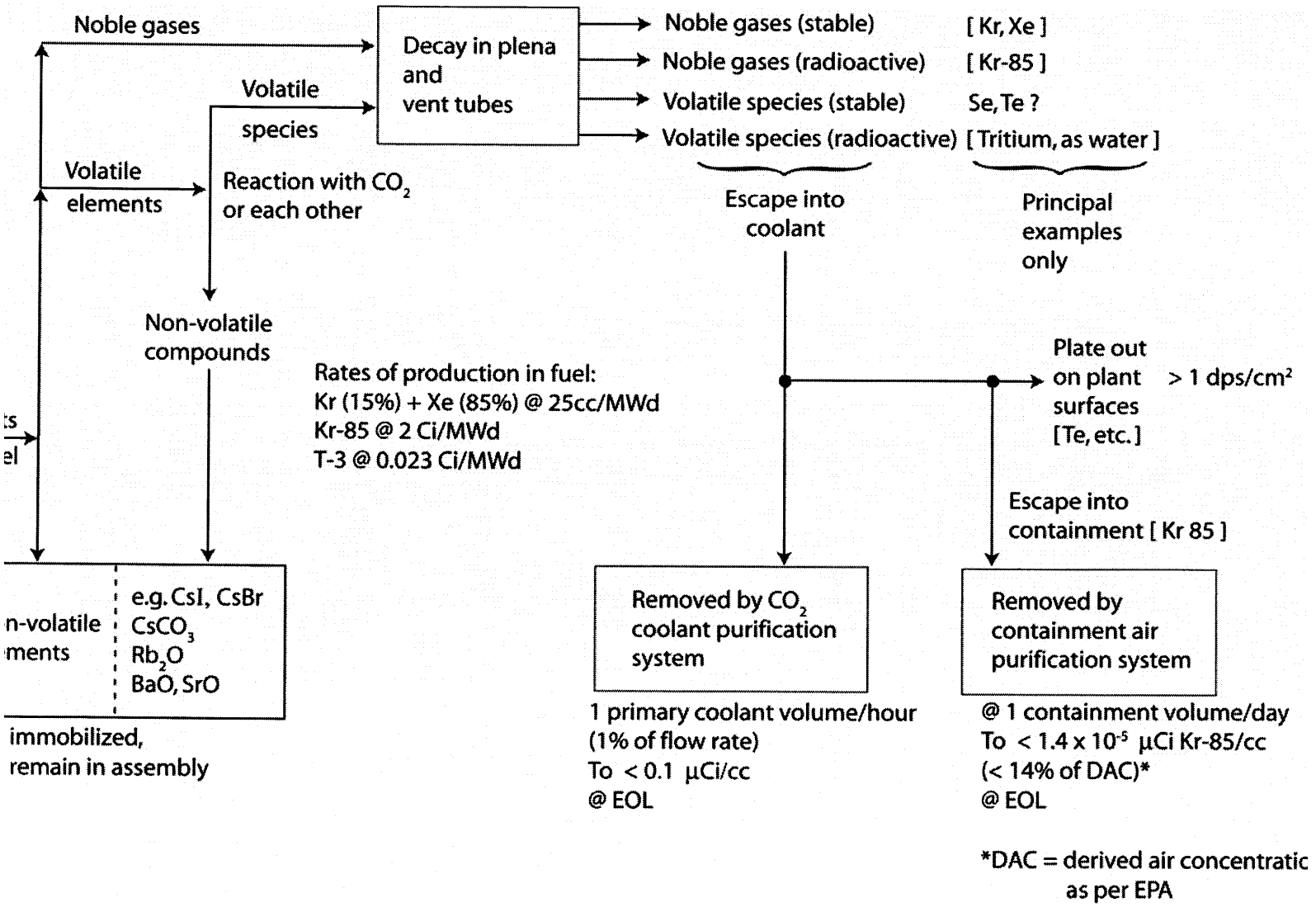

ummary of Fission Product Transport Processes

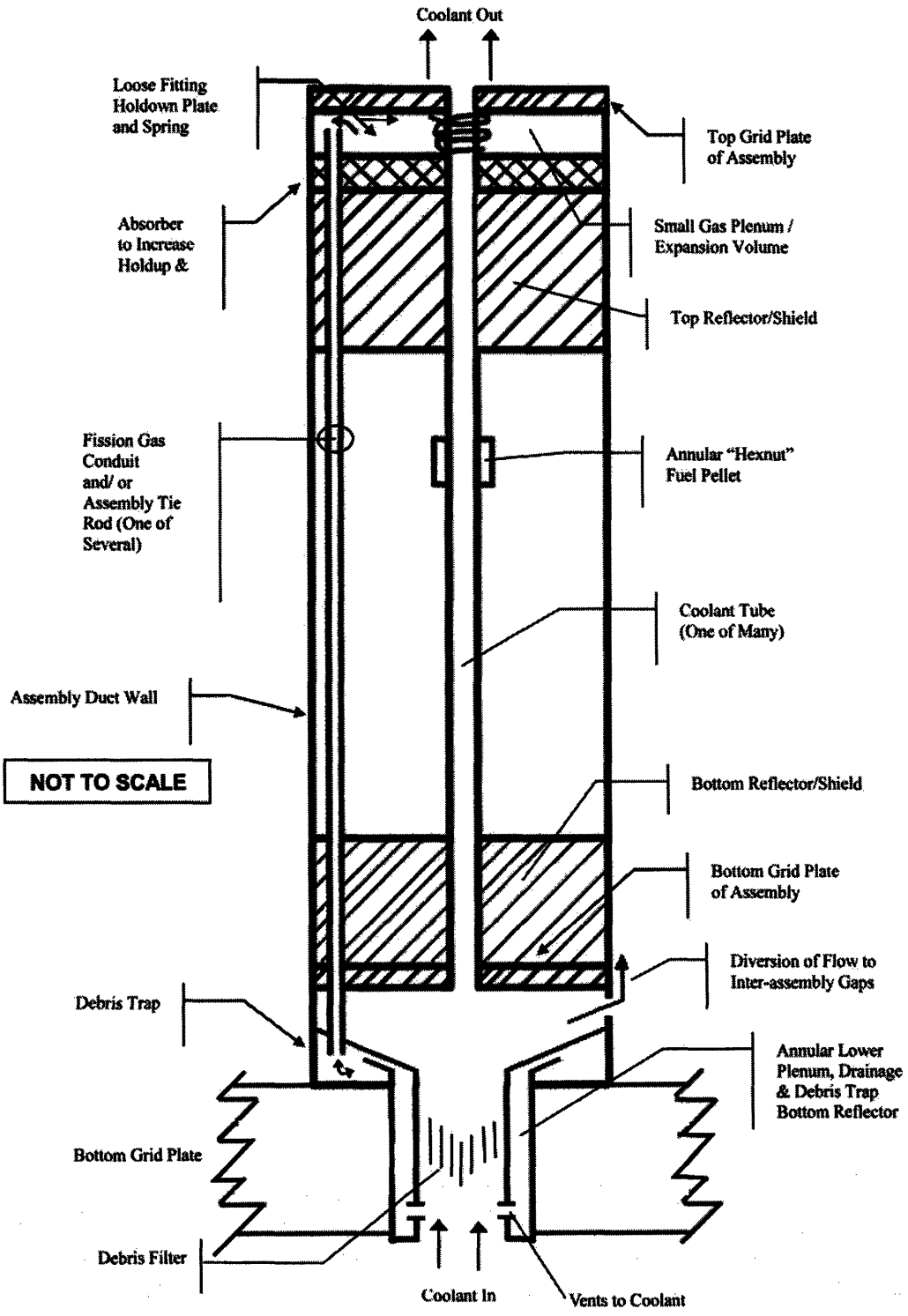

Figure 8.2: Final Vented Fuel Assembly Configuration

8.2 Physics of Venting and Identification of Troublesome Nuclides

A series of models for fission product transport from the fuel, to the gap, to the upper axial plenum, and on along the vent path were identified. For the sake of conservatism, it was assumed that all of the mobile radionuclides were immediately released from the fuel following their production. In addition, transport time through the upper axial reflector was neglected, as was thermal diffusion. The decision to ignore both modes of transport considerably increases the conservatism in all following estimates of fission product throughput by the vent system. The final result of the discussion of transport mechanisms was the use of a model based on classical diffusion along concentration gradients, in conjunction with the largest diffusion coefficient yielded by a group of estimates.

A broad range of potential fission products, both radioactive and volatile, were of interest in the present study. Noble gases were of particular importance due to their high yields in fission and great degree of mobility through the fuel matrix. Also investigated were volatile species, including several alkali metals, alkaline earth metals, halogens and chalcogens, some of which are radioactive, and all of which undergo chemical reaction with other fission products, coolant or structural materials. Because so many of the species previously listed for study are members in a radioactive decay chain, their respective parents and daughters were also investigated during the present work for the sake of completeness.

Because a simple calculation revealed that a radionuclide would take hundreds of hours to traverse even the shortest of vent paths, all nuclides with half lives shorter than nine hours were eliminated from consideration, owing to the fact that they would yield insignificant quantities at the outlet of the vent path. Following this step, maximum coolant activity levels were found for each of the remaining nuclides in the study, using a simulation developed from the models developed during the investigation of fission product transport. The results of these calculations revealed that several of the radioisotopes did not introduce any activity to the primary coolant during the lifetime of the fuel. Many others introduced so little activity that if the entire contents of the primary system were released to the containment structure, the derived air concentration limit for

these nuclides would not be exceeded. These nuclides were therefore removed from further consideration, leaving a total of fourteen radionuclides and nineteen stable volatile species as isotopes of interest in the venting process. These nuclides are shown in tables 8.1 and 8.2. Because ^{85}Kr and ^{137}Cs produced much greater activities than the other species investigated, they were taken as bounding cases for future investigations.

Table 8.4: Radioactive Fission Products of Concern in Venting

Isotope	Half Life
^{3}H	12.33 y
^{85}Kr	10.76 y
^{86}Rb	18.63 d
^{129}I	1.57×10^{7} y
^{131}I	8.02 d
^{129m}Te	33.6 d
^{131}Ba	11.5 d
^{133}Xe	5.24 d
^{132}Cs	6.48 d
^{134}Cs	2.0648 y
^{135}Cs	2.30×10^{6} y
^{136}Cs	13.16 d
^{137}Cs	30.07 y
^{140}Ba	12.75 d

Table 8.5: Volatile Fission Products of Concern in Venting

Isotope	Half Life	Isotope	Half Life
^{3}H	12.33 y	^{136}Cs	13.2 d
^{78}Se	Stable	^{137}Cs	30.1 y
^{79}Se	Stable	^{134}Ba	Stable
^{80}Se	Stable	^{135}Ba	Stable
^{82}Se	Stable	^{136}Ba	Stable
^{79}Br	Stable	^{137}Ba	Stable
^{81}Br	Stable	^{138}Ba	Stable
^{82}Br	35.3 h	^{140}Ba	12.8 d
^{85}Rb	Stable	^{124}Te	Stable
^{127}I	Stable	^{125}Te	Stable
^{129}I	1.57×10^{7} y	^{126}Te	Stable
^{131}I	8.02 d	^{128}Te	Stable
^{133}Cs	Stable	^{129m}Te	33.6 d
^{135}Cs	2.30×10^{6} y	^{130}Te	Stable

In order to determine the effect of vent path extension on the primary coolant inventory of radionuclides, it was necessary to compare the results of calculations for a range of vent path configurations which used different numbers and volumes of plena. Because the program developed to simulate fission product transport does not take into account the presence of plena, a simple correction factor, based on the ratio of the total available volume to the vent tube volume, was adopted in order to account for the volumes associated with the plena. Thus, for the selected vent path configuration, with six 100 cc vent tubes and 3000 cc of free plenum volume, the effective path length was 1848 cm. This figure represents the product of the correction factor with twice the 154 cm vent tube length. At a vent tube length of 1848 cm, and with no purification of the coolant, the end-of-lifetime inventories of the radioactive nuclides of concern are those given in table 8.3.

Table 8.6: End-of-Lifetime Primary Coolant Activities for Final Vent Configuration

Isotope	Coolant inventory, a	Activity (Ci)
^{3}H	4.109×10^{23}	19768
^{85}Kr	9.856×10^{24}	5.43×10^{5}
^{86}Rb	1.520×10^{11}	1.77×10^{-6}
^{129}I	7.535×10^{25}	2.85
^{131}I	6.866×10^{10}	1.86×10^{-6}
^{129m}Te	2.663×10^{17}	1.73
^{131}Ba	1570	2.97×10^{-14}
^{133}Xe	5.784×10^{7}	2.34×10^{-9}
^{132}Cs	0	0
^{134}Cs	7.413×10^{19}	21.2
^{135}Cs	4.747×10^{26}	123
^{136}Cs	3.264×10^{11}	5.37×10^{-6}
^{137}Cs	3.338×10^{26}	6.59×10^{6}
^{140}Ba	1.227×10^{14}	0.00208

The results of the calculations using different vent path configurations revealed that for most nuclides, the coolant activity at first decreases sharply with vent path extension, and then decreases more slowly, as shown in Fig. 8.3. This information was instrumental in selecting the final vent path configuration, because of the differing abilities of the various vent path configurations to guard against fission product release during changes in system pressure.

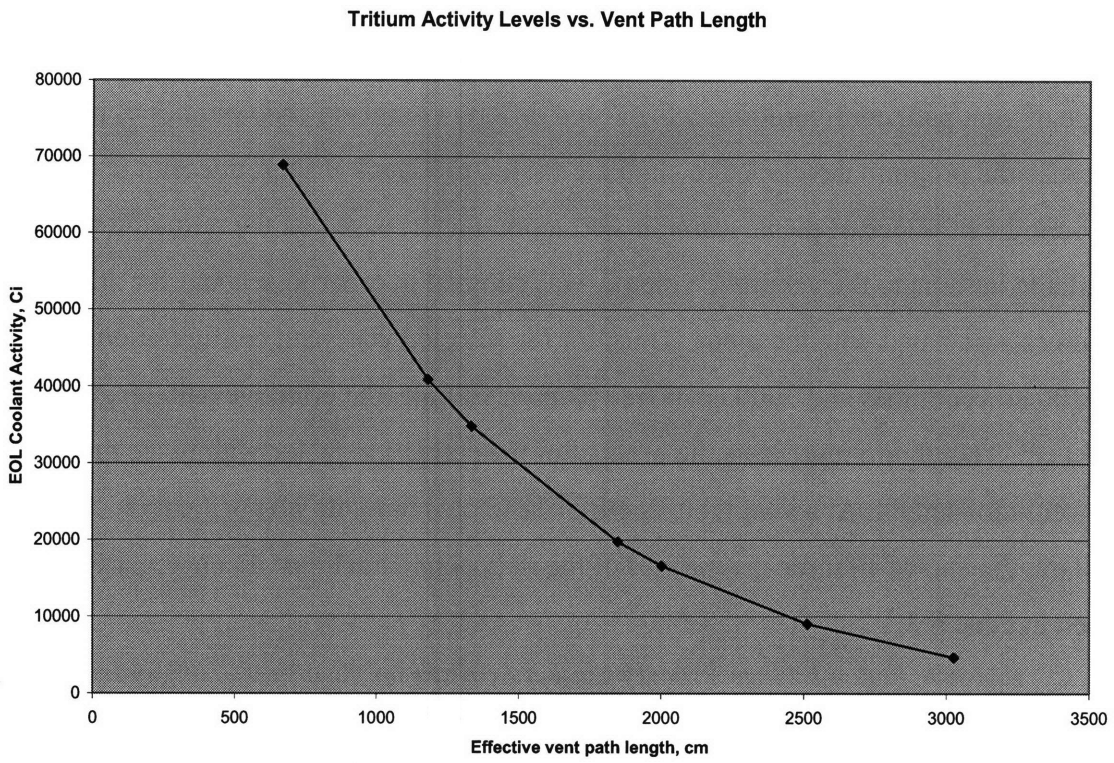

Figure 8.3: EOL Primary Coolant Tritium Activity as a Function of Vent Path Length

8.3 Fission Product Chemistry

As discussed in the section on fission products of interest to the venting process, a number of both stable and radioactive fission products are chemically volatile. These products include the halogens, chalcogens, alkali metals, and alkaline earth metals. These species are deemed important due to their radioactivity, in some cases, and in other cases, their potential for immobilization of radioactive species prior to their exit from the vent path. For this reason, a number of potential interactions were investigated, including reactions between fission products, and reactions of fission products with coolant. Following the identification of likely reactions and their products, the computer program HSC 6.1 was used to determine the equilibrium state of a "mixed pot" of reactants, representing the primary coolant before purification. This investigation revealed that the majority of fission products form stable salts or carbonates after reaction with coolant or other fission products. The only remaining volatile species were selenium and tellurium, of which only a small fraction reacted, as well as iodine, which remained free in much smaller quantities.

Table 8.4:Equilibrium Reaction Products

Species	Equilibrium Quantity, gram moles
CH_4	1.819×10^{-15}
H_2	3.648×10^{-10}
HCOOH	3.785×10^{-15}
HI	5.358×10^{-21}
$BaBr_2$	1.072×10^{-20}
CsBr	142.48
RbBr	2.7153
CsI	9.1399
RbI	3.7049×10^{-2}
$BaCO_3$	8997
Cs_2CO_3	4269
CsOH	2.120×10^{-14}
H_2O	2.059×10^{-2}
Rb_2CO_3	467.42
RbOH	7.289×10^{-14}
$SrCO_3$	0.05500
TeO_2	2.750×10^{-17}
I	2.1387×10^{-14}
Se	180.3
Te	1997

Note: shaded species are immobilized.

The compounds formed during the reactions investigated were of particular importance because many of them are solids at reactor operating temperatures, and as such, tend to deposit on steel surfaces. Additionally, some free atoms also deposit on these surfaces, often becoming bound into the oxide layer on the surface of the steel. Therefore, the physical state of each compound present at equilibrium was determined, in order to aid in an estimation of the primary surface contamination which would likely occur as a result of the presence of the deposition of radioactive compounds. It was assumed that all compounds with melting points greater than 500 degrees Celsius deposit on the debris trap at the lower end of the fuel assembly; these compounds are shaded in table 8.4. The estimate determined that contamination of primary system surfaces would be high enough to preclude hands-on primary system maintenance, which is limited to surfaces of less than 1 dps/cm^2 (^{129m}Te alone is estimated to result in surface contamination of 1×10^5 dps/cm^2). However, because hands-on maintenance of direct cycle systems is rarely conducted due to additional complicating factors, this result was hardly discouraging. Instead, it was noted that contamination bound to the primary

system's surfaces would provide additional holdup of these species, and prevent their release to the containment structure during a loss of coolant event. Additionally, it was demonstrated that the compounds under study are generally highly soluble in water (most have solubilities greater than 100g/100g H_2O), and that decontamination of many surfaces could take place simply by washing.

8.4 Primary Coolant Purification

Purification of primary coolant is necessary in all nuclear power systems, but becomes particularly important in the GFR due to the release of fission products directly to the coolant. Coolant purification systems traditionally remove water, particulate matter, and volatile chemical species. The nature of the GFR's vented fuel design requires robust performance in removal of these impurities, as well as the removal of fission gases like Xe and Kr, and oxygen and carbon monoxide produced through radiolysis. The removal of ^{85}Kr, the source of the bulk of the primary coolant activity, is especially important. For this reason, a number of potential techniques for removal of Kr and other impurities from the primary coolant were investigated. Among these potential techniques were use of sorbent materials, molecular sieving, cryogenic distillation and permeation through membranes and capillary tubes.

Cryogenic distillation was quickly rejected as a possibility for removal of Kr and Xe from the waste stream. While this method has often been used in removal of these species from other gases, the fact the CO_2 freezes above cryogenic temperatures makes it at least impractical, and likely impossible, to remove noble gases from CO_2 using cryogenic distillation. Selective permeation through membranes and capillary tubes was deemed an attractive option for purification due to its passively safe performance in many industrial settings, but will require additional testing to demonstrate its feasibility of use in the high pressure environment of the GFR primary loop. In the event that high pressures render selective permeation impossible for use with the primary coolant, the technique still remains a strong candidate for daily purification of containment facility air.

Because a great deal of uncertainty exists in the performance of many common purification methods at the high pressures required of the GFR, only a general framework for a coolant purification system can be outlined at present. The removal of dusts and

large particles will be a crucial first step which will enhance the performance of the later stages of the purification process. Next, desiccation must occur in order to remove tritiated water from the waste stream. Following this, any unreacted volatile species should be pulled out of the stream by either a metallic chemisorber or by a surface treated molecular sieve. Following this step, noble gases, mostly Kr and Xe, must be removed from the waste stream by either selective permeation through capillary tubes or adsorption on a charcoal or zeolite bed. The final step, in the event that a charcoal bed is used for removal of noble gases, is the use of a secondary filter to remove charcoal dust, and the subsequent return of the purified gas to the primary system.

8.5 Impact of Pressure Transients

Chapters 3 and 4 described the steady state diffusion of fission products along the vent path. However, this transport occurs very slowly, and so it is necessary to consider the increased rate of radionuclide transport tied to both small and large fluctuations in vent system pressure. In addition, it is vital to the safe operation of the vented fuel assembly that the vent system be capable of responding quickly to a large, sudden decrease in primary coolant system pressure, so that cladding overpressure does not result. Equations describing critical flow of gases were used to determine the time required for a fuel assembly to equalize pressure in the event of a sudden decrease to atmospheric pressure. This calculation revealed that the assembly could reach atmospheric pressure in only 0.8 s, much faster than plausible for the primary coolant system to reach equilibrium with the containment. This indicated that the cladding would be safe from overpressure during a LOCA or similarly large pressure transient. A calculation using RELAP showed the ability of eight different vent path setups to prevent cladding overpressure. A simple criterion to confirm this protection is to have the ratio of the vent path flow area to the total assembly gas volume less than the ratio of a LOCA-sized break to the total primary system volume. This criterion is indeed satisfied for the GFR, confirming that the vent system will prevent cladding overpressure.

By use of the ideal gas law, it was possible to derive equations describing the accordion-like expansion and contraction of plenum contents during the small pressure transients commonly known as "breathing". These hand-calculated estimates were again supported through the use of RELAP, and the fraction of the gas mass expelled from each

plenum during a breathing transient was found. These results, coupled with the results of plenum radionuclide inventory calculations made possible by a variation on the previously used MATLAB model, allowed the estimation of the activity release to the primary coolant which resulted from a single breathing transient. These results are reproduced in table 8.5.

Table 8.5: Summary Results of Breathing Calculations

Case	Plenum	Hand calculated fraction released to primary	RELAP fraction released to primary	^{85}Kr Activity Release (Ci)	^{133}Xe Activity Release (Ci)
1	1000 cc	0.3	0.401	3609	52.0
2	2000 cc	0.3	0.366	9080	48.3
3	2000 cc	0	0.0592	1467	7.81
	1000 cc	0.9	1	9627	3.44×10^{-6}
4	1000 cc	0	0	0	0
	1000 cc	0.6	0.795	11221	9.64
5	2000 cc	0	0	0	0
	2000 cc	0.25	0.481	7735	1.65×10^{-6}
	1000 cc	1	1	3705	0
6	2000 cc	0	0	0	0
	1000 cc	0.2	0.785	7556	2.70×10^{-6}
	1000 cc	1	1	5698	4.42×10^{-12}
7	1000 cc	0	0	0	0
	1000 cc	0	0.169	2383	0.0158
	1000 cc	0.9	1	8752	1.50×10^{-7}
8	1000 cc	0	0	0	0
	2000 cc	0.45	0.536	7494	18.3

Note: Case 8 is final selection (see Fig 8.2)

It was found that for short-lived radionuclides, the greatest activity release occurred for the shortest vent paths, as longer vent paths, with a greater number of plena, effectively guard against escape of the most recently released nuclides. However, for long-lived nuclides, which do not benefit significantly from additional delay time, the greatest activity release resulted from the longer vent paths, which had higher plenum inventories available for release. Further efforts are recommended to determine the frequency of such transients and the resulting radiological consequences.

For the consequences of a LOCA, the worst case scenario was assumed: total release of both the primary coolant inventory and the inventories of each plenum into the containment atmosphere. In order to assess the desirability of a number of different vent path configurations, the total release associated with each configuration was determined.

Under the assumption of unpurified coolant, it was clear that the configurations with the shortest effective vent path lengths corresponded to the greatest total activity release. However, comparison with the assumption of hourly primary coolant purification demonstrated that the shortest vent paths result in the lowest total activity release. This occurs because, while increased vent path length and increased coolant purification both act to reduce the radionuclide population, purification is by far the dominating effect, as can be seen in table 8.6. For this reason it is more prudent to speed the transport of longer-lived radionuclides, particularly long-lived species like ^{85}Kr, to the purification system, thereby decreasing the vent system activity inventory available for release in the event of a blowdown. It was concluded that use of a short vent path would prove most beneficial in this regard. The final configuration recommended, as shown in figure 8.1, is a compromise between confinement of short-lived species and purging of long-lived species. The configuration additionally exhibited one of the fastest times to pressure equalization during a sudden drop in system pressure, release of moderate levels of long-lived species and low levels of short-lived species during breathing transients, and fair performance at preventing high levels of activity release during a LOCA.

Table 8.6: Summary Results of EOL Blowdown Activity Release Calculations

Case	Unpurified LOCA release of ^{85}Kr (Ci)	Purified LOCA release of ^{85}Kr(Ci)
1	8.49×10^6	8674
2	5.01×10^6	17860
3	2.40×10^6	23605
4	4.25×10^6	17045
5	5.59×10^6	29717
6	1.11×10^6	34012
7	2.01×10^6	22133
8	2.40×10^6	22585

Note: Case 8 is final selection (see Fig. 8.2).

8.6 Conclusions

The reference design of the GFR has been advanced through the investigation of the venting of fission products from its innovative tube-in-duct fuel assembly. Several significant contributions have been made as a result of the present work. First, the mechanisms by which fission products leave the fuel and are transported along the vent path were identified. Secondly, a small subset of the nuclides which may enter the vent path have been identified as being of concern due either to their radioactivity or chemical

volatility. Of these, two nuclides, ^{85}Kr and ^{137}Cs, were identified as species which can effectively serve as conservative limiting cases in future studies of vented fuel performance. ^{137}Cs is particularly notable due to its tendency to form stable compounds with other species, thereby preventing their release or increasing their holdup time. Third, a primary coolant purification system was outlined which should have the capability to maintain the low coolant activity levels important to assuring the safety of workers in the containment facility, and ultimately the general public. Finally, an investigation of the behavior of the vented fuel assembly during pressure transients established that the fuel assembly will not fail due to cladding overpressure, and revealed the radiological consequences of both small pressure transients and large scale loss of coolant accidents. This analysis aided in the selection of the final approach to fuel venting.

Most important, however, is an assessment of the potential licensability of vented fuel assemblies for service in the GFR. Because the venting of fuel results in the bypass of the cladding as a barrier to fission product release, designs for vented fuel will be met with particular scrutiny by regulators. However, the plan for vented fuel implementation discussed in the present work adds several measures of safety. For example, a robust outer containment building surrounds the pressure vessel, acting as an additional barrier to the release of radionuclides from the core. In addition, while radionuclides are expected to circulate through the primary system, requirements for coolant purification have been set which result in a containment radiation field lower than can be expected to significantly impact workers. Finally, while some may argue that the venting of radionuclides and volatile fission products to the coolant will result in much greater risk in the event of an accident, it should be recalled that the use of vented fuels also provides considerable safety enhancement. For example, the increase in gap conductivity afforded by venting allows fuel to be more efficiently cooled. In addition, venting eliminates the threat of cladding overpressure, which can be of particular concern in direct-cycle gas-cooled systems due to the effects of breathing transients. For all of these reasons, it is concluded that the benefits of fuel venting outweigh its risks, and that the use of vented fuel assemblies in the GFR should be licensable.

8.7 Future Work

As in any research endeavor, there remain a number of areas in which further work could contribute to the design. With the focus on venting to directly to coolant, the possibility of venting to a grid-plate collection system has not been of emphasis in the present work. This configuration, studied in an earlier work [McKee, 2007], has been left as a fallback option. Note that the recommended configuration is easily modified to vent either into a grid plate plenum or to the coolant merely by moving the vent holes from the inside to the outside of the assembly bottom plenum as shown in Fig. 8.2.

In addition, there are areas within the vent-to-coolant design which would be benefited by additional work. For example, as the tube-in-duct fuel assembly is a new concept, further investigation of transient behavior would be beneficial to an understanding of the assembly. While the effects of pressure transients on vent system response have been analyzed in detail in the present work, other types of transients, such as changes in system temperature or in reactor power have not yet been investigated. Because both would likely have lesser impact on the operation of the system than the pressure transients studied in the present work, they are considered bounded by the present analysis, but remain open for future study.

Experimentation using either irradiation of an assembly or simulated fission product transport through a mockup of the vented assembly would also prove highly insightful. As the estimates of fission product release from the fuel and the vent system are based on the results of prior experiments [Campana, 1974] and are thought to be conservative, some level of experimentation should be conducted to determine exactly how conservative these estimates are. Experimentation could also be used to shed light on some previously unstudied subjects, such as the delay of radioactive and volatile species by reflector and shield materials, and the deposition of the products of chemical reactions onto steel surfaces. The MIT Research Reactor has hosted in-pile loops which could readily be converted into a facility for such tests.

On the topic of reflector materials, there is also room for future effort. The reference GFR design laid out by Handwerk established titanium as the reflector material of choice, after exhaustive comparison with other common reflector materials. However, some materials not previously considered show strong promise as both reflectors and as

dense materials which could be used to retard the transport of fission products. $PbSO_4$ is one such candidate, with a very high density of 6.2 g/cm^3, which allows it to both reflect neutrons effectively and slow transport of fission product atoms. Magnesium silicate, Mg_2SiO_4, is another potential candidate which is attractive due to its very low neutron absorption cross section. Titanium oxide and zirconium oxide are also well-known absorbers which could retard escape of chemically volatile species while permitting gases to diffuse to the vent system.

The consideration of advanced and alternative materials is important in other areas as well, including the purification of primary coolant. While techniques for removal of undesirable isotopes have been discussed in detail in chapter 6 of this work, it should be noted that advances in materials science and engineering are constantly providing new means for purifying gases, through the use of advanced materials for filtering and membrane separation. Thus any future endeavors into purification of coolant in a vented system should be conducted with an eye to recent innovations in separation technologies.

Similarly, as the total purification system described in the present work has not yet been constructed and tested, experimentation should be performed so that it can be demonstrated that the required purification rates are achievable using the described methods. The experimental setup described in this report appears suitable for future studies of this type. Further experimentation on purification strategies would also prove quite useful in improvement of cryogenic distillation techniques for Kr removal, as well as in other strategies.

The present work has been limited to the analysis of vented assemblies in a particular assembly geometry, with a particular choice of coolant. However, it would likely be feasible to vent fuel in a number of configurations. Venting in traditional pin fuel could be attractive, especially when that fuel is cooled by a gas. Holdup of fission gases in this scenario could be achieved by extension of the top of the fuel pin to include an annular plenum. Alternatively, the same setup could be used at the base of each fuel pin, where cooler temperatures would slow transport by both diffusion and breathing. This setup is similar to the diving bell configuration described in previous LMFBR work [O'Neill, 1965].

This approach to venting also shows promise in modern LMFBR designs. First, the breathing phenomenon which increases radionuclide transport in the GFR does not take place in the LMFBR due to the use of a virtually incompressible liquid sodium coolant. In addition, the presence of a cover gas above the liquid metal in an LMFBR allows the coolant to give up fission gases to the cover gas, while retaining non-gaseous (and shorter lived) products in the coolant. This could potentially provide a dramatic simplification in coolant purification, as compared to purification in the GFR.

Similarly, considerable thought has been given to the use of an alternative venting method, most likely taking the form of a forced stream of helium which is bled off to a sequestration and collection system at the end of the vent path. When helium gas is present inside the assembly, it becomes possible to use carbide fuels, which have a higher thermal conductivity than oxide fuels and can thus be used to achieve cooler fuel or higher power density. In addition, the use of helium allows the presence of activated carbon absorber materials for purification, which is not possible in a CO_2 atmosphere because of the risk of oxidation associated with the presence of free oxygen. The helium presents another advantage: by monitoring the primary coolant for the presence of helium, the operator can detect breaches in the cladding. Clearly, there may be some advantages to operating with helium as a feed material for the venting process, though these benefits should be carefully analyzed and weighed against the other effects of such an approach, including reduction in holdup of radionuclides, the higher gap thermal conductivity afforded by helium (as compared to carbon dioxide), and the required equipment for collection and sequestration of radionuclides, which would necessarily be separate from the primary coolant purification system.

In any case, it appears that such a helium "feed and bleed" approach to venting would be quite useful when implemented in conjunction with vibrationally compacted (VIPAC) fuels, which are of current interest at MIT.

References

M. Anbar, P. Perlstein, "Mechanisms of Radiolysis of Carbon Dioxide," *Transactions of the Faraday Society,* 62(1966).

E. Baum, H. Knox, T. Miller, eds. *Chart of the Nuclides*, 16th ed. Knolls Atomic Power Laboratory, 2002.

M. Benedict, T. Pigford, H. Levi, *Nuclear Chemical Engineering,* 2nd ed. McGraw-Hill, 1981.

J. Blessing, R. Ellefson, B. Raby, G. Brucker, R. Waits, "Recommended Practice for Process Sampling for Partial Pressure Analysis, " Journal of the American Vacuum Society A, 25(2007).

M. Bolmsjö, B. Persson, "Trapping and Reuse System for Radioactive Xenon in Nuclear Medicine," *Physics of Medical Biology*, 23(1978).

F. Brightman, C. Chapman, J. Garland, R. Hargreaves, E. Higham, "The Windscale Experiments: Circuit Activity Measurements," *Gas Cooled Reactors Today*, Vol. 3, Proceedings of the conference held in Bristol, September 1982.

R.J. Campana and J.R. Lindgren, "Irradiation Testing of Design Models for the GCFR Pressure Equalization System", *Nuclear Engineering and Design*, 26(1974), pp.201-214.

C. Chapman, D. Freck, R. Woolley, "Progress in Research on the Retention of Caesium and Iodine Fission Products by the Gas Circuit Surfaces in AGRs,' *Gas Cooled Reactors Today*, Vol. 3, Proceedings of the conference held in Bristol, September 1982.

C. Chen, Y. Sun, Z. Huang, C. Liu, S. Wu, "The Diffusion of Tritium and Helium-3 in 21-6-9 Stainless Steel During the Storage of Tritium at High Pressure and Room Temperature," *Physica Scripta*, T103 (2003).

E.L. Cussler, *Diffusion: Mass Transfer in Fluid Systems*, Cambridge University Press, 1984.

W. M. Deen, *Analysis of Transport Phenomena*, Oxford University Press, New York, 1998.

Drierite Co. "Laboratory Equipment: Gas Purifier," Online. [Available] www.drierite.com.

J.J. Duderstadt and L. J. Hamilton, *Nuclear Reactor Analysis*, John Wiley & Sons, 1976.

L. Durbin and R. Kobayashi, "Diffusion of Krypton-85 in Dense Gases," *Journal of Chemical Physics*, 37(1962).

R. Gallie, P. Hewitt, "Eighteen Years' Operating and Development Experience with the Windscale AGR," *Gas Cooled Reactors Today*, Vol. 1, Proceedings of the conference held in Bristol, September 1982.

J. Gan, "Assessment of Failure Mechanisms for GFR Vented Fuel Pins Using Hexoloy Cladding," Proceedings of the International Conference on Reactor Physics, Nuclear Power: A Sustainable Resource, Interlaken, Switzerland, September 2008.

W.R. Gee, "Design Considerations for Operation of the Fast Flux Test Facility with Fuel Fission Gas Emission," GEAP-10057, July 1969.

K. Gezelius, M. Driscoll, P. Hejzlar, "Design of Compact Intermediate Heat Exchanger for Gas-Cooled Fast Reactors," MIT-ANP-TR-103, May 2004.

M. Haissinsky, M. Magat, *Tables of Constants and Numerical Data: Selected Constants and Radiolytic Yields*, Pergamon Press 1961.

C.S. Handwerk, P. Hejzlar and M.J. Driscoll, "Core Design and Performance Assessment for a Supercritical CO_2-Cooled Fast Reactor," MIT-ANP-TR-113, May 2007.

P. Hofmann, J. Spino, "Chemical Interactions Between Simulated Fission Products and Zircaloy-4 at Elevated Temperatures, Including Influence in Ductility and Time-to-failure," *Journal of Nuclear Materials,* 102(1981).

D. Ianovski, K. Minakata, S. Kanjo, A. Koga, S. Yamatsuki, K. Tanaka, T. Fukumatsu, M. Nishikawa, Y. Igarishi, "Adsorption of Noble Gases on H-Mordenite," *Journal of Nuclear Science and Technology*, 39(2002).

B. Kalin, V. Yakushin, E. Fomina, "Tritium Barrier Development for Stainless Steel by its Aluminizing in a Lithium Melt," *Fusion Engineering and Design,* 41 (1998).

J.R. Lamarsh, *Introduction to Nuclear Engineering*, 3rd ed. Prentice Hall, 2001.

D. Lide, ed. *CRC Handbook of Chemistry and Physics, 88th ed.* National Institute of Standards and Technology, 2007.

Y.Long, M.S. Kazimi, R. G. Ballinger, J.E. Meyer, "Modeling the Performance of High Burnup Thoria and Urania Fuel," MIT-NFC-TR-044, July 2002.

S. McKee, "Feasibility Study for Utilization of Fission Gas Venting in a S-CO2 Cooled Fast Reactor," MIT Nuclear Engineering Department, August 2007.

F. McLafferty, *Interpretation of Mass Spectra*, University Science Books, 1980.

P. Monson, Jr., "Krypton Retention on Solid Adsorbents," Department of Energy Document DP-1615, January 1982.

Office of Nuclear Energy, *Global Nuclear Energy Partnership Strategic Plan,* Department of Energy Document GNEP-167312, January 2007.

D. R. Olander, *Fundamental Aspects of Nuclear Reactor Fuel Elements,* ERDA, USA, 1974.

H. Olson, H. Brey, F. Swart, "The Fort St. Vrain High Temperature Gas-Cooled Reactor: Evaluation and Removal of Primary Coolant Contaminants," *Nuclear Engineering and Design,* 61(1980).

G.L. O'Neill et al, "A Technical and Economic Evaluation of Vented Fuel for Sodium-Cooled Fast Ceramic Reactors," GEAP-4770, May 1965.

M.A. Pope, P. Hejzlar and M.A. Driscoll, "Thermal Hydraulics of a 2400 MWth Supercritical CO_2-Direct Cycle GFR," MIT-ANP-TR-112, September 2006.

K. Raznjevic, *Handbook of Thermodynamic Tables,* 2nd ed. Begell House, Inc., New York, 1995.

D. Rigual et al. "Interim Report on Task 2: Loops for Corrosion Tests in Supercritical CO_2 in the Presence of Radiolysis," MIT-GFR-010.

Roine, A. HSC *Chemistry ® 6.0 User's Guide*, Outotec Research Information Center, Pori, Finland, August 10, 2006.

C. Satterfield, *Mass Transfer in Heterogeneous Catalysis,* MIT Press, 1970.

E. Shwageraus, E. Fridman, E. Abramski, A. Galperin, "BGCore - A Comprehensive Package for Reactor Core and Fuel Storage Analysis", Proc. of 23rd Conference of the Nuclear Societies in Israel, Dead Sea, Israel, February 15-16, 2006.

S. Stern, S. Leone, F. Onorato, S. Wang, "Separation of Krypton and Xenon from Reactor Atmospheres by Selective Permeation," DOE Grant No. AT(11-1)3536, 1978.

B. Tissue, "Quadrupole Mass Spectrometry," Science Hypermedia, Online. [Available] http://elchem.kaist.ac.kr/vt/chem-ed/ms/quadrupo.htm.

J.A. Turnbull, et al. "The Diffusion Coefficients of Gaseous and Volatile Species During the Irradiation of Uranium Dioxide," *Journal of Nuclear Materials*, 107(1982), pp. 168-184.

A.E. Waltar and A.B. Reynolds, *Fast Breeder Reactors*, Pergamon Press, Oxford, 1981.

Y. Wang, "Estimation of N-16 Dose Rate for Direct Cycle CO_2 Gas Cooled Fast Reactors," MIT-GFR-032, August 2005.

R.H.S. Winterton, *Thermal Design of Nuclear Reactors*, Pergamon Press, Oxford, 1981.

R. Yang, *Adsorbents: Fundamentals and Applications*, John Wiley & Sons, Inc. 2003.

M. Yao, R. Wang, Z. Liu, X. He, J. Li, "The Helium Purification System of the HTR-10," *Nuclear Engineering and Design,* 218(2002).

Appendix A: MATLAB inputs

This appendix contains two MATLAB scripts and one function, current.m. The first script determines, for a decay chain of up to three nuclides, the influx and quantity of each in the primary coolant. The second script compares the current at a user-defined vent path length with the current at a second user-defined vent path length in order to determine the activity inventory of each plenum. The function current.m determines the fraction of produced nuclides which reach the end of the vent path during a fixed time interval.

The user-defined inputs for both scripts include the number of nuclides in the chain, the decay constants and fission yields for each, and the length of the vent path. Samples of the output for the first script can be found in table 4.5, among many others, and samples of the output for the second script can be found in tables 7.15-7.18.

```
%Initialize variables
clc
clear all
numdecay = input('Enter the number of isotopes in the decay chain:');
yield_1 = input('Enter the first fission yield:');
lambda_1 = input('Enter the first decay constant in inverse hours:');
lambda_1 = lambda_1*24;
yield_2 = input('Enter the second fission yield:');
lambda_3=0;
if numdecay > 2
    lambda_2 = input('Enter the second decay constant in inverse hours:');
    lambda_2=lambda_2*24;
    yield_3 = input('Enter the fission yield of the stable granddaughter:');
else
    lambda_2 = 0;
    yield_3 = 0;
end
H = 154;
lifetime = 6700;
P = 2400;
L = input('Enter length of vent tube, cm:');
d_gas = .0037;
d_gas = d_gas*3600*24;
J_1(1:lifetime/10)=0;
J_2(1:lifetime/10)=0;
J_3(1:lifetime/10)=0;
J_1p(1:lifetime/10)=0;
J_2p(1:lifetime/10)=0;
J_3p(1:lifetime/10)=0;
J_o1(1:lifetime/10)=0;
J_o2(1:lifetime/10)=0;
J_o3(1:lifetime/10)=0;
J_1out(1:lifetime/10)=0;
J_2out(1:lifetime/10)=0;
J_3out(1:lifetime/10)=0;
C_1(1:lifetime/10)=0;
C_2(1:lifetime/10)=0;
C_3(1:lifetime/10)=0;
```

```
quan1 = 2.7E21*yield_1*P*10;                %quantity of nuclide 1 produced in 10 d at half fuel height
quan2 = 2.7E21*yield_2*P*10;
quan3 = 2.7E21*yield_3*P*10;
%Determine outlet current at each time t
for t=2:lifetime/10-2
    for tau=t+1:lifetime/10
        tt = (tau-t-0.9)*10;
        J_o1(tau)=current(L+H/2,d_gas,tt,lambda_1)*quan1*10;
        J_o2(tau)=current(L+H/2,d_gas,tt,lambda_2)*(quan2+(1-exp(-lambda_1*tt))*quan1)*10;
        J_o3(tau)=current(L+H/2,d_gas,tt,lambda_3)*(quan3+(1-exp(-lambda_2*tt))*(quan2+(1-exp(-
lambda_1*tt))*quan1))*10;
        J_o1junk = J_1out(tau) + J_o1(tau);
        J_o2junk = J_2out(tau) + J_o2(tau);
        J_o3junk = J_3out(tau) + J_o3(tau);
        J_1out(tau) = J_o1junk;
        J_2out(tau) = J_o2junk;
        J_3out(tau) = J_o3junk;
    end
    C_1(t)=C_1(t-1)*exp(-lambda_1*10)+J_1out(t);
    C_2(t)=C_2(t-1)*exp(-lambda_2*10)+(1-exp(-lambda_1*10))*C_1(t-1)+J_2out(t);
    C_3(t)=C_3(t-1)+(1-exp(-lambda_2*10))*((1-exp(-lambda_1*10))*C_1(t-1))+J_3out(t);
end
if numdecay == 3
t=[1:lifetime/10-3];
    plot(10*t,C_1(t), '-',10*t,C_2(t),'--',10*t,C_3(t),':')
xlabel('time, days')
ylabel('quantity, atoms')
title('cumulative outlet quantity vs time, whole core')
legend('First isotope', 'Second isotope','Third isotope')
elseif numdecay == 2
    t=[1:lifetime/10-3];
    plot(10*t,C_1(t),'-',10*t,C_2(t),'--')
xlabel('time, days')
ylabel('quantity, atoms')
title('cumulative outlet quantity vs time, whole core')
legend('First isotope', 'Second isotope')
end
```

```
function c = current(H,D,t,lambda)
c=H/(4*sqrt(D*pi))*exp(-(H^2/(4*D*t))-lambda*t)/t^1.5;
end


%Initialize variables
clc
clear all
numdecay = input('Enter the number of isotopes in the decay chain:');
yield_1 = input('Enter the first fission yield:');
lambda_1 = input('Enter the first decay constant in inverse hours:');
lambda_1 = lambda_1*24;
yield_2 = input('Enter the second fission yield:');
lambda_3=0;
if numdecay > 2
    lambda_2 = input('Enter the second decay constant in inverse hours:');
    lambda_2=lambda_2*24;
    yield_3 = input('Enter the fission yield of the stable granddaughter:');
else
    lambda_2 = 0;
    yield_3 = 0;
end
H = 154;
lifetime = 6700;
P = 2400;
d_gas = .0037;
d_gas = d_gas*3600*24;
ent=input('Enter equivalent vent path length at plenum entrance');
ex=input('Enter equivalent vent path length at plenum exit');
J_1(1:lifetime/10)=0;
J_2(1:lifetime/10)=0;
J_3(1:lifetime/10)=0;
J_1in(1:lifetime/10)=0;
J_2in(1:lifetime/10)=0;
J_3in(1:lifetime/10)=0;
```

```
J_1out(1:lifetime/10)=0;
J_2out(1:lifetime/10)=0;
J_3out(1:lifetime/10)=0;
inv1(1:lifetime/10)=0;
inv2(1:lifetime/10)=0;
inv3(1:lifetime/10)=0;
d1dt=0;
d2dt=0;
d3dt=0;
%find change in plenum inventory at each time t
%increment inventory by this amt.
quan1 = 2.7E21*yield_1*P*10;                %quantity of nuclide 1 produced in 10 d at half fuel height
quan2 = 2.7E21*yield_2*P*10;
quan3 = 2.7E21*yield_3*P*10;
for t=1:lifetime/10-2
    for tau = t+1:lifetime/10
        tt = (tau-t-0.9)*10;
        J_1(tau) = current(H/2+ent,d_gas,tt,lambda_1)*quan1*10;
        J_2(tau) = current(H/2+ent,d_gas,tt,lambda_2)*(quan2+(1-exp(-lambda_1*tt))*quan1)*10;
        J_3(tau) = current(H/2+ent,d_gas,tt,lambda_3)*(quan3+(1-exp(-lambda_2*tt))*(quan2+(1-exp(-
lambda_1*tt))*quan1))*10;
        J_1junk = J_1in(tau)+J_1(tau);
        J_2junk = J_2in(tau)+J_2(tau);
        J_3junk = J_3in(tau)+J_3(tau);
        J_1in(tau)=J_1junk;
        J_2in(tau)=J_2junk;
        J_3in(tau)=J_3junk;
    end
end
for t=1:lifetime/10-2
    for tau = t+1:lifetime/10
        tt = (tau-t-0.9)*10;
        J_1(tau) = current(H/2+ex,d_gas,tt,lambda_1)*quan1*10;
        J_2(tau) = current(H/2+ex,d_gas,tt,lambda_2)*(quan2+(1-exp(-lambda_1*tt))*quan1)*10;
        J_3(tau) = current(H/2+ex,d_gas,tt,lambda_3)*(quan3+(1-exp(-lambda_2*tt))*(quan2+(1-exp(-
lambda_1*tt))*quan1))*10;
        J_1junk = J_1out(tau)+J_1(tau);
        J_2junk = J_2out(tau)+J_2(tau);
```

```
        J_3junk = J_3out(tau)+J_3(tau);
        J_1out(tau)=J_1junk;
        J_2out(tau)=J_2junk;
        J_3out(tau)=J_3junk;
    end
end
for t=2:lifetime/10-2
    d1dt=J_1in(t)-J_1out(t)-lambda_1*inv1(t-1);
    d2dt=J_2in(t)-J_2out(t)-lambda_2*inv2(t-1)+lambda_1*inv1(t-1);
    d3dt=J_3in(t)-J_3out(t)+lambda_2*inv2(t-1);
    inv1(t)=inv(t-1)+d1dt;
    inv2(t)=inv(t-1)+d2dt;
    inv3(t)=inv(t-1)+d3dt;
end
```

Appendix B: RELAP Inputs

This appendix contains inputs for two RELAP cases: blowdown of the vent system to atmospheric pressure and a breathing transient. Variations on these two input files were used to investigate the behavior of eight different vent path configurations during pressure transients. Sample output of this code can be found in tables 7.3-7.11.

```
=Blowdown test
*
* Prepared in September 2007
* Stephanie A. McKee
*three plenum case, different sizes
*******************************************************************************
0000001    11 *modifies coding for supercritical pressure conditions
*-------------------------------------------------------------------------------
0000100       newath        transnt
*-------------------------------------------------------------------------------
0000101       run
*-------------------------------------------------------------------------------
0000102       si
*-------------------------------------------------------------------------------
0000120    101010000 0.0 co2 plenum
*-------------------------------------------------------------------------------
*        runtime minstep maxstep option mineditfreq majeditfreq restartfreq
0000201     25.   1.0e-6 0.005  0003    10         10         1000
*-------------------------------------------------------------------------------
* Trip number definitions
20600000        expanded
*-------------------------------------------------------------------------------
20600010  time 0 ge null 0 0.0 1
20600020  time 0 ge null 0 1e6 1
*-------------------------------------------------------------------------------
*hydro    component name     component type
1010000   plenum              pipe
*-------------------------------------------------------------------------------
*hydro    # vol
1010001     6
*hydro    area     volume number
1010101    .0446      01
1010102    8.4e-5     02
1010103    .0446      03
1010104    8.4e-5     04
1010105    .0446      05
1010106    8.4e-5     06
*hydro    length   volume number
1010301    .0448      01
1010302    1.54       02
1010303    .0224      03
1010304    2.0        04
1010305    .0224      05
1010306    2.0        06
*hydro    volume   volume number
1010401    0.0        01
1010402    0.0        02
1010403    0.0        03
1010404    0.0        04
1010405    0.0        05
1010406    0.0        06
*hydro    incl. angle  volume number
1010601    90.0         01
1010602    90.0         02
1010603    90.0         03
1010604    90.0         04
```

```
1010605   90.0        05
1010606   90.0        06
*hydro    roughness   hd diam     volume number
1010801   0.0         0.0         01
1010802   0.0         0.0         02
1010803   0.0         0.0         03
1010804   0.0         0.0         04
1010805   0.0         0.0         05
1010806   0.0         0.0         06
*hydro    vol con   volume number
1011001   0000010   01
1011002   0000010   02
1011003   0000010   03
1011004   0000010   04
1011005   0000010   05
1011006   0000010   06
*hydro    jun con   junc number
1011101   00000100   01
1011102   00000100   02
1011103   00000100   03
1011104   00000100   04
1011105   00000100   05
*hydro    con wrd pressure  int energy
1011201   003      2.0e7    923.0  0.0 0.0 0.0 01
1011202   003      2.0e7    923.0  0.0 0.0 0.0 02
1011203   003      2.0e7    923.0  0.0 0.0 0.0 03
1011204   003      2.0e7    923.0  0.0 0.0 0.0 04
1011205   003      2.0e7    923.0  0.0 0.0 0.0 05
1011206   003      2.0e7    923.0  0.0 0.0 0.0 06
*hydro    liq. flow vap. flow
1011301   0.0      0.0      0 1
1011302   0.0      0.0      0 2
1011303   0.0      0.0      0 3
1011304   0.0      0.0      0 4
1011305   0.0      0.0      0 5
*-------------------------------------------------------------------
*hydro    component name      component type
1040000   outlet              valve
*-------------------------------------------------------------------
*hydro    from       to       area     floss    rloss      vcas
1040101   101010000  105000000 8.4e-5   0.0      0.0        00100
*
*hydro    vel/flw    f flow   g flow   j flow
1040201   1          0.0      0.0      0.0
1040300   mtrvlv
*hydro    open trip #    close trip #    rate   init pos.table
1040301   0001           0002            10000. 0.0        0.0
*-------------------------------------------------------------------
*hydro    component name      component type
1050000   exvol               snglvol
*-------------------------------------------------------------------
*hydro    area       length     volume
1050101   0.01       0.0        200.0
*hydro    horz ang   vert ang   deltaz
1050102   0.0        0.0        0.0
*hydro    roughness  hyd d      fe
```

```
1050103    0.0        0.0        10
*hydro     ebt        pressure   temp
1050200    003        14000000.0     923.0
*----------------------------------------------------------------------
.

=Breathing test
*
* Prepared in September 2007
* Stephanie A. McKee
*three plenum case, different sizes
*******************************************************************************
0000001    11 *modifies coding for supercritical pressure conditions
*----------------------------------------------------------------------
0000100       newath         transnt
*----------------------------------------------------------------------
0000101       run
*----------------------------------------------------------------------
0000102       si
*----------------------------------------------------------------------
0000120    101010000 0.0 co2 plenum
*----------------------------------------------------------------------
*         runtime minstep maxstep option mineditfreq majeditfreq restartfreq
0000201     25.   1.0e-6 0.005   0003    10         10         1000
*----------------------------------------------------------------------
* Trip number definitions
20600000       expanded
*----------------------------------------------------------------------
20600010  time 0 ge null 0 0.0 1
20600020  time 0 ge null 0 1e6 1
*----------------------------------------------------------------------
*hydro     component name      component type
1010000    plenum              pipe
*----------------------------------------------------------------------
*hydro     # vol
1010001     6
*hydro     area     volume number
1010101    .0446       01
1010102    8.4e-5      02
1010103    .0446       03
1010104    8.4e-5      04
1010105    .0446       05
1010106    8.4e-5      06
*hydro     length   volume number
1010301    .0448       01
1010302    1.54        02
1010303    .0224       03
1010304    2.0         04
1010305    .0224       05
1010306    2.0         06
*hydro     volume   volume number
1010401    0.0         01
1010402    0.0         02
1010403    0.0         03
1010404    0.0         04
1010405    0.0         05
```

```
1010406   0.0       06
*hydro    incl. angle  volume number
1010601   90.0      01
1010602   90.0      02
1010603   90.0      03
1010604   90.0      04
1010605   90.0      05
1010606   90.0      06
*hydro    roughness  hd diam    volume number
1010801   0.0       0.0        01
1010802   0.0       0.0        02
1010803   0.0       0.0        03
1010804   0.0       0.0        04
1010805   0.0       0.0        05
1010806   0.0       0.0        06
*hydro    vol con   volume number
1011001   0000010   01
1011002   0000010   02
1011003   0000010   03
1011004   0000010   04
1011005   0000010   05
1011006   0000010   06
*hydro    jun con   junc number
1011101   00000100  01
1011102   00000100  02
1011103   00000100  03
1011104   00000100  04
1011105   00000100  05
*hydro    con wrd pressure  int energy
1011201   003       2.0e7    923.0  0.0 0.0 0.0 01
1011202   003       2.0e7    923.0  0.0 0.0 0.0 02
1011203   003       2.0e7    923.0  0.0 0.0 0.0 03
1011204   003       2.0e7    923.0  0.0 0.0 0.0 04
1011205   003       2.0e7    923.0  0.0 0.0 0.0 05
1011206   003       2.0e7    923.0  0.0 0.0 0.0 06
*hydro    liq. flow vap. flow
1011301   0.0       0.0      0 1
1011302   0.0       0.0      0 2
1011303   0.0       0.0      0 3
1011304   0.0       0.0      0 4
1011305   0.0       0.0      0 5
*-------------------------------------------------------------------------
*hydro    component name      component type
1040000   outlet              valve
*-------------------------------------------------------------------------
*hydro    from      to        area     floss    rloss     vcas
1040101   101010000 105000000 8.4e-5   0.0      0.0       00100
*
*hydro    vel/flw   f flow    g flow   j flow
1040201   1         0.0       0.0      0.0
1040300   mtrvlv
*hydro    open trip #   close trip #    rate   init pos.table
1040301   0001          0002            10000. 0.0       0.0
*-------------------------------------------------------------------------
*hydro    component name      component type
1050000   exvol               snglvol
```

```
*-------------------------------------------------------------------
*hydro     area       length     volume
1050101    0.01        0.0        200.0
*hydro     horz ang    vert ang    deltaz
1050102    0.0         0.0         0.0
*hydro     roughness   hyd d       fe
1050103    0.0         0.0         10
*hydro     ebt         pressure    temp
1050200    003          700000.0     250.0
*-------------------------------------------------------------------
```

.